UNIVERSITY OF LIVERPOOL

Structural Damage Identification by Kriging Model Based Model Updating Methods

Thesis submitted in accordance with the requirements of the University of Liverpool for the degree of Doctor in Philosophy

By

Xiuming Yang

September 2019

Abstract

Although model updating as a methodology has been widely studied and applied in the past decades, it has a great potential for further development. This research focuses on the development and application of model updating method in the field of damage identification. The updating program is coded by Matlab and some numerical simulation data are provided by Nastran. This thesis includes the introduction of basic model updating theory and experimental measuring instruments, and original contributions have been made in the following aspects:

Method: Many theoretical models were created using finite element software. Considering that the stiffness and mass matrices of such a model are difficult to extract, an evolutionary algorithm (such as the genetic algorithm) is usually used to solve the optimization problem in model updating. In the specific implementation, each response needs to be calculated by a finite element run, which is very time-consuming. The traditional response surface-based methods replace the response calculation by a computational software package by constructing a mathematical model to simulate the response changing with the updating parameters. However, this kind of methods is difficult to be applied to the response with dramatic changes, and the number of responses is limited. In order to overcome these shortcomings, this thesis proposes a new model updating strategy based on Kriging model. This strategy broadens the types of responses that can be utilized by the response surface-based model updating methods and avoids the burden of constructing response surfaces for each response separately. Based on this strategy, the model updating based on the response surface of the frequency response function is successfully implemented.

Response: Modal strain energy (MSE) is a very sensitive response to damage and was mainly used in damage index methods. This thesis develops its application in the field of model updating and proposes a model updating method based on its sensitivity. A major challenge in the application of this method is to obtain accurate MSE measurement data. The specific solution is demonstrated in the experimental test and data processing parts. The proposed method successfully identifies the damage caused by the cracks in a beam-like structure.

Structure: Seam weld is one of the common ways to join components in an assembled structure. However, there are few studies on its modelling and how to properly reflect structural dynamic properties. This thesis studies the way of constructing a seam welded joint using CSEAM element available in Nastran and obtains accurate theoretical models through effective model updating. Moreover, a new method based on the proposed strategy and the MSE is developed for the damage identification of two structures with such a joint, each of which is a common T-shaped structure consisting of two plates welded together. The model updating of this structure is a typical problem that the response surface-based method must be used to reduce the computational cost. The method proposed in this study has good performance in damage identification and computational efficiency improvement.

Acknowledgements

First of all, I would like to convey my sincerest gratitude to my supervisors Professor Xinglin Guo and Professor Huajiang Ouyang, who have given me great encouragement and support for my PhD. Thanks you Professor Xinglin Guo for taking me into the field of experimental mechanics and providing me a comfortable and free research environment. Thanks you Professor Huajiang Ouyang, your patience, rigorousness, responsibility and dedication are the most outstanding scenery on my research path.

I would like to thank the Dual PhD program of University of Liverpool and Dalian University of Technology, which has provided me a precious opportunity to study at both universities and covered my tuition fees at the University of Liverpool.

Special thanks to people who have given me great help. Thanks to Shancheng Cao for teaching me to use experimental instruments and providing valuable experience for my research. Thanks to Professor Dongsheng Li and Professor Yan Zhao for their valuable suggestions. Thanks to Ray for helping me with the experiment and always caring about my safety.

I would also like to thank my colleagues and academic companions at the Dalian University of Technology and the University of Liverpool for their company and academic support, which makes my research life interesting and colourful.

Finally, thanks to my parents. Thanks for everything you have done for me.

Contents

Abstract ..... **I**

Acknowledgements ..... **III**

Contents ..... **V**

List of Figures ..... **IX**

List of Tables ..... **XIII**

Nomenclature ..... **XV**

Acronyms ..... **XVII**

Chapter 1 – Introduction **1**
1.1 Background and motivation 1
1.2 Aim and objectives 4
1.3 Original contributions 6
1.4 Outline of the thesis 8

Chapter 2 – Literature review **11**
2.1 Introduction 11
2.2 Dynamic responses 11
2.2.1 Natural frequency 11
2.2.2 Mode shape 12
2.2.3 Modal flexibility 15
2.2.4 Mode shape curvature/ Modal strain energy (MSE) 16
2.2.5 Frequency response function (FRF) 17
2.3 Model updating methods 18
2.3.1 Direct methods 20
2.3.2 Sensitivity based model updating methods 21
2.3.3 Evolutionary algorithms based model updating method 25
2.3.4 Response surface-based methods 28
2.3.5 Uncertainty quantification in model updating 31
2.4 Weld joint modelling 32
2.5 Conclusions 34

Chapter 3 – Experimental test conditions **35**
3.1 Introduction 35
3.2 Experimental modal analysis 35
3.3 Scanning laser vibrometer 41
3.4 Conclusion 48

Chapter 4 – Basic theory of model updating method **49**
4.1 Introduction 49
4.2 Sensitivity-based methods using natural frequencies and mode shapes 49
4.2.1 Selection of updating parameters 49
4.3 Genetic algorithm-based model updating 57

4.3 Numerical Simulation 60
4.4 Sensitivity-based methods using FRFs 63
4.4.1 Basic theory 64
4.4.2 Case study using simulated FRF data 67
4.5 Conclusions 71

Chapter 5 - Modal Strain Energy Based Model Updating Method for Damage Identification on Beam-like Structures 73
5.1 Introduction 73
5.2 Background 73
5.3 Basic theory 76
5.3.1 Sensitivity of element modal strain energy 76
5.3.2 Calculation of residuals 77
5.3.3 Data processing 79
5.3.4 Model updating procedure 81
5.4 Numerical simulation 83
5.5 Experimental setup and results 90
5.6 Influence of damping 96
5.7 Conclusion 98

Chapter 6 - A Kriging model-based finite element model updating method for damage detection. 101
6.1 Introduction 101
6.2 Background 101
6.3 Kriging based model updating method 104
6.3.2 Kriging model in model updating 107
6.3.3 Efficient Global Optimization 110
6.4 Numerical example 115
6.5 Experimental study 119
6.6 Conclusions 128

Chapter 7 - Finite element modelling and damage detection of seam weld 129
7.1 Introduction 129
7.2 Background 129
7.3 Seam welded joint modelling 131
7.3.1 General seam welded joint modelling methods 131
7.4 Theory of model updating of seam welded joint 142
7.5 Numerical simulation 145
7.6 Experimental results 152
7.8 Conclusions 160

Chapter 8 - Conclusions and future work 163
8.1 Conclusions 163
8.2 Future work 166

Appendix A: 169

Nastran input file (.bdf) for Normal Modes analysis (SOL 103) of welded structures using CSEAM elements with PARTPAT format. 169

References **173**

List of Figures

Figure 2-1 Classification of model updating methods. 20
Figure 3-1 Impact test tools: (a) Hammer; (b) Accelerometer. 36
Figure 3-2 EMA through impact test. 39
Figure 3-3 Shaker. 40
Figure 3-4 Schematic of the experimental set-up. 41
Figure 3-5 Actual experimental set-up. 44
Figure 3-6 Position distribution of measuring points. 44
Figure 3-7 FRF measurement of point 11. 45
Figure 3-8 Settings of FastScan. 46
Figure 3-9 Comparison of Measurements: (a) Mode shape measured by Fast scan; (b) Mode shape measured by common method; (c) Modal displacement at on each measurement point by the two methods. 47
Figure 4-1 Flowchart of the sensitivity-based model updating method. 56
Figure 4-2 Flowchart of the GA method. 58
Figure 4-3 4-DoF mass-spring system. 60
Figure 4-4 Updating results of the 4 ways: (a) Without noise; (b) Noise contaminated. 62
Figure 4-5 Geometry of a truss model. 68
Figure 4-6 Actual and updating results for damage scenario 1 (top graph for mass and bottom graph for stiffness). 69
Figure 4-7 Numbers of acceptable NF for the three methods with different numbers of measured DoFs. 70
Figure 4-8 Actual and updating results for damage scenario 2 with 3% white Gaussian noise polluted data (top graph for mass and bottom graph for stiffness). 70
Figure 5-1 1-D Gaussian distribution with σ=1. 80
Figure 5-2 Simulate simply supported beam and its geometry. 83
Figure 5-3 Beam model with damage of a crack built in Patran. 84
Figure 5-4 MSE calculation: (a) Comparison of element MSEs of 1st mode from different sources; (b) Curvature of the 1st mode. 85

Figure 5-5 Element MSEs of 1st mode calculated by theoretical model with different values. 86
Figure 5-6 Updating results of the data from curvature method: (a) Damage severity represented by $\mathbf{1}-\mathbf{p}_d$; (b) MSE comparison. 87
Figure 5-7 Updating results of the data from real result: (a) Updated parameters change from 1; (b) MSE comparison. 88
Figure 5-8 Photos of test on a cantilever beam: (a) Experimental setup; (b) Measurement points set up by PSV-500 system. 91
Figure 5-9 MSE calculation based on the experimental data. 93
Figure 5-10 Updating results of the experimental data shown by reduced proportion. 94
Figure 5-11 Comparison of MSE of different modes between the intact model, calculated by the curvature method and the updated model: (a) Mode 1; (b) Mode 2; (c) Mode 3; (d) Mode 4. 95
Figure 5-12 Beam with grounded viscous dampers (view of part of the beam that covers the crack). 96
Figure 5-13 The 1st mode MSE calculation results comparison. 97
Figure 5-14 Updating results of the 2 cases. 98
Figure 6-1 Real response surface of (a) First order frequency; (b) FRF(1,1). . 103
Figure 6-2 (a) The expected improvement of a one-variable function calculated by the Kriging model constructed through five sample points; (b) A graphical interpretation of the expected improvement at x=0.7. 112
Figure 6-3 Flow chart of the proposed model updating method. 113
Figure 6-4 Flow chart of the proposed updating strategy. 115
Figure 6-5 The cantilever beam used for numerical simulation. 116
Figure 6-6 The response surface of the objective function when only two parameters are variable: (a) The Kriging model prediction; (b) Real response surface. 118
Figure 6-7 The updating results of the Kriging method, GA method and AF approach compared with the ‘real’ damage. 118
Figure 6-8 Overview of the three-story structure (Source: Courtesy of [190]). 120
Figure 6-9 Theoretical model for the test structure. 122

Figure 6-10 The FRF of the first floor of the real structure and the updated model: (a) Absolute value of $H(1,1)$; (b) Absolute value of the real part of $H(1,1)$; (c) Absolute value of the imaginary part of $H(1,1)$. 123
Figure 6-11 The objective function of 50Hz when only m1 and m2 are variable using experimental data of state 1. 124
Figure 6-12 The response surface of the objective function when only m1 and m2 are variable: (a) Before improvement; (b) After improvement. 125
Figure 6-13 Updating results of the different states of the two methods compared with the real value. 127
Figure 7-1 Three ways of modelling for comparison: (a) Shell elements with nodes overlapped; (b) Solid elements connected by solid elements; (c) Shell elements connected by CSEAM elements. 132
Figure 7-2 Illustration about the creation of CSEAM element: (a) Seam weld between two shell patches; (b) Dimensions of the seam element. (Source: reference [195] with permission from Nastran). 134
Figure 7-3 Demonstration about how CSEAM element is built in Nastran: (a) Semi-finished structure in Patran; (b) CSEAM elements built directly in Patran. 135
Figure 7-4 Force and moment transferred from the reference points to other points connected by RBE3: (a) From reference point to the centre of gravity; (b) From the centre of gravity to other points; (Source: reference [198] with permission from Nastran). 137
Figure 7-5 Mode shapes of the structures connected by CSEAM elements: (a) Mode 1 of the Semi-finished structure; (b) Mode 1 of the full structure; (c) Mode 2 of the Semi-finished structure; (d) Mode 2 of the full structure. 138
Figure 7-6 Illustration about modifying the location of start point GS (Provided by MSC Technique Support with permission to use). 139
Figure 7-7 Seam element cross section at start point GS (Source: reference [150] with permission from Nastran). 140
Figure 7-8 Illustrations of two T-shape models used in simulation by Patran: (a) Fine mesh with merged-node joint (b) General mesh with CSEAM element joint. 146

Figure 7-9 MSE distribution of the structure: (a) Mode 1; (b) Mode 2; (c) Mode 9. 148
Figure 7-10 Experimental data of the 1st Mode of the 1st model: (a) Extracted mode shape; (b) MSE of calculated by equation (7.9); (c) MSE of the coarse mesh corresponding to the 2nd model. 149
Figure 7-11 Response surface of the objective function: (a) Real response surface of the 1st step; (b) Kriging model of the 1st step; (c) Real response surface of the 2nd step; (c) Kriging model of the 2nd step 150
Figure 7-12 Comparison of element MSEs across the weld seam. 151
Figure 7-13 Designed parameters of the T-shape structures (unit: mm): (a) Horizontal plate; (b) Vertical plate; (c) Weld connection for T1; (d) Actual appearance. 153
Figure 7-14 Two damage scenarios: (a) Weld connection for T2; (b) Weld connection for T3. 153
Figure 7-15 (a) Theoretical model connected by CSEAM elements; (b) MSE distribution of the 3rd mode. 155
Figure 7-16 Grid of measurement points. 156
Figure 7-17 Performance of Gaussian smoothing technique applied on calculating x-direction curvature measurements: (a) Measured mode shape; (b) x-direction angular displacement calculated from (a); (c) x-direction angular displacement calculated from smoothed (c); x-direction curvature calculated from (b); (d) x-direction curvature calculated from smoothed (c); (e) Curvature squared from (d); (f) Final MSE density measurements. 157
Figure 7-18 (a) Experimental and updated MSEs comparison of T2; (b) Experimental and updated MSEs comparison of T3; (c) The 3rd mode theoretical MSE distribution of T2; (d) The 3rd mode theoretical MSE distribution of T3; 159

List of Tables

Table 3-1 Nature frequencies of the specimen. 45
Table 3-2 Test time comparison. 47
Table 4-1 Natural frequencies (Hz) of the system. 61
Table 4-2 Damage scenarios of the truss structure. 68
Table 4-3 Updating limits of the three methods. 69
Table 5-1 Information of crack configurations. 90
Table 5-2 Natural frequencies of the damaged beam and the used driving frequencies of the shaker. 91
Table 6-1 Natural frequencies of the theoretical and damaged model of the cantilever (unit: Hz). 116
Table 6-2 The required number of running the FE program of the Kriging method, and the GA method (which is repeated 3 times). 119
Table 6-3 Summary of structural state conditions. 120
Table 6-4 The required number of running the FE programs of the Kriging method and the GA method for different states. 127
Table 7-1 Natural frequencies of the stiffened plate. 133
Table 7-2 Natural frequency improvement after updating. 147
Table 7-3 Actual location and updating results of the gap. 151
Table 7-4 The measured weights (unit: kg) and calculated mass densities (unit: kg/m3) of the plates. 154
Table 7-5 Measured frequencies (unit: Hz) and updated *E* (unit: GPa) and ν of the horizontal plates. 154
Table 7-6 Model updating of the *E* (unit: GPa) of the welding part based on natural frequencies (unit: Hz). 154
Table 7-7 Updating results of T2 and T3 (unit: cm). 159
Table 7-8 Computation time comparison of the 2 methods (unit: s). 159

Nomenclature

a, e/x	Subscript or superscript to indicate theoretical and experimental
D	Dynamic characteristic
d	Superscript to indicate damaged
dis	Measured displacement vector
EI	Bending stiffness
E	Young's modulus
$ei(\mathbf{x})$	Expected improvement
$F(\omega)$	Output function in the frequency domain
$\mathbf{F}(\omega)$	Fourier transform vector of external forces
$\mathbf{f}(t)$	Force vector
f	Frequency
$G(x)$	Gaussian distribution
h	Distance between 2 measurement points/thickness
$H(\omega)$	Frequency response function
$\mathbf{H}(\omega)$	Frequency response function matrix
h	Frequency response function vector
j	The imaginary unit
$k1, k2 \ldots k6$	Stiffness of Springs
L	Likelihood function
$\mathbf{M}, \mathbf{C}, \mathbf{K}$	Mass, damping and stiffness matrix
$m1, m2 \ldots m4$	Mass
m, s	Subscript to indicate master and slave
p	Vector of updating parameters
$\mathbf{p}_i$	Vector of updating parameters in the *i*th iteration
r	Mode order
R, **R**	Correlation and correlation matrix
$S_{X,X}(\omega)$	Averaged auto power spectrum of the input

$\overline{S_{F,X}(\omega)}$	Averaged cross power spectrum between the input and output
$\mathbf{S}$	Sensitivity matrix
$\hat{s}^2(\mathbf{x})$	Mean squared error
t	Time
T	Transpose
$v, v_x\ v_{xx}$	Displacement, angular displacement and curvature in y direction
$\mathbf{W}$	Weighting matrix
w	Weighting value/ out-of-plane displacement
$X(\omega)$	Input function in the frequency domain
$\mathbf{X}(\omega)$	Fourier transform vector of displacement responses
$\mathbf{x}(t)$	Displacement vector
$\mathbf{X}, \mathbf{x}, \mathbf{Y}$	Input matrix, input vector, output matrix
x	Updating parameter
$\mathbf{y}$	Vector of the dynamic features
$\mathbf{y}_{\mathrm{m}}$	Measured features
$z(\mathbf{x}_i)$	Stochastic process
α, β	Coefficient
$\boldsymbol{\varepsilon}$	Residual vector
ε	Residual/ stopping criterion
θ	Decay rate of correlation
λ	Eigenvalue
υ	Poisson's ratio
ξ	Modal damping ratio
σ	Standard deviation
$\boldsymbol{\varphi}$	Eigenvector/mode shape
ω	Frequency variable

Acronyms

1-D	One dimensional
2-D	Two dimensional
COMAC	Coordinate modal assurance criterion
DI	Damage identification
DOE	Design of experiments
DoFs	Degrees of freedom
EGO	Efficient global optimization
ei	Expected improvement
EMA	Experimental modal analysis
FDAC	Frequency domain assurance criterion
FE	Finite element
FFT	Fast Fourier transform
FRF	Frequency response function
GA	Genetic algorithm
LANL	Los Alamos National Laboratory
LHS	Latin hypercube sampling
MAC	Modal assurance criterion
MOMD	Minimum order of magnitude difference
MPC	Multi-point constraint
MSE	Modal strain energy
PSO	Particle swarm optimization
SA	Simulated annealing
SLV	Scanning laser vibrometer

Chapter 1 – Introduction

1.1 Background and motivation

In the development of modern society, a variety of engineering structures such as automobiles, bridges, satellites and offshore platforms provide a great convenience for human activities. People are constantly pursuing better performance, lower cost and more reliable safety diagnosis and maintenance for these structures. In this process, the finite element (FE) method is the most widely used numerical method in engineering analysis. Based on this theory, many FE analysis software like ANSYS, Abaqus and Nastran were born.

At present, establishing an FE model for structural design, optimization and behaviour prediction has been widely recognized by the industry and is an important part of computer-aided design and manufacturing. Compared with traditional theoretical analysis and experimental research, the application of the FE method for analysis can greatly reduce the time cost and economic cost especially for large complex structures and is also convenient to provide a theoretical guarantee for the feasibility of different design schemes.

However, an FE model is essentially a simplification of a real structure, which is bound to introduce a certain degree of modelling errors. In addition, when producing the actual structure based on the design blueprint, it is difficult to ensure that the geometric dimensions and material parameters are in full agreement with the design values. If these errors exceed the permissible range, the confidence in the actual structural response based on the FE method will be considerably decreased. Therefore, it is necessary to calibrate the FE model through some easily measurable characteristics of the actual structure before predicting the behaviour of the structure in a special circumstance. This led to the emergence and development of FE model updating techniques [1].

The dynamic and static responses of an actual structure obtained through experimental testing are the most reliable, despite measurement errors. The basic idea of model

updating is to make the FE model produce the theoretical response which is as consistent as possible with the experimental data by adjusting the selected uncertain structural parameters. After this, the FE model can more reliably reflect actual structural characteristics. Therefore, the FE model updating is essentially an inverse problem of determining structural parameters from responses. Minimizing the difference between the predicted result and the measured data is an optimization process for a specific objective function. After years of development, the FE model updating has become a relatively mature technology and has been successfully applied to many engineering applications such as bridges [2], space vehicles [3] and composite structures [4].

In the above examples, the model updating parameters represent the global characteristics of the structure or sub-structure, which means those parameters usually belong to many elements. On the other hand, one major application of the model updating is about parameters specific to individual elements or local parameters, which are often used for damage identification. In this field, the difference between the results from the theoretical model and the actual structure is attributed to damage. By using the model updating method, the influence of the damage can be effectively reflected by the parameter change of a particular element or a local parameter. Generally speaking, damage will cause the reduction of the stiffness of the element at the damage location. By comparing the stiffness changes of the FE model before and after the structural damage has occurred, the localization and quantification of the structural damage can be effectively performed. Of course, for damage identification, the parameters to be modified are not limited to the material properties of each element. Geometric parameters, such as the position and depth of a crack, and boundary conditions are also included.

Damage identification is also a popular research topic in the past few decades [5]. Many large engineering structures face damage problems that occur after long-term service or accidental disasters. Once the accumulation of damage leads to the failure of the function of the structure, it may cause a great loss of people's lives and property. Therefore, it is necessary to perform effective health monitoring and damage detection for these structures in order to perform maintenance and protection in time. In the field

of damage identification, non-destructive testing methods that do not require disassembly and destruction of the original structure are the most welcome. It can be divided into global detection technology and local detection technology. The latter, such as the ultrasonic method, the X-ray method, etc., need to know in advance the approximate area of the damage, also the area is required to be measurable. In comparison, global detection technology is more flexible and versatile, which can also provide the necessary information support for local detection technology.

The global detection technique is also based on structural static and dynamic response information. Some methods emphasize experimentally measured response data for diagnosis, while others require a detailed mathematical model, called model-based approaches. The most commonly used mathematical model is undoubtedly the FE model, and the FE model updating method can make the model more accurate and credible. Model updating is often used as a prior step to apply these damage identification methods, especially for the methods that require intact structural test data method. In addition, the damage identification method based on model updating itself is a subclass of model-based methods. Compared with other damage identification methods, the advantages of modal updating based methods are that the location and quantity of the damage can be determined at the same time, the updated parameters reflecting damage have a physical meaning, the impact of damage is more intuitive, and the test data obtained under different conditions can be considered at the same time. On the other hand, this kind of methods also needs to face the adverse factors such as the change of the element parameters does not completely represent the actual damage, and it is like to arrive at (incorrect) updating parameter values that compensate each other.

At present, vibration-based damage detection is most commonly used in global damage detection. Structural vibration response data tend to provide more information than static response data. A vibration test is also simpler than a static test because it does not require initial displacement calibration of the sensor and its requirement for the shape of the structure is low.

This thesis focuses on the application of the model updating method in the field of damage identification using dynamic response data, for following reasons. (1) Ease of verification. The introduction of damage can make the difference between the actual structure and the theoretical model become intuitive and obvious, thus the judgment of the model updating result can be objective and reliable. Also, the verification can be done by generally used beam, plate and frame structures in the laboratory. (2) Establishment of new methods and new sensitive responses. In the model updating of large and/or special structures, due to the great influence of modelling errors, in most cases, the FE model which can provide close frequencies to the experimental data is sufficiently satisfactory. On the other hand, in the application of damage detection on simple structures, accurate localization of the damaged element is required, which will encourage researchers to continually pursue a new response which is more sensitive to damage and develop the model updating method based on that response. Of course, reliable behaviour prediction and damage identification for large complex structures is always the direction of researchers' efforts. The current research results make a positive contribution to meet the needs of society. Model updating as a key technology still has a great potential to be untapped.

1.2 Aim and objectives

In the study of model updating methods, the sensitivity method is a mature solution strategy [6]. As a method of iteratively solving the objective function by minimizing the residual between the theoretical response and the measured response, it has been proved to be a very successful method. Based on this strategy, a large number of sensitivity-based model updating methods using different types of dynamic and static responses are explored and applied to different engineering structures.

However, the application of the sensitivity method requires known stiffness, mass and damping matrix. For large complex structures that rely on FE analysis software to build the model, the extraction of these matrices is difficult. Moreover, special elements and constraints are often included in the FE models to describe complex boundary conditions and connections, which makes it hard to apply the sensitivity method. These have led to the limited application of sensitivity-based model updating methods in such

structures. Therefore, directly invoking the commercial software to calculate the theoretical response is more convenient. The model updating method combined with commercial software is a better choice.

Benefiting from the rapid development of artificial intelligence algorithms, many model updating methods based on such algorithms [7], like genetic algorithm (GA), particle swarm optimization (PSO) and simulated annealing (SA), have been proposed. These powerful mathematical tools can be used to solve complex optimization problems with high nonlinearity without the need to calculate a sensitivity matrix. Theoretically, with the help of these algorithms, most model updating problems of large complex structures can be resolved in 3 steps: (1) Build the FE model by software. (2) Construct a reasonable objective function. (3) Solve the optimization problem through these artificial intelligence algorithms which invoke the software to calculate the analytical responses. However, in practical applications, since artificial intelligence algorithms require a very large number of computation of the objective function to obtain a result, the computational efficiency has become a major problem that plagues the method. Much time is consumed in the process of invoking FE software for calculation, which makes the solution time of a single problem unsatisfactory.

Aiming at this problem, the response surface-based model updating method is proposed and developed [8]. Its core idea is to construct a mathematical model to predict the response output of the commercial software. The model is usually built through a certain number of given input parameters and their corresponding output responses calculated by the software. For a random input, if the calculation result of this mathematical model is close enough to the software, it can be used to provide theoretical responses for the artificial intelligence algorithm instead of invoking the commercial software. As the calculation speed of the mathematical model is much higher than running the FE software, the efficiency of solving such a model updating problem will be significantly improved. The response surface-based model updating method is a new branch in the model updating field. However, at present, only a limited variety of responses and a small number of updating parameters can be utilized in this

method, and there are still many problems that need to be overcome. The improvement and application of this method are a main effort of this thesis.

In addition, in order to validate the proposed method by design of experiments, this research explores the use of the finite elements provided by well-known commercial FE analysis software, Nastran, to model seam welded joints. In modern industry, many structures are assembled from different parts via special joints for easy production. These joints, such as bolted joints and welded joints, are inherently complex in modelling and often numerous. Therefore, it is not suitable to build these connections to use sophisticated FE models but to replace them with some special, usually simplified, joint elements. The calibration of these connecting elements to correctly reflect the mechanical properties at the joints is also one of the application areas of the model updating method. In the process of model modification relying on modelling and computation by FE software, the application of the response surface method is indispensable. Thus, the test on a seam weld connected structure is an important part of the experimental verification of this thesis.

1.3 Original contributions

The main original contributions of this research are as follows:

(1) A new model updating strategy based on Kriging model is proposed. This strategy changes the traditional idea of constructing a surrogate model for the response of a theoretical FE model by response surface method but focuses on constructing the agent model of the objective function to solve the updating problem. In this way, many responses which change sharply, with strong nonlinearity, with the updating parameters can be used in the surrogate model based model updating method. The problem that it is difficult to build a mathematical model to describe these responses is transformed into the problem of how to reasonably construct the objective function to make its response surface smooth and reliable in the vicinity of the optimal solution. Therefore, other types of responses, for example, frequency response function, which would be difficult to use together with the traditional response surface methods, can

now be used due to advantage in this new strategy. . This strategy is very versatile, and most of the responses can be put into use directly according to this idea.

(2) Based on this strategy, the model updating method based on the response surface of the frequency response function (FRF) is studied. FRF is one of the most widely used three major responses in structural dynamics and has the advantage of no mode extraction error. This study proposed an efficient way to utilize it in the response surface-based model updating method. A usable objective function is constructed and the damage identification based on this is successfully performed. The results also show that with the newly proposed solution strategy, the number of response surfaces required to be constructed is extremely low, and the number of selectable model updating parameters has been increased to nine.

(3) Most of the literature on weld joint modelling is about simulating the welding process or analysing the fatigue and residual stress of the joint. The literature reflecting the dynamic behavioural modelling of joints, especially for seam welded joints, is very rare. The FE modelling of such joints should be simple, precise and easy to generalize. Therefore, as a specially designed element in an FE commercial software package whose application is very rare, the seam connection element (i.e. CSEAM in Nastran) is selected. A guideline on how to use this element to build an FE model of seam-welded structures and how to correctly reflect the dynamic characteristics of joints by effective model updating method is presented.

(4) Based on the CSEAM element, this thesis further considers how to use the joint model and the model updating method for damage identification. Here the damage is introduced as a weld defect, which is designed as the partial loss (gap) of weld at the joint. Since the dynamic features of the joint is difficult to measure directly, it must be identified by the response of the connected parts. The modal strain energy (MSE) is selected as the response and a suitable objective function is constructed to implement the model updating method based on the Kriging model, and the damage identification of the weld gap on the T-shaped structure is successfully completed.

(5) As a derivative of vibration mode shape, MSE is very sensitive to damage. However, in the past, MSE has been mainly used in the literature of detecting damage by damage index methods. There is no application of MSE in the field of model updating. This research explores how to utilize MSE to do model updating by the sensitivity method. A specific scheme including formulation, optimization process, response measurement and data processing is presented, and the scheme is successfully used to identify multiple cracks in beam-like structures.

List of publications:

- Yang, X., Guo, X., Ouyang, H. and Li, D., 2017. A Kriging model based finite element model updating method for damage detection. Applied Sciences, 7(10), p.1039.

- Yang, X., Ouyang, H., Guo, X. and Cao, S., 2017 Model Strain Energy Based Model Updating Method for Damage Identification on Beam-like Structures. Journal of Structural Engineering. Submitted

- Yang, X., Ouyang, H., Guo, X. and Li, D., 2020. Finite Element Modelling and Damage Detection of Seam Weld. In Proceedings of the 13th International Conference on Damage Assessment of Structures (pp. 51-62). Springer, Singapore.

- Yang, X., Guo, X., Ouyang, H. and Li, D., 2017, May. A new frequency matching technique for FRF-based model updating. In Journal of Physics: Conference Series (Vol. 842, No. 1, p. 012013). IOP Publishing.

1.4 Outline of the thesis

This thesis contains 8 chapters. Most of these chapters are self-contained and can be read independently. The structure of this thesis is given as follows:

Chapter 1 introduces the background of the model updating methods, the motivations, objectives and the original contributions of this thesis, and the thesis outline.

Chapter 2 provides a literature review of dynamic response based damage identification methods, model updating methods and weld joint modelling methods, which covers the development of these methods and important research results.

Chapter 3 introduces the theory of experimental modal analysis, testing instruments and a testing example demonstration.

Chapter 4 presents in detail the basic theory of two mature model updating methods: the sensitivity-based model updating method and the genetic algorithm-based model updating method. Sensitivity-based model updating methods are divided into two categories: using modal data and using FRF data. It also describes the improvement to the FRF-based methods made in this research.

Chapter 5 proposes an MSE sensitivity-based model updating method. A penalty function is added to the objective function to control the variation range of the updating parameters. The specific process for obtaining accurate MSE measurements is demonstrated. The proposed method is applied to identify the cracks of beam-like structures.

Chapter 6 presents a Kriging model-based model updating method. This method effectively utilizes FRF data, which are difficult to use in traditional response surface-based methods, for model updating. A numerical simulation of a cantilever beam and the test data of a laboratory three-story structure are used to verify the robustness of the method. In addition, the core solution strategy of this Kriging model-based method is summarized and is shown to be easily applicable to other dynamic responses.

Chapter 7 studies how to use the CSEAM element designed by Nastran to model seam welded joints. It also shows that the theoretical model can correctly reflect the measured frequency data by updating the Young's modulus of the CSEAM elements. In addition, damage is introduced in the form of a weld gap. Based on the experimental data, the damage in 2 T-shaped structures is successfully identified by the proposed method, which utilizes MSE data through the strategy summarized in Chapter 6.

Chapter 8 outlines the key conclusions achieved in the research and makes some suggestions for future work.

Chapter 2 – Literature review

2.1 Introduction

In this chapter, a literature review is provided, which is divided into 3 categories, dynamic responses, model updating method and weld joint modelling. For dynamic responses, different kinds of dynamic properties used in damage identification and their related methods are reviewed. For model updating method, the development of this method from the past to the present is covered. Some methods are no longer popular, some methods are mature, and some methods have a great potential in this field. For weld joint modelling, papers about two kinds of weld joints, spot weld and seam weld, are reviewed.

2.2 Dynamic responses

Theoretically, all dynamic responses which are sensitive to damage can be used in damage identification. Some reviews of vibration-based structural damage identification are provided by Doebling, et al. [9], Fan and Qiao [5], Cao, et al. [10] and Yan, et al. [11]. Generally, the depth of damage identification can be divided into four levels: existence, location, severity and residual service life. Most damage identification methods can be classified as at level 2 and level 3. In this section, some most widely used dynamic features are reviewed, which makes it convenient to introduce the different kinds of model updating method in the next section.

2.2.1 Natural frequency

Natural frequency, mode shape and modal damping are 3 basic modal parameters describing the dynamic characteristics of structures. It is well known that measured natural frequencies have the highest signal-to-noise ratio and can be obtained very accurately in the laboratory. In addition, the frequency data can be acquired by simple single-point measurements, and its experimental time is much less than the mode shape test.

Early natural frequency-based damage identification studies can be traced back to Cawley and Adams [12, 13], where it was found that the changes in natural frequencies could be used to detect, localize and roughly quantify damage in structures. However, this method is susceptible to noise in the measurement. After years of development, many improvements and new methods have been proposed, for example, Messina, et al. [14] presented a multiple damage location assurance criterion that utilized the changes in natural frequencies between damaged and undamaged states to predict the location and size of the damage.

In 1997, Salawu [15] reviewed damage identification methods based on frequency variation by that time. It was concluded that the natural frequency alone cannot provide sufficient information for the localization of damage, for example, a crack in a location of a beam may cause the same amount of frequency change as a crack in a different location. Also, very high frequencies have to be used to cover various damage situations, which makes these methods easily influenced by noise and theoretical assumptions. The proper way is to use only test data from the first few frequencies in damage identification.

2.2.2 Mode shape

Unlike the natural frequencies, a series of sensors are required to measure mode shape data and usually noise contamination in these data is much higher than the frequency data. However, the advantage of using mode shapes for damage identification is also quite obvious. Apparently, mode shape data contain enough spatial information and thus is more useful in damage localization, especially for multi-damage identification problems. Besides, natural frequencies of structures are susceptible to environmental factors such as temperature and humidity, while these factors have a very small effect on mode shapes.

An FE model is necessary for natural frequency-based damage detection methods, but not for all mode shape-based methods. Thus, the latter can be divided into 2 categories, model-based methods and non-model based methods, and will be introduced in turn.

(1) Similar to frequency-based methods, the idea of model-based methods is to establish a relationship between the damage location and/or severity and the mode shape change though an FE model. The mode shape change is calculated from test data of the intact and damaged models. If the intact model measurements are not available, the FE model is usually used to generate baseline data instead.

Based on Messina, et al. [14]'s work, Shi, et al. [16] proposed a sensitivity- and statistical- method to localize structural damage. This method can utilize incomplete mode shape data directly without the requirement of matching the full FE model. Another way of using incomplete mode shape data is to expand it into complete ones. Chen and Bicanic [17] put forward a method of using the Gauss-Newton least-squares technique to predict damage. Parloo, et al. [18] presented a method to localize and assess damage based on the use of mode shape sensitivities and the least square method. A comparison with other damage localization methods was also shown using the test data from a clamped wooden board and an I-40 highway bridge. The change of natural frequencies and modes can also be used together, called modal data, which is shown in Ren and De Roeck [19, 20]'s work to identify damage of reinforced concrete beam with free boundary conditions.

In a real application, it is important to compare the difference between the theoretical mode shape data to its experimental counterpart. Hence, the function of the modal assurance criterion (MAC) [21] is defined to provide a measure of consistency between a mode shape pair. Certainly, The MAC values between the same modes before and after damage is less than 1, which can be used as a simple damage indicator. An extension of the MAC is the coordinate modal assurance criterion (COMAC) which can be used to localize damage. In Salawu and Williams [22]'s paper, the dynamic response measurements of a bridge before and after structural repairs was provided and compared. It was shown that the change of COMAC values could be used to detect the positions of two of the three damages and showed the best performance. On the other hand, the change in natural frequencies and damping values were not obvious.

(2) For the health diagnosis of large complex structures, FE modelling for these structures consumes much time and test data of the intact structures are required to

build an accurate FE model, which is usually not available. Therefore, model-based damage identification methods are more suitable for long-term health monitoring, rather than occasional on-site diagnosis.

In order to meet the engineering needs, many researchers focus on developing a non-model based, or response based, or modern signal processing based, branch of damage identification methods. These methods do not require any theoretical model but diagnose directly based on the measured mode shape data. Their core idea is that damage induces high-frequency signal change of the mode shape data in its neighbourhood. If a suitable mathematical tool can be found to accurately describe this change, this indicator can be used to determine the location of the damage and estimate its severity.

The fractal dimension is such a tool, which was introduced by Hadjileontiadis, et al. [23] to find the sudden change in the spatial variation of the mode shape responses to detect damage. The proposed fractal dimension-based crack detector can successfully identify the damage of a one-crack cantilever beam and is attractive due to its simple calculation. This method was also extended to crack damage detection of 2-D plates by Hadjileontiadis and Douka [24]. Hadjileontiadis' methods were all applied to the fundamental mode shape; if high mode shapes were considered, the sudden change caused by the crack would be overwhelmed by the spatial variation of the mode shapes themselves. To overcome this problem, Wang and Qiao [25] put forward a generalized fractal dimension method to increase the influence of the complexity caused by the crack. Such a method was applied to a beam-type structure using the data measured under uniform load surface which was considered to be the least sensitive to the experimental errors.

Another well-known tool is the wavelet transform, which can be used to extract the features of the mode shapes in multiple scales. The extracted wavelet transform coefficients are proportional to the higher derivatives of the selected model shape data sequence. Thus, the damage features can be obtained from these coefficients.

The first attempt to apply wavelet theory in damage identification was made by Liew and Wang [26]. It was found that wavelet transform based method could detect a transverse crack on a simply supported beam easily and did not require data of the high-order modes. However, the response data processed was the deflection of the beam which oscillated under initial excitation. In Wang and Deng [27]'s work, wavelet transform was applied directly to analyse deflection or displacement response for damage detection. Douka, et al. [28] used the 'symmetrical 4' wavelet to identify damage of a plate having a uniform-depth crack which was parallel to one edge. Chang and Chen [29] extended the application of the wavelet-based method to identify multiple cracks in a beam.

Obviously, the direct use of vibration mode data does not fully exploit its potential in the field of damage identification. In addition to the above mathematical tools, there are many other attempts to be introduced as follows.

2.2.3 Modal flexibility

Modal flexibility can be estimated by the first few mode shapes accurately. It was suggested by Pandey and Biswas [30] that the changes in flexibility matrix could be used directly to reflect the location of damage. This method was also validated on wide-flanged beams in [31] and only 3 of the lowest modes were enough to build the flexibility matrix. Zhao and DeWolf [32] presented a sensitivity study which compared the performance of natural frequencies, mode shapes and modal flexibility in damage detection. Results showed that the modal flexibility was more likely to indicate damage than the others. Duan, et al. [33] proposed a proportional flexibility matrix-based method to identify damage of structures under environmental excitation where only output was required. Wu and Law [34] applied the changes in uniform load-induced curvature to localize damage on 2-D plate structures. The uniform load-induced curvature can be regarded as a derivative of the modal flexibility and is robust to the truncation error.

2.2.4 Mode shape curvature/ Modal strain energy (MSE)

It was demonstrated by Li, et al. [35] that the defect on a plate would directly lead to the sudden change of the strain on the edge of the damaged area. This phenomenon implies that the mode shape derivatives are more sensitive to damage than mode shapes themselves. In the past few decades, strain-based damage identification research has attracted the attention of many scholars. A literature review presented by Li [36] briefly introduced these methods using different strain-based parameters, such as strain (curvature) mode shape, strain energy, strain frequency response function, etc. In this subsection, mainly the curvature mode shape-based and strain energy-based methods are reviewed.

As second derivatives of mode shapes, mode shape curvatures can be derived by a central difference approximation or obtained by measured strains (curvature is proportional to the bending strain). In Pandey, et al. [37]'s work, it was shown that the absolute changes in the curvature mode shape could be used directly to localize damage. These changes increase with damage size. Abdel Wahab and De Roeck [38] proposed a curvature damage factor, which represented the mean value of the curvature change at a point of all modes. This factor was used to detect damage on a prestressed concrete bridge, Z24. It was suggested that a fine mesh was required in calculating the curvatures, but generally, the curvatures of lower modes are more accurate.

Ratcliffe [39] used the Laplacian operator to calculate the curvature mode shapes and tried to detect damage based on the distinctive shape of a continuous curvature. To deal with the problem that the distinctive shape does not exhibit apparent singularity when the damage is small, Ratcliffe proposed a gapped smoothing method that established a localized cubic polynomial curve to fit each segment of the curvature mode shape and calculate the difference between the fitted curve and the curvature that reflected damage. This method was successfully applied in detecting damage of a steel beam with a slot cut and was also used to localize the delamination in a composite beam [40].

Curvature mode shapes have been recognized by many researchers as being very sensitive to damage. Although this sensitivity can be further amplified by the wavelet transform [41, 42], the accuracy of the measurement of the vibration mode data is the factor that restricts the practical application of this kind of methods.

Unlike the curvature mode shape, MSE is a response used to compare differences between elements. MSE was first used by Stubbs and Kim [43] and Stubbs, et al. [44] to detect damage in beam-like structures. The basic assumption of this method is that the damage is primarily located at a single sub-region, then the fractional strain energy (MSE of an element over MSE of a whole mode) of other parts will remain relatively constant before and after damage. Cornwell, et al. [45] extended this method to plate-like structures. In all of these applications, MSE was obtained by integrating the square of curvature and the measurements of the intact structure are required for comparison. Li, et al. [46] proposed an improved modal strain energy method, which took the influence of frequency into consideration, to detect damage in offshore platform structures.

Another way of calculating MSE is based on the mode shape and element stiffness matrix. Obviously, an FE model is required before the calculation. The MSE based methods can also be easily applied to truss and frame type structures, which is an advantage that the curvature-based methods do not have. Shi et al. [47-49] directly utilized the change ratio of MSE of each element to localize damage. Some MSE based damage quantification methods were also proposed in these papers but they are not as accurate as the MSE based localization methods. In some papers, it was preferred to use another response to quantify the damage. For example, Law, et al. [50] used MSE change to detect the damage location with incomplete measurements and estimated the severity of damage based on the sensitivity of natural frequency. Moradipour et al. [51, 52] made some improvements to the calculation formula of MSE for damage identification.

2.2.5 Frequency response function (FRF)

FRF can be measured directly in vibration tests, from which modal parameters can be extracted. Therefore, the FRF has the advantage of no extraction error and contains

more vibration information, and is also used by researchers in damage identification methods. Wang, et al. [53] proposed an algorithm based on the perturbation equation of FRF data to determine a damage vector indicating the location and magnitude of the damage of a plane 3-bay frame structure. Owolabi, et al. [54] used the first few natural frequencies and their corresponding FRF amplitudes to identify crack damage in aluminium beams. Sampaio and Maia [55] utilized the frequency domain assurance criterion and the response vector assurance criterion to build the damage indicator reflecting the location and relative severity of the damage.

Similar to the mode shape curvature, the FRF curvatures at the specified frequency before and after damage can also be used to locate damage directly. It was recommended by Sampaio, et al. [56] that the selected range of the frequencies should better be lower than the first resonance or anti-resonance. In Maia, et al. [57]'s work, a detailed comparison of the damage identification performance of different damage indices formed by FRF shape, FRF shape slope, FRF shape curvature as well as mode shape, mode shape slope, mode shape curvature was provided. It was concluded that the FRF based methods perform better and the false alarm problem should be given special attention.

2.3 Model updating methods

In dynamic analysis, the initial FE model of a structure usually predicts a different response from the experimental data. The errors listed below are the typical reasons for this discrepancy:

- Model simplification errors, which may be caused by the difficulty of modelling joints, boundary conditions, nonlinearity and damping.
- Model parameter errors, which may be caused by the uneven distribution of structural material properties, measurement errors of dimensional parameters and unknown damage.
- Model order and structure discretization errors.

Due to the above errors, it is necessary to modify the FE model before it is put into use.

Model updating theory has been widely studied and applied in different engineering fields such as aerospace, mechanical and civil engineering in the past few decades, and has been successful.

In this section, the literature on model updating methods is reviewed. These publications are mainly divided into five categories based on different solution strategies and a brief summary of these categories is provided in Figure 2-1. The measurement data used in these methods are the various dynamic responses previously discussed, and the problems addressed tend to be in the field of damage identification. It should be pointed out that the role of model updating is to find an optimal solution that minimizes the discrepancy between the theoretical predictions and the test data, and the outcome of damage identification depends on the sensitivity of the response itself.

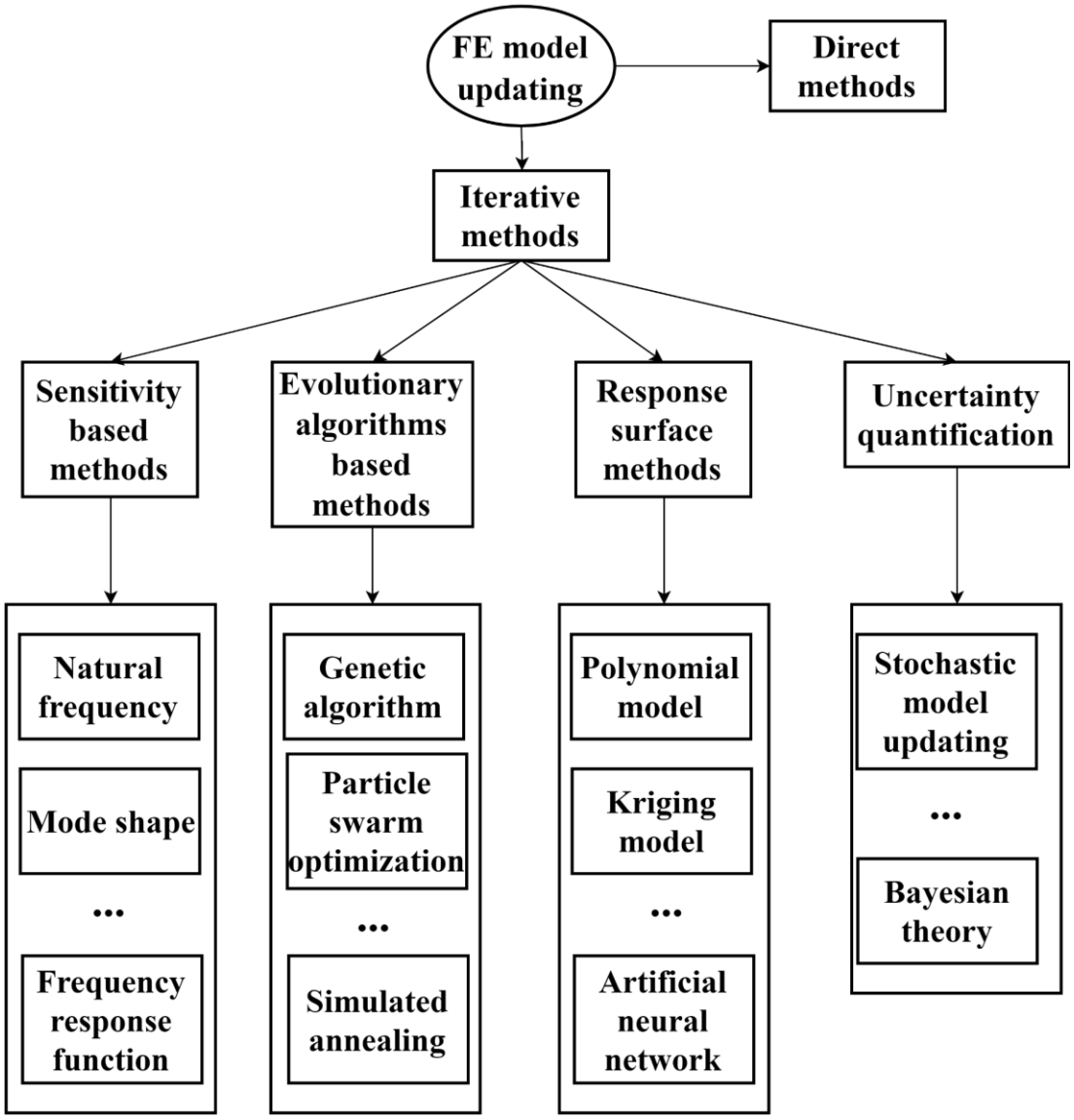

Figure 2-1 Classification of model updating methods.

2.3.1 Direct methods

The earliest model updating methods focus on modify the matrix of the dynamic system (mass matrix, stiffness matrix, and sometimes damping matrix) to make the predicted numerical results match the experimental results. Such methods are referred to as the direct methods. By assuming that the mass matrix is known in advance, Baruch [58] derived formulas to get the optimally corrected stiffness matrix and the optimally corrected flexibility matrix. Baruch [59] also utilized the stiffness matrix as the reference basis, which was updated by the static tests, to modify the measured mode shapes and the mass matrix. In Wei [60]'s work, the mass and stiffness matrices

were corrected together by the Lagrange multiplier technique. Friswell, et al. [61] presented an approach to minimize the difference in damping and stiffness matrices.

These methods are mostly based on the special relationships between these matrices, such as the eigenvalue equation and the orthogonality constraints, to construct mathematical expressions of the updated results. Although the mathematical expressions of the formulas are very complicated, the calculation is very simple, and the corrected theoretical response is very close to the measured data.

However, the updating process of the direct method does not consider maintaining the physical meaning inside those matrices. The modified mass or stiffness matrix is often polluted and no longer has characteristics such as symmetrical and sparsity. This will cause the updated theoretical model to lose its original physical meaning. The modified model can only provide theoretical responses that are close to the test results. It can neither predict the unmeasured data effectively nor link the changes of the matrix before and after the correction with the changes of the physical parameters of the structure. Therefore, the direct method has gradually been abandoned by scholars.

In order to overcome the above shortcomings of the direct method, it has been found that it is more reasonable to update the structural physical parameters rather than the matrices, and the model updating problem can be solved by iterative methods, which will be introduced in the following sections.

2.3.2 Sensitivity based model updating methods

A complete FE model updating program contains the following steps, which are detailed by Friswell and Mottershead [62].

1. Construct the FE model.
2. Vibration testing, including choosing the response used.
3. Comparing numerical results with test results, dealing with the incomplete measurements.
4. Parameter selection for model updating.
5. Estimation techniques/Model updating methods

The sensitivity-based methods are a kind of early, classic and mature iterative model updating method. The method is based on linearizing the relationship between the response of the FE model and the updated parameters to construct a sensitivity matrix. Typically, a Taylor expansion describing the relationship is used, and the sensitivity matrix is equal to the linear portion of the expansion.

Model updating is essentially an optimization problem that pursues the minimization of residuals between theoretical response and experimental data. The sensitivity-based method is a solution similar to the method of steepest descent. Usually, it uses the sensitivity matrix to construct the linear relationship between the modified parameters and the response residuals, acquires the best solution at current iteration by the least-squares method, and then obtains the optimal solution of the updating parameters through multiple iterations by the least-squares method. According to the types of the responses used, sensitivity methods can be roughly classified into modal data-based methods and FRF based methods.

(1) Modal data-based methods

Modal data refers to natural frequencies, mode shapes and damping, which have been introduced in Section 2.2. Generally, in model updating, the material properties of structural elements or substructures, such as Young's modulus, are selected as updating parameters. In order to obtain the sensitivity matrix, the first derivative of the modal data to these parameters needs to be calculated. One well-known method was proposed by Fox and Kapoor [63], which calculated the change rate of eigenvalues and eigenvectors of the undamped system. Some other derivative calculation methods have also been proposed to consider damping and to seek high computational efficiency, etc. [63-67].

Mottershead, et al. [6] conducted a comprehensive and systematic discussion of sensitivity-based model updating methods and demonstrated their application to a baseline Lynx helicopter. That work also included the use of special updating parameters like offset nodes and generic elements. Gorl and Link [68] updated a theoretical model based on experimental data of intact and damaged models, respectively. Then the damage parameters of the benchmark steel frame were extracted.

Sarvi, et al. [69] showed the performance of using an enhanced Levenberg-Marquardt algorithm, designed for the nonlinear least square problem in the updating process. Moaveni, et al. [70] applied model updating to detect damage in a masonry infilled RC frame. The RC frame was tested on a shake table and the damage was induced by applying simulated earthquake excitation based on the historical records. Finally, the progressive damage can be successfully identified based on the natural frequency and mode shape measurements obtained between each earthquake simulation.

A basic assumption in the sensitivity-based method is that the optimal solution obtained from the experimental data should be near the initial value of the theoretical model parameters. Therefore, on the one hand, it should be checked whether the FE modelling is accurate and whether the experimental data is close to the theoretical data before the updating to ensure that the solution does not converge to a certain local extremum. On the other hand, in each iteration, the step size of the parameter change should be controlled to pursue the shortest optimal solution. This is mainly achieved by a regularization method, which was demonstrated in detail in reference [6]. For the development and application of the regularization method itself, references [71-75] are recommended.

(2) FRF data-based methods

As mentioned above, FRF data contains abundant information and no extraction error, which can be easily used to construct a set of overdetermined equations in sensitivity based methods. Since the theoretical FRF value is obtained from the transfer function whose first derivative is not easy to calculate, the sensitivity matrix of the FRFs is usually calculated by both the theoretical and experimental FRFs. Imregun, et al. [76] showed a classic version of the formula derivation about the sensitivity matrix. In this formula, At least one full column of FRF data must be used to calculate the sensitivity of the correction parameters to the residuals of each FRF data and theoretical values in that column. To deal with the incomplete measurements, Imregun suggested to directly replace the unmeasured responses by their analytical values. The dynamic reduction method [62] can also be applied to achieve the reduction of the FE model or the expansion of the experimental data. Gang, et al. [77] introduced the pseudo master

degrees of freedom (DoFs) when only FRF is measured at only a few of DoFs to improve convergence.

If there is a special need that the whole FRF matrix measurement should be used in the updating, Esfandiari, et al. [78] suggested using the decomposed form of the FRF matrix by the mode shapes and natural frequencies to calculate the measured FRF matrix. Obviously, in this way, the FRF data will be polluted by extraction errors. But the number of available data will increase as the mode shapes of the damaged structure can be replaced by those of the analytical model to some extends. There is a balance between the number of data and the extraction errors when considering which formula of the FRF sensitivity is more suitable for solving different problems. Esfandiari [79] also proposed a new model updating method using the frequency domain strain data which was calculated by the mode shape strain measurements based on a similar formula.

In the frequency domain, theoretical FRF data may change dramatically with the updating parameter change, especially the FRFs near a natural frequency. Thus, it is not wise to calculate the residual between the theoretical and experimental FRF data at the same frequency, as some residuals may be much bigger than others which may amplify the test and modelling errors and the level of the ill-conditioning of the sensitivity matrix. In modal data-based methods, MAC values are used to select a matching modal shape. Similarly, Pascual et al. [80, 81] proposed the frequency domain assurance criterion (FDAC) to match the corresponding theoretical FRF column to the measured FRF column. The sensitivity equation was changed to consider a frequency shift between theoretical and experimental FRFs. Asma and Bouazzouni [82] presented a method which selected the frequency of theoretical FRF by searching the shortest distance between the theoretical and experimental FRF points, which also showed good convergence performance. Besides the theoretical FRF frequencies, the selection of the frequencies of measured FRFs is also important. Usually, it is not recommended to use the frequencies near the resonance or anti-resonance points as the FRFs may be highly influenced by the test errors and damping (unless damping is the study target). Kwon and Lin [83] proposed a frequency selection method to ensure the measure FRF used did not contain similar information and some special indices were defined to evaluate the degree of ill-conditioning of the sensitivity matrix.

D'Ambrogio and Fregolent [84] provided suggestions about how to select experimental DoFs and the experimental FRF data in certain frequencies to reduce the ill-conditioning problem.

D'Ambrogio and Fregolent [85] proposed an anti-resonance based model updating method, which was another way of utilizing FRF data. Lin and Zhu [86] derived formulas for using measured response function data under base excitation to do model updating. To take the influence of damping into account, Pradhan and Modak [87] put forward a normal response function method using complex FRFs, which performed well when it was applied in viscously and structurally damped systems. In Garcia-Palencia and Santini-Bell [88]'s work, the updating of the damping matrix was done as a second step separately from the mass and stiffness matrix, and the measured FRFs at resonance were specifically used to update the damping ratios. Arras and Coppotelli [89] presented an enhanced formulation for the FRF based method whose residual vector was defined upon the correlation functions.

The iterative method can maintain the physical meaning of the parameters before and after the updating, making such methods have high practical application value. Sensitivity based method is a subclass of the iterative method. It is especially good at solving the problems with a large number of updating parameters. The other branches of the iterative method will be introduced in later chapters.

2.3.3 Evolutionary algorithms based model updating method

Based on the fact that the essence of FE model updating is an optimization problem which seeks to minimize the residual between theoretical prediction and actual measurement data, it can be naturally associated with the use of methods other than sensitivity method to solve it, which leads to the introduction of computational intelligence methods including different kinds of evolutionary algorithms. Two systematic introductions and reviews of the model updating methods using computational intelligence were provided by Marwala [90] and Alkayem, et al. [7].

Evolutionary algorithms can be regarded as very effective mathematical tools for solving optimization problems. They are population-based optimization algorithms that ultimately identify optimal solutions through a wide range of searches and

comparisons. They have the advantages of not calculating the gradient of the objective function, not relying on the position of the initial point, and not easily converging on the local solution in the solution process, which makes them very good at solving complex and highly nonlinear optimization problems.

In model updating, evolution algorithms should be applied after both the updating parameters and the objective functions are designed. Under normal circumstances, these algorithms will directly give updated results. Such methods are primarily classified by the type of evolutionary algorithms used.

(1) Genetic algorithm (GA)

GA originated from computer simulation studies of biological systems. It is a random global search and optimization method that mimics the evolutionary mechanism of biological evolution in nature [91].

Akula and Ganguli [92] applied GA for model updating of a helicopter rotor blade based on natural frequencies. Almeida and Awruch [93] used GA based model updating method to obtain the optimal designs of composite laminated structures under different force conditions. Canyurt, et al. [94] developed a laser welding strength model using GA to evaluate the strength of the welding strength based on wire type, shielding gas, laser energy, etc. In Marwala [95]'s work, the objective function was constructed based on the information extracted from the FRF data by wavelet transform. GA was used to get the results which showed that the wavelet data performed better than directly used FRF data. Perera and Ruiz [96] proposed a 2-steps damage identification method using GA for large-scale structures. The position of the first damage was roughly estimated by using the damage function. Then, a multiobjective function was defined to identify the damage.

(2) Particle swarm optimization (PSO)

PSO is an evolutionary algorithm inspired by simulating bird predation behaviour. This method was developed by Kennedy and Eberhart [97].

Lin, et al. [98] applied PSO to estimate parameters of nonlinear dynamic rational filters. Kathiravan and Ganguli [99] used PSO to design the best ply angles of a composite box-beam structure which could be used as the main load-carrying members of helicopter rotor blades. It was found that the PSO could provide globally best designs. Seyedpoor [100] proposed a two-stage damage detection method in which PSO was used in the second stage to evaluate the extent of the damage based on mode shape measurements. In Liu, et al. [101]'s work, PSO was used in the parameter identification problem of permanent magnet synchronous motors. Perez and Behdinan [102] improved the basic PSO for constrained structural optimization problems. Hassan, et al. [103] provided a comparison between the PSO and GA, and found that both methods could give high quality solutions and their difference was PSO had a higher computational efficiency dealing with unconstrained nonlinear problems while GA performed better when applied to constrained nonlinear problems.

(3) Simulated annealing (SA)

Simulated annealing is a probabilistic algorithm used to find approximately optimal solutions in a large search space in a certain time, which was proposed by Kirkpatrick, et al. [104]. It is often used when the search space is discrete.

McGookin and Murray-Smith [105] applied SA to optimize the nonlinear controllers of submarine manoeuvring. In that work, the SA's global search performance was not as good as GA. Pedamallu and Ozdamar [106] proposed a hybrid SA method to solve a general constrained optimization problem. Levin and Lieven [107] recommended a special version of SA which was the most effective of all the versions for model updating purposes. They also concluded that the choice of updating parameters was of paramount importance.

Other evolutionary algorithms such as tug-of-war optimization [108] and cyclical parthenogenesis algorithm [109] were also used in model updating and damage identification. With the development of the evolutionary algorithm itself, new methods will be proposed constantly. Most of them can give good optimization results, only with different computing efficiency for different problems.

Since there is no need to calculate sensitivity, many dynamic characteristics such as MAC that are difficult to be utilized in the sensitivity-based method can be directly added to the objective function to be solved by an evolutionary algorithm [110]. This helps researchers to directly find the most effective responses and parameters for model updating. The main disadvantage of the evolutionary algorithm is the efficiency problem, especially when the FE software needs to be called for the theoretical response calculation. The solution to this problem will be covered in the next section.

2.3.4 Response surface-based methods

The response surface, also known as the meta-model or surrogate model, was first developed as an experimental design method and has been gradually applied to other engineering fields. Myers [111] summarizes the research results of the method in the initial development stage. Rutherford, et al. [112] introduced and compared some of the new response surface construction methods, updating methods and sampling methods at that time.

The main role of the response surface method is to use explicit mathematical tools to represent the relationship between the input and output of a system. For structures that need to be modelled with FE software, the FE model itself may be complicated, but some responses, such as frequencies and MAC, may vary smoothly and gently with the change of updating parameters. If an accurate mathematical model can be constructed to reflect the relationship between them, the mathematical model can be used instead of the FE software to calculate the response in the updating process. In this way, the problem can be easily solved by the artificial intelligence method, and the time consumption of the calculation process is greatly reduced.

Of course, the premise of the response surface method is that the number of updating parameters is small, otherwise the difficulty of constructing a response surface will be greatly increased. Nevertheless, the practicability of response surface methodology is still obvious, and it is a relatively new methodology in the field of model updating.

In the response surface method, the polynomial model is a very common mathematical tool used to construct the mapping between input and output. Fang and Perera [113]

presented a response surface-based model updating method using the second-order polynomial model. In this work, the complete construction flow of the response surface was demonstrated, including mathematical tool selection, sampling design, output feature selection, and model accuracy checking. Natural frequencies were used to identify damage and a multi-objective optimization algorithm provided by Matlab was used to solve the optimization problem. 3 cases were used to verify this method including the data from the I-40 bridge. Deng and Cai [2] applied a similar method to update an existing bridge.

Ren and Chen [114] used two special indicators together with the mean square value to check the accuracy of the response surface. Fang and Perera [8] introduced D-optimal design to reduce the number of samples used for response surface fitting and improving efficiency. Chakraborty and Sen [115] utilized the moving least-squares method to calculate the coefficients of the response surface which was good at capturing the nonlinearity and the local variations. This method added weighting to each sampling point, which tried to predict a response mainly using the sampling points near it. However, this method required a response surface to be reconstructed each time a response was predicted, which increased the computational burden.

Besides the polynomial model, there are also other mathematical tools to build the surrogate model, such as radial basis function, Kriging model and support vector regression [116]. Zhou, et al. [117] utilized the radial basis function to construct the response surface and applied modal updating on a 1/40 scale model of a cable-stayed bridge. Wan and Ren [118] used the Gaussian process model to build the meta-model of the residuals for model updating.

The principle of the Gaussian process is very similar to that of Kriging, which is popular in many fields due to its superior nonlinear fitting characteristics. Gao, et al. [119] applied the Kriging model to identify a single arbitrary crack for plate-like structures. The locations of the crack tips were selected as updating parameters and the stochastic particle swarm optimization algorithm was used to solve the optimization problem. The result showed that the crack can be determined by initial samples of fewer than 200. Liu, et al. [120] combined the Kriging model and the component mode

synthesis to update a 1 /10 scaled arch bridge model. Wang, et al. [4] constructed a Kriging model of the acceleration frequency response functions in the model updating of the composite structure of a honeycomb sandwich beam. Yin, et al. [121] applied Kriging model for model updating of a truss structure by FRF data. Joy, et al. [122] implemented a Kriging model for delamination prediction in composite structures based on frequencies and mode shapes. Xie, et al. [123] constructed a Kriging model between frequencies and crack depths for multiple cracks identification in beam structures. Lu, et al. [124] improved the Kriging model by adding a quadratic polynomial term in the original formula. The new surrogate model had higher accuracy in the dynamic probabilistic analysis of an aeroengine compressor blisk. One of the main advantages of using the Kriging model to construct a response surface is that it can estimate the degree of error of the predicted response and allows new sampling point to be filled at the location of the point where the error is large to reconstruct the Kriging model with smaller error near certain areas. Jin and Jung [110] illustrated how to apply this 'sequential surrogate modelling' based on validation samples to do model updating.

In addition to constructing a surrogate model with updating parameters as input and dynamic responses as output to assist in computation, it is also a feasible idea to directly construct a mathematical model with the dynamic responses as the input and the updating parameters as the output. In this way, inputting the measured responses into the constructed model can directly obtain the updated result to determine the location and extent of the damage, and the optimization process is no longer needed.

This kind of methods can be referred to as machine learning-based methods, and some successful applications are as follows. Zapico, et al. [125] applied the neural network technique to update a steel frame using natural frequencies. Zhu and Zhang [126] utilized the least squares support vector machines to construct the mapping between the natural frequencies and the designed parameters in the updating of GARTEUR aircraft model. Marcy, et al. [127] used the artificial neural network to localize damage in beams using measured mode shape data.

2.3.5 Uncertainty quantification in model updating

In the practical application of model updating, the updating result will inevitably be affected by errors, such as measurement error and assembly error. Although some robust methods can still obtain relatively accurate results, the fact is that the updating results obtained in different situations will be different. In very difficult cases, it is easy to make a misjudgement. This uncertainty introduced by various errors leads researchers to study the problem of model updating from the statistical point of view.

The model updating method for quantitative analysis of uncertainty is a very recent research endeavour. A statistical model such as a probability density function can be used to model the uncertainty of the updating parameters. Then, the statistical features of the model can be passed to the probability description of the response of the FE model, which is usually done by the Monte Carlo technique. Finally, the parameters are updated based on the actually measured response distribution. The advantage of this kind of methods is that not only the updating results of the parameters but also the confidence evaluation of the results can be given. A framework for this confidence assessment was presented by A Hanson and Hemez [128].

Mares et al. [129, 130] developed a stochastic model updating method to determine the means and standard deviations of the updating parameters by making the simulated data cloud converge upon the measured data cloud. This method was then applied to a set of benchmark structures connected by spot welds. Mares, et al. [131] also adopted the Bayesian analysis to solve a similar problem. Fonseca, et al. [132] identified the uncertainty of the position of a lumped mass on a cantilever beam using the maximum likelihood method. Khodaparast, et al. [133] proposed a new perturbation method to simulate the propagation of uncertainties.

In Andriosopoulou, et al. [134]’s work, a lab-scale composite aerostructure was clamped at one end (bolted connection) and the damage scenarios were designed as the reduction in the tightening torque of the clamped end. Many experiments measuring FRF data were performed with assembly-induced uncertainty. It can be clearly seen that when all the data was drawn in one picture, the test data for the minor damage case was almost covered by the healthy case. Therefore, it was difficult to

obtain convincing results using deterministic damage detection methods. However, in the analysis of uncertainty, such as the multiple model based method and the principal component analysis based method used in the paper, those minor damage cases could be clearly distinguished from the healthy state.

The model updating method of uncertainty quantification involves a wide range of topics, and only a part of them is described in this section. To have a more comprehensive understanding of this topic, readers can refer to the literature review written by Simoen, et al. [135].

2.4 Weld joint modelling

The form of welding is essentially the atomic-level interdiffusion between the materials being joined. Metals, glasses and thermoplastic polymers can all be joined by welding under the combined action of heat and pressure. So far, a great number of welding processes has been invented and applied in industrial equipment production. Some of them which are commonly used such as gas welding, arc welding, resistance welding and friction welding, were described in detail by Messler [136]. Besides, Hughes [137] showed what a welding inspector should do to check and ensure the quality of a welding product.

Except for basic knowledge of welding process, much research on different aspects of the weld has been completed. Firstly, the modelling and control of the welding process are concerned. Neto and Neto [138] presented a literature review on friction stir welding modelling. By fine-tuning of some process and material parameters, the welding process could become more reliable. Shen and Chen [139] developed a shell and solid combined model to simulate the temperature history and distribution, welding distortion and residual stress after the welding process, which was less time-consuming compared with a solid model.

FE modelling and simulation of the structure after welding is also of great interest. To study the residual stresses and distortions induced by the T- joint welding of two plates, Peric, et al. [140] used a shell/three-dimensional modelling technique to improve the

computational efficiency and accuracy of FE analysis. Nadimi, et al. [141] investigated residual stress problems, whose object was the butt welding of two dissimilar pipes. Nuruzzaman, et al. [142] adopted the notch stress approach for weld joint modelling to predict stress distribution. Al-Samhan and Darwish [143] worked on predicting the strength of weld-bonded joints with different welding forms.

As welding joints often become areas of high-stress concentration, different kinds of failure must be studied and considered in the design process. Fang, et al. [144] introduced the Kriging model to optimize the spot weld to find locations of spot-welded joints with maximum fatigue life. Matos and Dodds [145] applied the Weibull stress model to study the nonlinear fracture behaviour of welded steel frames. Song, et al. [146] studied numerically the magnification factors for semi-elliptical cracks numerically on the weld root of a T-butt joint. Hu, et al. [147] proposed a method for crack damage identification of welded steel structures by the propagation of Lamb waves.

One purpose of this research is to use reliable solder joint modelling to properly reflect the dynamic characteristics of the structure, paving the way for subsequent damage identification. A recent literature review on this aspect was provided by Zahari, et al. [148]. Within this topic, the study on spot welding has been quite mature. Xu and Deng [149] proposed several types of simplified FE models for spot-welded joints. The stiffness of the joint of these models was compared with that of converged three-dimensional FE models when the joint is subjected to different forces. Additionally, as a widely used commercial software, Nastran provides CWELD element which was specially designed for spot weld modelling[150]. The theory behind this element was given in reference [151]. Based on this element, Husain, et al. [152] and Abdul Rani, et al. [153] applied FE modelling and updating on laser spot weld joints in a top-hat structure. Abu Husain, et al. also successfully performed damage identification [154] and uncertainty analysis [155], based on the model updating method, on that kind of structure.

As a comparison, research about modelling and model updating of a seam-welded joint has more potential to explore. Zeng, et al. [156] used the so-called local equivalent

welding element to predict the welding deformation of a plate-type structure. Chee and Bakar [157] simulated a simple T-joint structure by different element types and compared their natural frequency and mode shape predictions with the measured data. Similar work was done by Rahman, et al. [158] on a stiffened plate. Garifullin, et al. [159] used a surrogate model to optimize the initial rotational stiffness of welded tubular joints with fillet welds. These methods were successful in their own field. But it is better to find a common way that model the connection of the two welded parts easily and the parameters of the connection part can be adjusted for model updating which would make dynamic response predictions more accurately.

For the case of a welded frame, Horton, et al. [160, 161] and Ahmadian, et al. [162] used partly rigid beam elements to connect beams and the lengths of the rigid parts was taken as updating parameters. When it comes to plates connected by seam welds, also with the help of FE analysis software Nastran, Zahari, et al. [163, 164] used rigid body element type 2 (RBE2) to model friction stir welding joint. Van Belle, et al. [165] compared the measurements and simulations of joined panels considering different joining techniques, whose model for seam weld connection was also RBE2. The shortcoming of their model is that the RBE2 element is rigid and nonadjustable. So they had to choose parameters of the two plates to update and no improvement can be made to the weld connection itself.

2.5 Conclusions

In this chapter, publications on the development of dynamic response based damage identification methods, model updating methods and the modelling methods of welded structures are reviewed. Readers can get a basic understanding of the advantages and shortcomings of these methods, especially the response surface method, MSE and weld joint modelling, which provide motivations for the research work of this thesis.

Chapter 3 – Experimental test conditions

3.1 Introduction

Experimental testing is an important part of this research. No matter how noise is introduced into the theoretical simulation, there is a gap between the theoretical simulation and the experimental data. Therefore, only the method that verified by the test data is convincing. The experimental data used in this thesis is tested in the laboratory environment, where the input and output measurements are both available. After the test signal is transmitted through the sensor, the experimental modal analysis (EMA) is used to obtain the frequency, mode shape and frequency response function data of the test structure.

In this chapter, the basic principles of vibration testing techniques (on the aspect of EMA) and the experimental equipment used are introduced. And an example is given to illustrate the acquisition of experimental data in detail.

3.2 Experimental modal analysis

Most structures can be made to resonate under certain conditions. Resonance usually appears as excessive and sustained motion, which can be generated by excitation at a specific frequency. Modal properties (natural frequency, mode shape and damping) are used to describe such dynamic characteristics, which are inherent properties of a structure. They are only related to the material properties and boundary conditions of the structure and do not depend on the applied external forces. EMA is a method of obtaining modal information of structures through experimental tests and has been extensively developed and widely used in the past few decades [166].

In the early days, modal testing was done by applying a sinusoidal excitation to a structure. Later, thanks to the fast Fourier transform (FFT) algorithm and the use of digital computers, the basic framework of EMA was built, which can be mainly divided into two steps:

- FRF measurements obtained by structural test and FFT.
- Modal features extracted by curving fitting.

Impact testing is a convenient, fast and low-cost way to find patterns in structures. It was developed in the 1970s and became a very popular modal test method to estimate the modal properties of structures. Its process is demonstrated here to show the theoretical details of EMA.

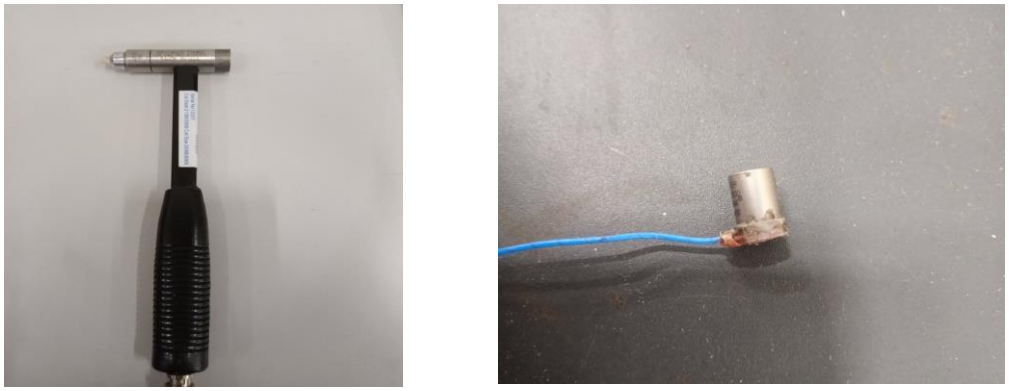

(a) (b)

Figure 3-1 Impact test tools: (a) Hammer; (b) Accelerometer.

The measurement tools required to perform an impact test are a hammer and accelerometers as shown in Figure 3-1. By the sensors in these tools, the time-domain signals of the force and response of an effective knock on the structure can be recorded and then converted into the frequency domain signals of the input and output by the FFT analyzer. After that, the frequency response function representing the input-output relationship between the two points of the structure can be obtained whose basic formula is

$$H(\omega) = \frac{F(\omega)}{X(\omega)} \tag{3.1}$$

where $H(\omega)$ is the frequency response function, $F(\omega)$ is the output function in the frequency domain, $X(\omega)$ is the input function in the frequency domain, ω is the frequency variable.

The physical meaning of FRF is the response of an output point of a structure under the unit force excitation of a specific frequency. In actual tests, the results are usually

obtained by means of multiple measurements. According to the different effects of noise sources, there are many averaging options to choose. The most common formulas are as follows

$$H(\omega) = \frac{\overline{S_{F,X}(\omega)}}{\overline{S_{X,X}(\omega)}} \tag{3.2}$$

where $\overline{S_{F,X}(\omega)}$ is the averaged cross power spectrum between the input and output, $S_{X,X}(\omega)$ is the averaged auto power spectrum of the input.

The FRF measurement contains the vibration information of the structure in a selected bandwidth frequency domain. The next step is to extract the modal information of the structure. Obviously, when the structure is in resonance, its FRF curve will reach a local peak. The frequency point at this time is the natural frequency. The FRF peak of each measurement point is used as the vibration mode shape, and the width of the resonance peak can be used to estimate the damping.

In vibration test systems, there are usually built-in programs that can directly provide modal information based on FRF measurements. This is done primarily by curve fitting, which approximates the experimental data curve by mathematical expressions containing specific parameters.

When an elastic structure is vibrated by an external force, its linear vibration can be described as

$$\mathbf{M}\ddot{\mathbf{x}}(t) + \mathbf{C}\dot{\mathbf{x}}(t) + \mathbf{K}\mathbf{x}(t) = \mathbf{f}(t) \tag{3.3}$$

where $\mathbf{M}$, $\mathbf{C}$ and $\mathbf{K}$ are the mass, damping and stiffness matrices, respectively. $\mathbf{x}(t)$ and $\mathbf{f}(t)$ are the displacement and force vectors at time *t*.

Equation (3.3) works in the time domain, which can be transformed into the frequency domain by Fourier transforms

$$\begin{aligned} \mathbf{X}(\omega) &= \mathbf{H}(\omega)\mathbf{F}(\omega) \\ \mathbf{H}(\omega) &= \left[-\mathbf{M}\omega^2 + \mathrm{i}\mathbf{C}\omega + \mathbf{K} \right]^{-1} \end{aligned} \tag{3.4}$$

where $\mathbf{X}(\omega)$ and $\mathbf{F}(\omega)$ are vectors of Fourier transforms of displacement responses and external forces at frequency ω, respectively. $\mathbf{H}(\omega)$ is the FRF matrix representing

displacement per unit harmonic force which is also called receptance, i denotes the imaginary unit. Equation (3.4) provides a theoretical way to predict the FRF of a structure. Usually, the mass, stiffness and damping matrices of the structure are obtained by the FE method, and the positions of the impact and accelerometers in the actual measurement should be arranged on the nodes of the FE mesh. Note that the theoretical prediction of the FRF at a particular location is affected by the mesh distribution but the measured data is independent of the mesh.

Here, it is assumed that the viscous damping model is used in the equation of motion of the structure. After omitting some intermediate derivation, the theoretical value of FRF (the receptance matrix element) can be estimated by the following expression using modal parameters as variables [167].

$$H_{ij}(\omega) = \sum_{r=1}^{n} \left(\frac{\varphi_{ir}\varphi_{jr}}{\mathrm{i}\omega - s_r} + \frac{\varphi_{ir}^{*}\varphi_{jr}^{*}}{\mathrm{i}\omega - s_r^{*}} \right) \qquad (3.5)$$

$$s_r = -\omega_r \xi_r + \mathrm{i}\omega_r \sqrt{1-\xi_r^2}$$

where $H_{ij}(\omega)$ is the *ij*-th entry of the FRF matrix at frequency ω, s_r is the complex pole of the *r*th mode, φ_{ir} and φ_{jr} are entries of the mass-normalised mode shape vector of the *r*th mode, ω_r is the frequency of the *r*th mode of the system without damping, * denotes complex conjugate; *n* is the number of DoFs of the system. ξ_r is the modal damping ratio for mode *r*, which can be estimated directly by the experiment or be further simplified by applying proportional damping assumption which defines the viscous damping matrix is a linear combination of the stiffness and mass matrix as

$$\mathbf{C} = \alpha\mathbf{K} + \beta\mathbf{M} \qquad (3.6)$$

where α and β are constants. Then, the ξ_r can be calculated by

$$\xi_r = \frac{\beta}{2\omega_r} + \frac{\alpha\omega_r}{2} \qquad (3.7)$$

In this way, only two parameters need to be determined to reflect the damping property of the structure.

Equation (3.5) shows a way to construct an FRF curve (one entry of the FRF matrix with frequency) from modal parameters. The actual values of those modal parameters can be determined by performing an effective curve fitting of the measured FRF curves.

It can be seen from the equation that when the excitation frequency of the structure is equal to a certain natural frequency, the FRF matrix will be mainly affected by the corresponding mode shape. At this point, every row or column of the FRF matrix will be approximately that mode shape. This allows a researcher to measure only one row or column of the FRF matrix to obtain all the required modal information, which significantly reduces the effort of modal testing.

Actual modal feature extraction algorithms tend to consider more factors, such as the influences of the out-of-band modes and to process multi-input-multi-output measurements. These methods are also constantly evolving for greater precision and stability. A well-known estimation method called PolyMAX is used in the LMS test system and was described in detail in [168].

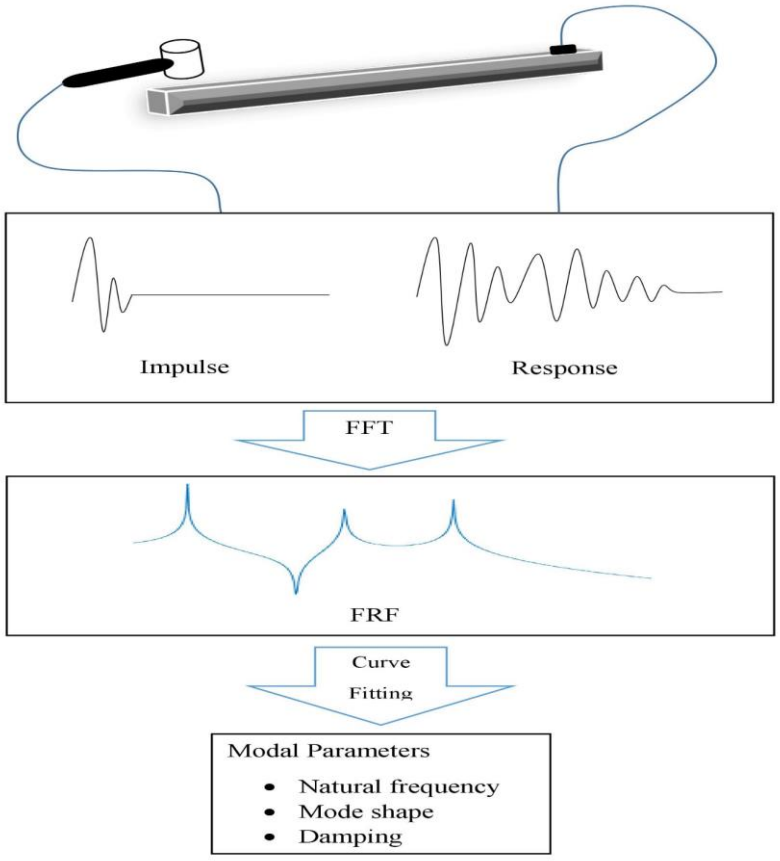

Figure 3-2 EMA through impact test.

So far, the general flow of the EMA through the impact test has been introduced as shown in Figure 3-2. In a specific experiment, there are also other steps, such as

selecting appropriate window functions, setting sampling frequency, and assessing the quality of test results by coherence. In addition, the experimenter's experience is also an important factor in getting good test results. Impact testing is a mature EMA method, and a more complete description can be found in references [169, 170]. This type of experiment is usually performed in the laboratory to reduce the interference of unmeasured external forces.

Figure 3-3 Shaker.

The test tools used in this research are not the hammer and accelerometer previously described. For external impact and measurement, in most cases the hammer is replaced by a shaker as shown in Figure 3-3. A Shaker is also a widely used test tool. It can provide a continuous external force excitation in a specific frequency bandwidth, which is usually controlled by the signal processing system, making the interested mode more possible to be excited. The test signal of a shaker-excited structure is stationary and continuous, which makes the test data more accurate. A shaker is usually connected to a specific location on a structure. This ensures that the position of the input force does not change. However, when using sensors to measure the response, a large number of sensors or manual adjusting the position of the sensors is required to obtain a complete set of test data, which brings certain inconvenience.

For the response measurement in this study, accelerometers are replaced by a scanning laser vibrometer, which is described in the next section.

3.3 Scanning laser vibrometer

In addition to classical impact testing, there are other testing tools that can be used in EMA. PSV-500 scanning laser vibrometer (SLV) is a modern vibration testing equipment, which is used to obtain experimental data in this study. In this section, the device layout, testing methods, advantages and disadvantages of the equipment are described in detail, and a specific test example is provided for demonstration.

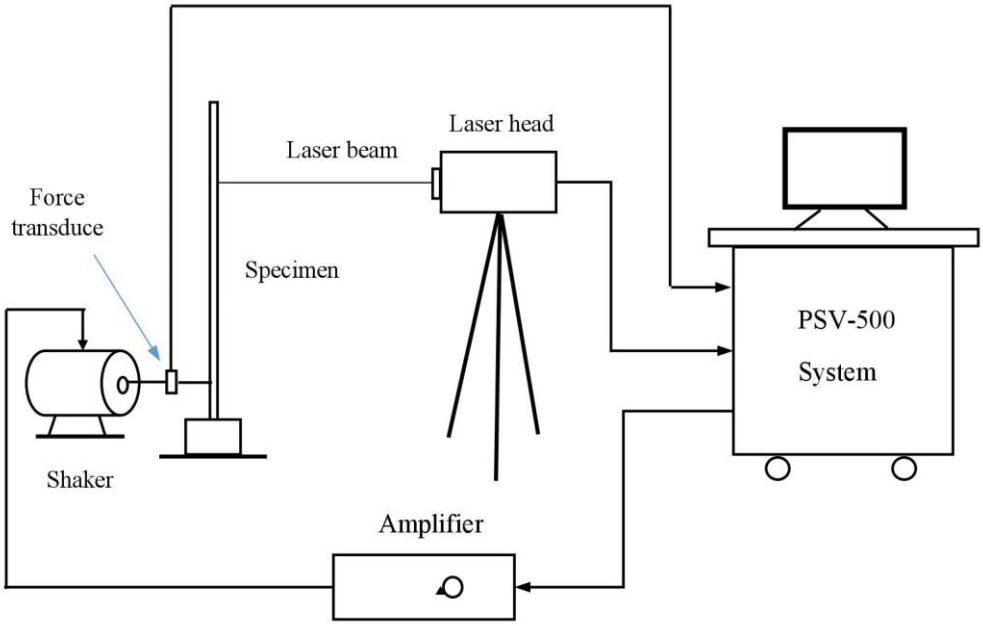

Figure 3-4 Schematic of the experimental set-up.

As shown in Figure 3-4, the entire experimental setup contains the following components.

- A laser head emits laser light to the surface of a specimen and utilizes the Doppler shift phenomenon to measure the velocity of the structural vibration. This research uses the 2-D plane acquisition function, which means that only out-of-plane motion data will be acquired.

- A force sensor is installed between the shaker and the specimen to measure the input force.

- A PSV-500 system is used to receive, process, present and save data collected by the laser head and the force sensor. It can also generate the input force signal to control the shaker.

- An amplifier is used to manually adjust the amplitude of the generated input force signal before it is transmitted to the shaker.

- A shaker is used to excite the specimen in a specific frequency band.

When EMA is conducted by impact testing, the mesh density of the measuring points is limited to the size of the accelerometers. In addition, during the test it is difficult to ensure the accuracy of the tapping position, and high-intensity physical exertion also brings some additional problems.

Compared with accelerometers, SLV can make non-contact measurements of a specimen so that its test results are not subject to additional mass interference. Besides, in a PSV-500 system, the position of the test points can be evenly distributed by the grid function and the laser beam can be controlled to move to the target accurately for measurement. In a complete scan test, a PSV-500 system can automatically complete the test of each measurement point. At the same time, a shaker can be installed at a fixed position of a test piece so that the position of the input force remains fixed for each measurement. These characteristics of the SLV make it a distinct advantage in vibration testing with a great number of measurement points [171]. It is less affected by external factors during the test and the testing speed is very fast as a specific testing process is completely controlled by a built-in signal processing software without human judgment.

However, there is not a built-in modal feature extraction algorithm in a PSV-500 system. This means that it can only perform the time-frequency conversion of the collected data, but cannot directly give the value of modal parameters. In addition, its laser test results are greatly affected by the selected velocity-measuring range. The measurement of a point will not be accurate enough if its vibration magnitude is much less than the measuring range. Moreover, the presence of the shaker can also cause a slight shift in the frequency measurement.

In this study, a PSV-500 SLV is used to measure the mode shape of a structure with very high-density measurement points. In the absence of a modal characteristic extraction algorithm, the commonly used method (which is referred to as common method in Figure 3-9) of obtaining the natural frequency and mode shape of the structure by using this device is to excite the specimen by force of a certain frequency band by the shaker using pseudo-random signal, and measure the FRFs of all the measuring points. Then, the natural frequencies are found from the resonance peaks on the FRF curves and the peak values of all measuring points for the same resonance frequency are recorded and form the mode shape of that frequency. When facing a large number of measuring points, another test strategy is used, which is mainly divided into the following two steps:

- **Step1**: The natural frequencies of the structure are obtained from the FRFs measured at a small number of measuring points.

- **Step2**: The mode shape of the structure at each natural frequency is measured in turn by the FastScan mode of the PSV-500 system.

An actual vibration experiment is used to demonstrate the vibration test procedure based on the FastScan mentioned above. The experimental layout is shown in Figure 3-5. The structure used in the experiment consists of two plates welded together and the vibration of one of the plates is measured. This specimen is mainly used in Chapter 7, where a detailed description can be found. This experiment can be seen simply as a test of the mode shape of a plate.

Figure 3-5 Actual experimental set-up.

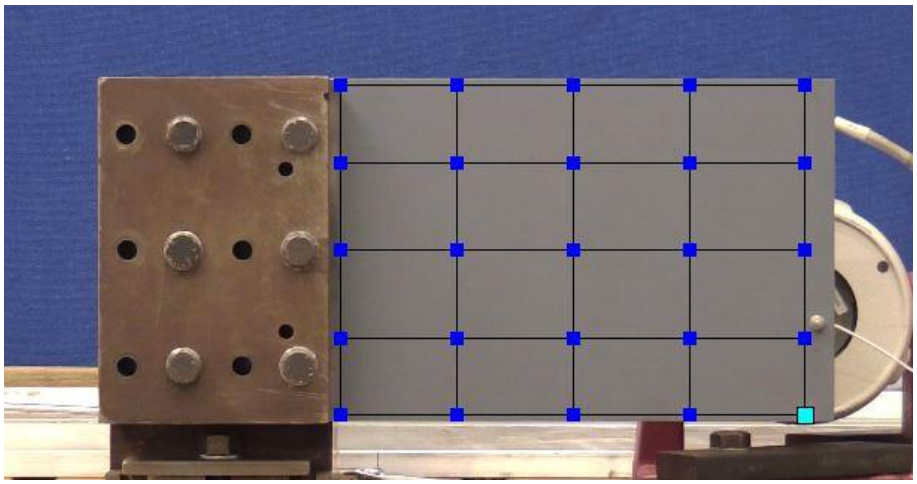

Figure 3-6 Position distribution of measuring points.

The distribution of the measuring points on the specimen is shown in Figure 3-6. According to step1, the FRF of point 11 (whose colour is cyan) is first measured which is shown in Figure 3-7. The peak positions of the curve can be used to determine the first 5 natural frequencies of the structure as shown in Table 3-1. In this step, the confidence of natural frequency measurements can be increased by looking at FRF peaks at multiple points or making multiple measurements on one point.

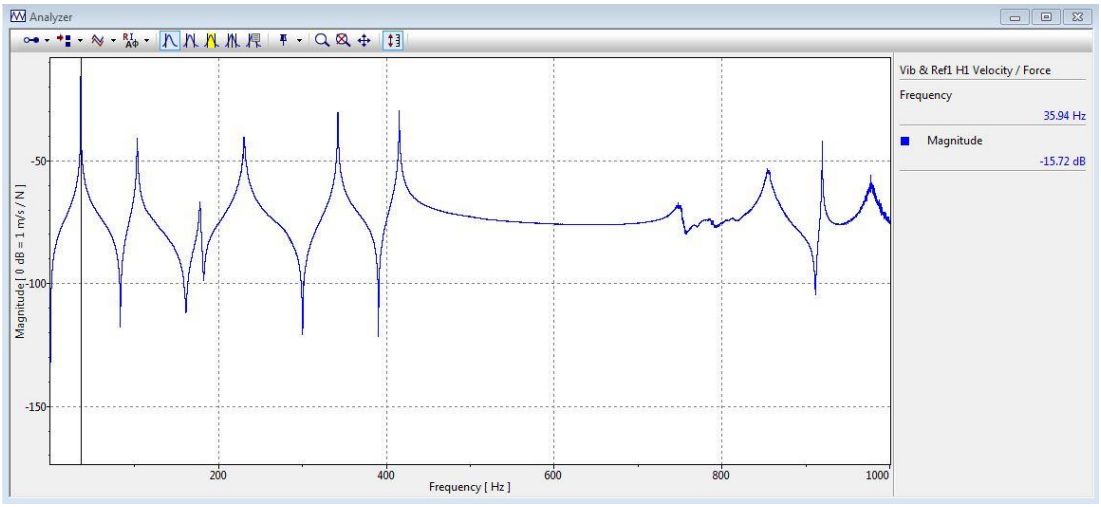

Figure 3-7 FRF measurement of point 11.

Table 3-1 Nature frequencies of the specimen.

Modes	Natural frequency (Hz)
1	35.94
2	103.28
3	177.97
4	230.47
5	342.34

Next, the first-order mode shape of the structure is measured as a demonstration by the FastScan mode in this experiment. In this mode, a specified frequency is inputted and the PSV-500system generates a sine wave signal of the frequency band near that frequency to control the shaker to apply an external force. Then, only the frequency domain data at that frequency are recorded, which significantly reduces the test time. Thus, the FRF measurements of all measuring points at this frequency are obtained.

The 1st natural frequency, 35.94Hz, and bandwidth of 3Hz are entered into the PSV-500 system as shown in Figure 3-8. The measured FRF magnitude values are taken as the mode shape data which is drawn in Figure 3-9 (a). The bandwidth depends on the needs and experience of the experimenter. A narrow bandwidth means a higher signal-to-noise ratio but it takes longer to scan.

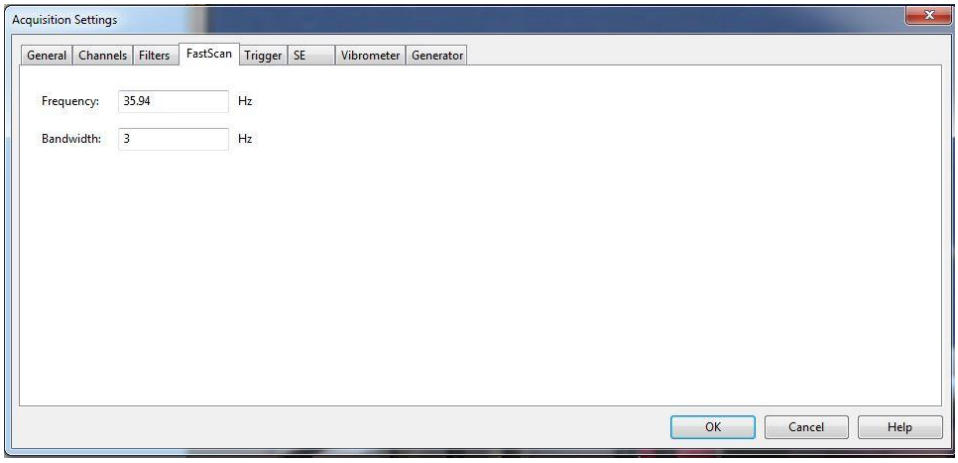

Figure 3-8 Settings of FastScan.

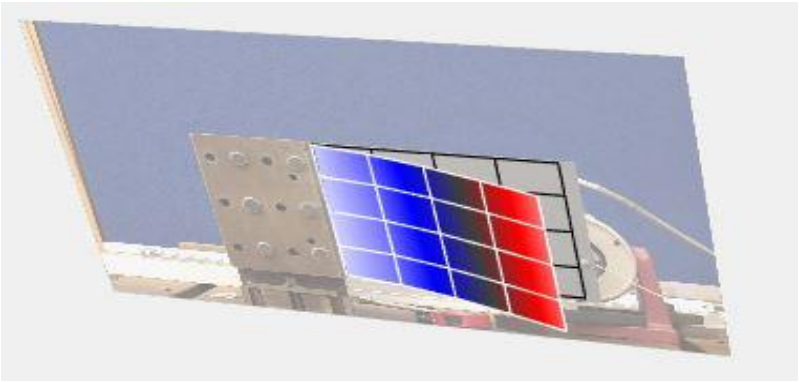

(a)

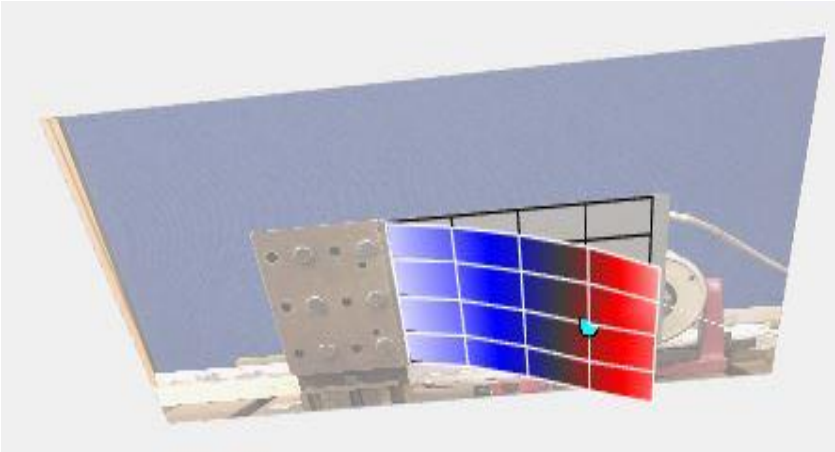

(b)

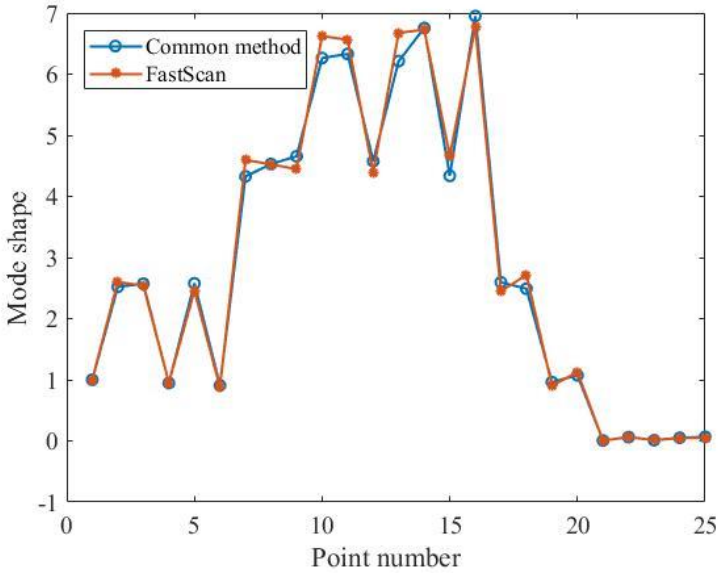

(c)

Figure 3-9 Comparison of Measurements: (a) Mode shape measured by Fast scan; (b) Mode shape measured by common method; (c) Modal displacement at on each measurement point by the two methods.

The 1st order mode shape measurement by the common method is also provided in Figure 3-9 (b). The two mode shape measurements look very similar and their exact values (normalized) are compared in Figure 3-9 (c). The results show that both methods can accurately capture the mode shapes of structures. The main difference between them is the time of measurement. As shown in Table 3-2, under the same condition that each point is measured three times, the time taken by FastScan to complete the test is much less than that of the common method.

Table 3-2 Test time comparison.

Test method	Test time(s)
FastScan	67
Common method	1202

So far, a complete process of measuring natural frequencies and mode shapes of structures using FastScan mode has been demonstrated. In the experimental tests of Chapters 5 and 7, to calculate the curvatures of structural mode shapes, it is necessary to use a very high-density grid of measuring points and perform a high number of

measurements of the velocity time history on each measuring point to obtain accurate mode curvatures. Therefore, FastScan, a fast measurement scheme, must be used to obtain the experimental data.

3.4 Conclusion

In this section, experimental modal analysis is introduced. The main test procedure for obtaining experimental data using a scanning laser vibrometer in subsequent chapters is described. It is important to have a good understanding of the basic principles and the specific purpose of the operation before performing the modal test.

Chapter 4 – Basic theory of model updating method

4.1 Introduction

It is very valuable to have a clear understanding of the basic theory of model updating. In this chapter, two classic and successful methods of model updating are introduced, which are sensitivity-based and GA-based model updating methods, respectively. The sensitivity-based method is divided into two parts which are modal property-based and FRF-based methods. For the FRF-based method, a new frequency matching technique is proposed to improve the convergence of the method. Sensitivity methods and artificial intelligence algorithms including GA are the two most widely used methods for solving optimization problems in model updating. Their ideas and algorithms continue to play an important role in later chapters.

4.2 Sensitivity-based methods using natural frequencies and mode shapes

4.2.1 Selection of updating parameters

In the beginning, it is important to understand what model updating can and cannot do. As mentioned in the previous two chapters, the function of model updating is to minimize the discrepancy between the 'responses' of the theoretical model and the actual structure by adjusting the values of the selected parameters. This discrepancy is mainly caused by simplification and incorrect description in the process of FE modelling. Among them, many problems cannot be solved by model updating [6]. For example,

- Use of a wrong type of elements like applying beam elements for a plate.
- Unexpected external forces.
- Discretization error caused by a too coarse FE mesh.
- The connection between the nodes is misplaced.
- Linear models are used to describe structures with obvious nonlinear characteristics.

Therefore, when the numerical results are significantly different from the experimental data, the modelling of the FE model itself should be checked first. After that, model updating can be used to reduce the discrepancies caused by uncertain parameters. Generally, the parameters that can be updated contain the following categories.

- Material parameters such as Young's modulus, mass density or Passion's ratio.
- Geometric parameters such as thickness or moments of area.
- Connection parameters which treat elastic connections as rigid.
- Specially designed parameters like treating cracks as rotational springs [172].

Now the question becomes how to choose the parameters to be updated. This step may even be more important than the model updating method itself. Because no matter whether the parameters to be modified are the source of the difference between theoretical results and experimental data, the model updating method will provide a 'best' solution. However, these parameters will actually become inaccurate or even lose their physical meaning after updating. The typical result is that the revised theoretical model can reproduce the experimental data quite accurately, but it cannot predict the dynamic characteristics outside the experimental test range. This will make the use of model updating method meaningless, because the response that can be tested by experiment is only for reference, and it is precisely those characteristics beyond the measurement range that are the focus of researchers.

At present, there is no general mathematical theory that can accurately determine the parameters to be updated. In practical application, the choice of parameters mainly depends on engineering experience. By analysing the blueprint of the target structure and referring to the actual test situation of the structure, researchers can make a judgment on the locations and parameters of the FE model which contains large errors. Usually, the most likely place for modelling errors is where structural theory assumptions or model simplification is the greatest. In addition, structural stiffness and boundary conditions are also important areas of concern. For complex structures with more components, sometimes a trial-and-error method is an effective solution strategy.

After preliminary selection of some modified parameters, sensitivity analysis can be carried out to further screen them as the model updating process expects to have as few parameters as possible. The sensitivity analysis is to determine how the specified dynamic characteristics of the structure are affected by the updating parameters on the basis of the current FE model, which can be quantified by calculating the rate of change of the dynamic characteristics with respect to the parameters:

$$\frac{\partial D}{\partial x_i} \approx \frac{D(x_i + \Delta x_i) - D(x_i)}{\Delta x_i} \tag{4.1}$$

where D and x_i are the dynamic characteristic and updating parameter, respectively. Equation (4.1) is a generalized way of calculating sensitivity using the finite difference method. There are already sensitivity formulas for some dynamic characteristics like natural frequencies and mode shapes, which will be introduced later.

The use of sensitivity analysis to select updating parameters is more of a consideration in solving optimization problems. A very large difference of sensitivity between two parameters will cause ill-conditioning of the sensitivity matrix, and the updating process may not converge. Therefore, it is necessary to calculate the sensitivity of each parameter and set a threshold to eliminate the parameters with a too low sensitivity. In fact, the highly sensitive updating parameters are indeed more likely to be the cause of the modelling error. However, this is not always true, and the sensitivity calculation is usually chosen in a local position of the parameter space, and it is often impossible to draw a general conclusion from a global perspective.

Parameter selection is an important part of model updating, but it is mainly based on the engineering experience of researchers. In practice, it is recommended to use test data of the fractional frequency band for model updating, and check whether the updated model can correctly predict the test data of remaining frequency band to judge the effect of model updating.

4.2.2 Procedure of sensitivity-based model updating method

Theoretically, the function between dynamic features of a structure and its updating parameters can be written as

$$\mathbf{y} = \mathbf{f}(\mathbf{p}) \tag{4.2}$$

where $\mathbf{y}$ is the vector of the dynamic features, $\mathbf{p}$ is the vector of updating parameters. Let $\mathbf{p}_i$ and $\mathbf{y}_i = \mathbf{f}(\mathbf{p}_i)$ denote the parameters and features of the FE model in the *i*th iteration, and $\mathbf{y}_{\mathrm{m}}$ denotes the measured features. The sensitivity method chooses to linearize the generally nonlinear relationship $\mathbf{f}$ using the first-order approximation of Taylor expansion series. In this way, the measured values are approached by

$$\begin{aligned} \mathbf{y}_{\mathrm{m}} &\approx \mathbf{y}_i + \left.\frac{\partial \mathbf{f}}{\partial \mathbf{p}}\right|_{\mathbf{p}_i} \Delta\mathbf{p} = \mathbf{y}_i + \mathbf{S}_i \Delta\mathbf{p} \\ \boldsymbol{\varepsilon}_i &= \mathbf{y}_{\mathrm{m}} - \mathbf{y}_i \approx \mathbf{S}\Delta\mathbf{p} \end{aligned} \tag{4.3}$$

where $\boldsymbol{\varepsilon}_i$ is the residual vector in the current iteration, $\mathbf{S}_i$ is the sensitivity matrix computed at the current value of the updating parameters $\mathbf{p}_i$. In model updating process, it is always required to ensure the number of the dynamic features is more than that of the updating parameters, which makes equation (4.3) overdetermined and can be solved by least-square methods as follows ($(*)^{\mathrm{T}}$ is transpose symbol.)

$$\Delta\mathbf{p} = \left[\mathbf{S}_i^{\mathrm{T}}\mathbf{S}_i\right]^{-1}\mathbf{S}_i^{\mathrm{T}}\boldsymbol{\varepsilon}_i \tag{4.4}$$

Then the FE model is updated with a new set of parameters

$$\mathbf{p}_{i+1} = \mathbf{p}_i + \Delta\mathbf{p} \tag{4.5}$$

Due to the existence of truncation errors in equation (4.3), multiple iterations are usually required to bring the theoretical response close to the test data. Therefore, the model updating starts from the initial value of the parameters and iterates using equations (4.4) and (4.5) until the value of $\mathbf{p}_i$ converges.

In this section, the experimental data are taken from the natural frequencies and modes shapes, which are directly related to the eigenvalues and eigenvectors of the structural free vibration equation. The first analytical formula for the eigenvalue and eigenvector sensitivity was proposed by Fox and Kapoor [63] which was about undamped systems:

$$\frac{\partial \lambda_j}{\partial p_k} = \boldsymbol{\varphi}_j^{\mathrm{T}}\left[-\lambda_j\frac{\partial \mathbf{M}}{\partial p_k} + \frac{\partial \mathbf{K}}{\partial p_k}\right]\boldsymbol{\varphi}_j \tag{4.6}$$

$$\frac{\partial \boldsymbol{\varphi}_j}{\partial p_k} = \sum_{l=1}^{n} a_{jkl} \boldsymbol{\varphi}_l$$

$$a_{jkl} = \frac{\boldsymbol{\varphi}_l^{\mathrm{T}} \left(-\lambda_j \dfrac{\partial \mathbf{M}}{\partial p_k} + \dfrac{\partial \mathbf{K}}{\partial p_k} \right) \boldsymbol{\varphi}_j}{\lambda_j - \lambda_l}; \qquad l \neq j \tag{4.7}$$

$$a_{jkj} = -\frac{1}{2} \boldsymbol{\varphi}_j^{\mathrm{T}} \left(\frac{\partial \mathbf{M}}{\partial p_k} \right) \boldsymbol{\varphi}_j$$

where λ_j and $\boldsymbol{\varphi}_j$ are the *j*th order eigenvalue and eigenvector, respectively, p_k is the *k*th updating parameter, $\mathbf{M}$ and $\mathbf{K}$ are mass and stiffness matrices.

To calculate the sensitivity of natural frequencies, equation (4.6) is applied together with the following formula according to the multiple relationships between them (represented by f) and the eigenvalues. Alternatively, a simpler way is to turn measured natural frequencies into the measured eigenvalues and to use those eigenvalues as experimental reference directly.

$$(2\pi f_j)^2 = \lambda_j$$

$$8\pi^2 f_j \frac{\partial f_j}{\partial p_k} = \frac{\partial \lambda_j}{\partial p_k} \tag{4.8}$$

In equation (4.7), the eigenvector sensitivity is calculated as a linear combination of all the eigenvectors and *n* is the number of the vectors actually used. The mode shape data can be used directly as eigenvectors and they had better be normalized by

$$\boldsymbol{\varphi}_j^{\mathrm{T}} \mathbf{M} \boldsymbol{\varphi}_j = 1 \tag{4.9}$$

It is worth noting that when modal data is used for model updating, it must be ensured that the theoretical prediction and experimental data correspond to the same physical mode. This is mainly judged by the degree of closeness of their mode shapes using modal assurance criterion (MAC) [62].

$$MAC_{ij} = \frac{\left| \boldsymbol{\varphi}_i^{\mathrm{T}} \boldsymbol{\varphi}_j \right|^2}{(\boldsymbol{\varphi}_i^{\mathrm{T}} \boldsymbol{\varphi}_i)(\boldsymbol{\varphi}_j^{\mathrm{T}} \boldsymbol{\varphi}_j)} \tag{4.10}$$

where $\boldsymbol{\varphi}_i$ and $\boldsymbol{\varphi}_j$ denote the theoretical mode and the measured mode, respectively. The value of MAC is between 0 and 1. A value of 1 means the highest match between the two modes.

In an undamped system, the modal data of the structure have only real parts. Real natural frequencies and real mode shapes are widely used in model updating methods because most structures are lightly damped. However, for a highly damped structure, Equation (4.6) and (4.7) will no longer be suitable to use. The formulas for calculating the eigenvalues and eigenvectors sensitivities of damped vibration systems is given in [67], which can be used in model updating methods especially for studying damping.

$$\frac{\partial \lambda_j}{\partial p_k} = \boldsymbol{\varphi}_j^{\mathrm{T}} \left[\lambda_j^2 \frac{\partial \mathbf{M}}{\partial p_k} + \lambda_j \frac{\partial \mathbf{C}}{\partial p_k} + \frac{\partial \mathbf{K}}{\partial p_k} \right] \boldsymbol{\varphi}_j \tag{4.11}$$

$$\begin{Bmatrix} \dfrac{\partial \boldsymbol{\varphi}_j}{\partial p_k} \\ 0 \end{Bmatrix} =$$

$$\begin{bmatrix} \lambda_j^2 \mathbf{M} + \lambda_j \mathbf{C} + \mathbf{K} & (2\lambda_j \mathbf{M} + \mathbf{C})\boldsymbol{\varphi}_j \\ \boldsymbol{\varphi}_j^{\mathrm{T}} (2\lambda_j \mathbf{M} + \mathbf{C}) & 0 \end{bmatrix}^{-1} \begin{Bmatrix} -(2\lambda_j \mathbf{M} + \mathbf{C})\boldsymbol{\varphi}_j \dfrac{\partial \lambda_j}{\partial p_k} - \left(\lambda_j^2 \dfrac{\partial \mathbf{M}}{\partial p_k} + \lambda_j \dfrac{\partial \mathbf{C}}{\partial p_k} + \dfrac{\partial \mathbf{K}}{\partial p_k} \right) \boldsymbol{\varphi}_j \\ -\dfrac{1}{2} \boldsymbol{\varphi}_j^{\mathrm{T}} \left[2 \left(\dfrac{\partial \lambda_j}{\partial p_k} \mathbf{M} + \lambda_j \dfrac{\partial \mathbf{M}}{\partial p_k} \right) + \dfrac{\partial \mathbf{C}}{\partial p_k} \right] \boldsymbol{\varphi}_j \end{Bmatrix} \tag{4.12}$$

where $\mathbf{C}$ is the symmetric damping matrix. Also note that the expression of eigenvalue in a damped system is different from that in an undamped system.

As mentioned in chapter 1, the model updating process can be regarded as an optimization process. The goal is to minimize the residuals between the numerical results and test data, which can be described as an objective function

$$J(\mathbf{p}) = \boldsymbol{\varepsilon}^{\mathrm{T}} \boldsymbol{\varepsilon} \tag{4.13}$$

where $\mathbf{p}$ is the updating parameter vector and $\boldsymbol{\varepsilon}$ is the residual vector as defined in equation (4.3). The sensitivity method finds this minimum by making the gradient of this objective function zero. There is an implicit assumption that the minimum is within the neighbourhood of the initial values of the updating parameters. Otherwise, the sensitivity method may converge to a local extreme point.

In actual application, the objective function can be extended to the following form

$$J(\mathbf{p}) = \boldsymbol{\varepsilon}^{\mathrm{T}} \mathbf{W}_{\varepsilon} \boldsymbol{\varepsilon} + \lambda_{\mathrm{r}} \Delta \mathbf{p}_i^{\mathrm{T}} \mathbf{W}_{\mathrm{p}} \Delta \mathbf{p}_i \tag{4.14}$$

where the residual weighting matrix $\mathbf{W}_\varepsilon$ is often used to balance the importance of different test data. A simple idea is that the first-order and the fifth-order natural frequencies have similar influences on the objective function, although their values may vary widely. Therefore, a reasonable choice is to set $\mathbf{W}_\varepsilon = \left[\mathrm{diag}(\mathbf{y}_\mathrm{m})\right]^{-2}$ to eliminate scale differences between test data of the same type. As for the weighting setting between different types of test data, such as natural frequencies and mode shapes are used at the same time, it mainly depends on the experience of the researcher.

The essence of sensitivity is the gradient of the objective at the current parameter position, which means that the prediction of a new theoretical response is only valid within a limited range of step size ($\Delta\mathbf{p}$). However, the step size obtained by the least-squares method can be very large, especially for sensitivity matrices with ill-conditioning problems. Therefore, a regularization method is used to increase the convergence probability of the sensitivity method. It adds a new term to the objective function (the second term in equation (4.14)) that requires that the parameter changes should be minimized at the same time to limit the step size during each iteration.

To minimize this extended objective function, in each iteration the change of each parameter can be estimated as

$$\Delta\mathbf{p} = \left[\mathbf{S}_i^\mathrm{T}\mathbf{W}_\varepsilon\mathbf{S}_i + \lambda_\mathrm{r}\mathbf{W}_\mathrm{p}\right]^{-1}\mathbf{S}_i^\mathrm{T}\mathbf{W}_\varepsilon\boldsymbol{\varepsilon}_i \tag{4.15}$$

The parameter weighting matrix $\mathbf{W}_\mathrm{p}$ is used to reflect the uncertainty in the initial parameter estimations and λ_r is a regularization parameter determined from an L-curve [71]. The regularization technique is mainly used when the model updating process cannot converge, caused by the ill-conditioning problem. More details of it can be found in [84].

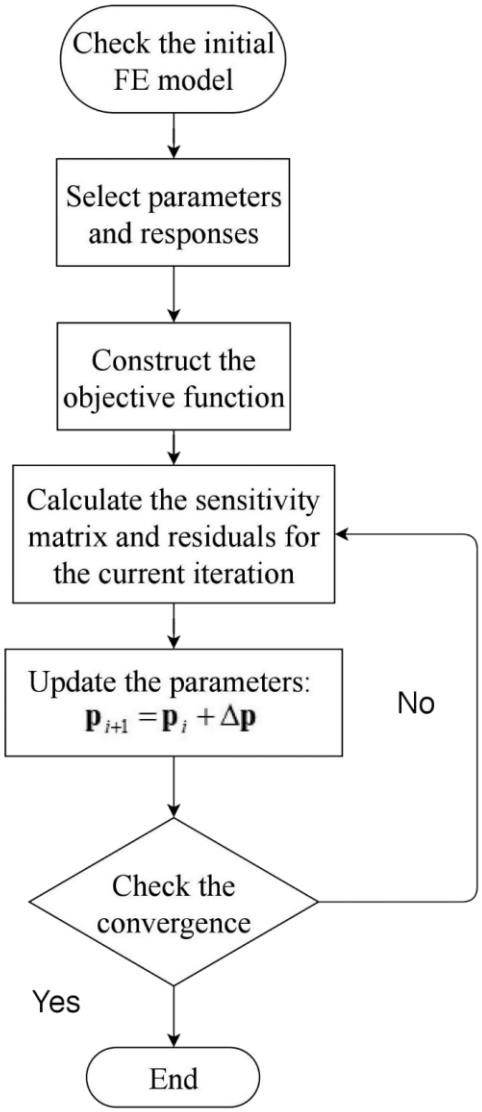

Figure 4-1 Flowchart of the sensitivity-based model updating method.

So far, the procedure of the sensitivity-based model updating method has been introduced, which is illustrated more clearly in Figure 4-1. In addition, the sensitivity formulas of the natural frequencies and vibration modes are given. In a specific model updating problem, usually, the frequencies are more important than the mode shapes. This is because the measured natural frequencies are much less affected by noise than the mode shapes.

4.3 Genetic algorithm-based model updating

GA is a heuristic algorithm based on global search and is one of the most successful evolutionary algorithms. Inspired by Darwin's theory of evolution, this algorithm searches for optimal solutions by simulating the process of natural selection, that is, only the fittest individuals can survive the cruel competition and spread their genes through producing offspring. It ultimately finds the best solution from a set of possible solutions. This process does not depend on the calculation of sensitivity, and its probability of converging to the global optimal solution is also higher than the sensitivity method. This advantage makes GA better at dealing with complex optimization problems such as wire routing and cognitive modelling [90]. In the field of model updating, GA can be directly connected to the construction of the objective function, in the flow chart of Figure 4-1, and then give the updating results. Many successful applications can be found as mentioned in Chapter 2. This section is mainly an introduction to the basic principles of GA.

To implement a genetic algorithm [90], as shown in Figure 4-2, there are five main stages to consider: initialization, selection, crossover, mutation, and termination, which are introduced separately.

(1) Initialization. For a given optimization problem, a set of individual solutions is first randomly generated as a population. The number of this initial population is proportional to the number of design variables and the population should cover the entire variable space as much as possible. Each individual is characterized by a set of parameters called a gene. All genes are arranged in sequence to form a chromosome to replace the original individual. The whole process is called ‘encode’.

Typically, binary digit strings are used to construct chromosomes. For example, '100000', where each digit represents a gene. In the specific encoding process, It is assumed that the variables’ change range is *m* and the number of digits in the binary digit string is *n*. Then *m* will be divided equally into 2^n points and the values of each variable will be represented by the binary digit string corresponding to their nearest segmentation point. The greater the value of *n*, the higher the accuracy of GA solution.

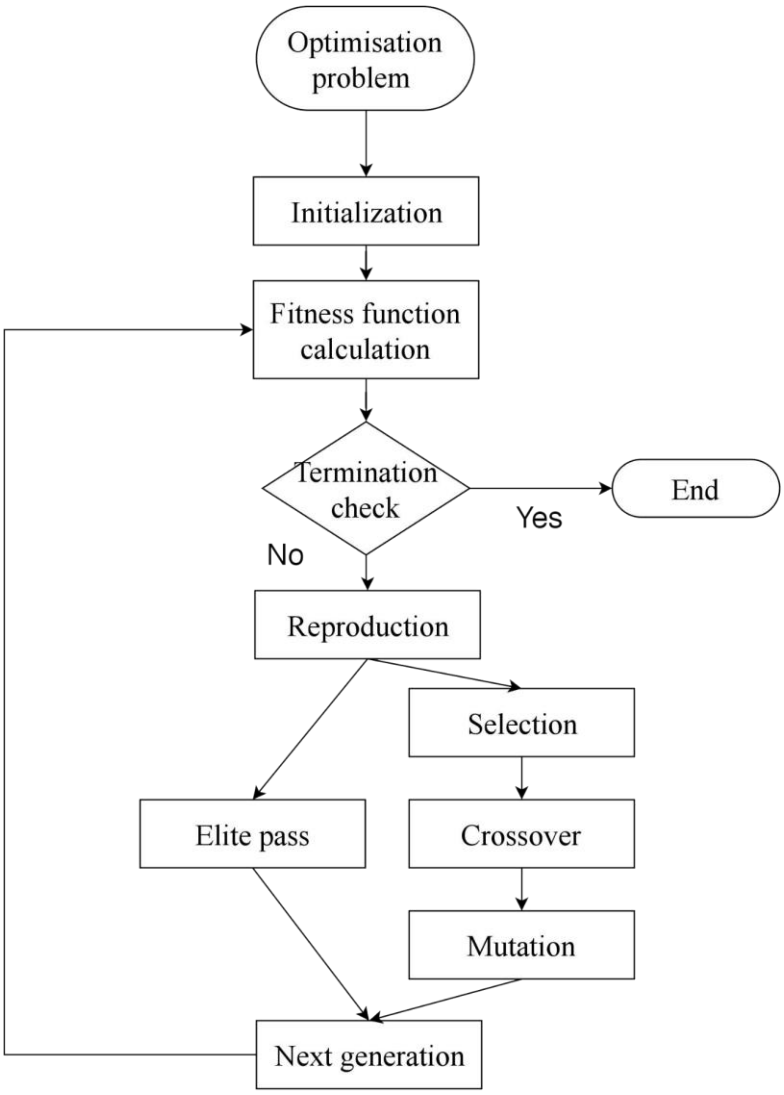

Figure 4-2 Flowchart of the GA method.

(2) Selection. GA is also an iterative-based approach, with a new generation of population generated in each iteration. The selection process is to select the fittest individuals and pass their genes to the next generation. Despite this, many selection functions tend to be stochastic in nature to ensure that some individuals with low fitness have the opportunity to be selected to ensure the diversity of the population genes and to avoid premature convergence of the search process to low-quality solutions. In this process, the fitness function determines the ability of each individual to compete with other individuals. It gives each individual a fitness score based on the

objective function of the optimization problem. This score is an important basis for the probability of individual survival and reproduction.

(3) Crossover. A pair of individuals are selected as parents, and crossover operators control them to produce offspring. A classic way of doing this is to choose a random crossover point on the parents' chromosomes and then exchange the genes on the left of the point to form two new offspring. For example, two chromosomes, a='000000', b='111111', are selected and the crossover point is considered to be in the middle. Then new offspring c=' 111000' and d=' 000111' will be generated.

The crossover operation mixes the genetic information of individuals with high fitness in the population. This has the potential to combine two excellent genes to form a better individual. Genes with poor fitness are gradually eliminated in natural selection.

(4) Mutation. In certain newly formed offspring, some of their genes can be subjected to mutation with a low probability. The mutation operation randomly flip a binary digit of chromosomes. For example, e='110011' becomes f='110101' after the mutation. Mutation is an effective way of enriching the population diversity, making GA have a higher probability of converging to the global optimal solution.

(5) Termination. The new generation of population formed in each iteration consists of two parts: the offspring produced by crossover and mutation, and the elite individuals (called elite children) surviving from the previous generation. This iterative process is repeated until a termination condition is met. The stopping criteria can be the maximum number of iterations or the maximum time has been performed, the best fitness value is less than or equal to the expected fitness limit (note that for minimum optimization problem, the less means the better.), the average change in the fitness function value is less than a tolerance (which means the population has converged) and so on.

When applied to model updating, the main disadvantage of GA is the low speed of the solution, which makes it difficult to implement for large-scale structures. Nevertheless, it provides great convenience for solving general model updating problems, and can

easily utilize some special dynamic features that cannot be solved by sensitivity method like the MAC value. A numerical simulation is provided to demonstrate the implementation and comparison of the sensitivity-based and the GA-based model updating method.

4.3 Numerical Simulation

In this section, a 4-DoF undamped mass-spring system adapted from [62] is considered for demonstration, as shown in Figure 4-3.

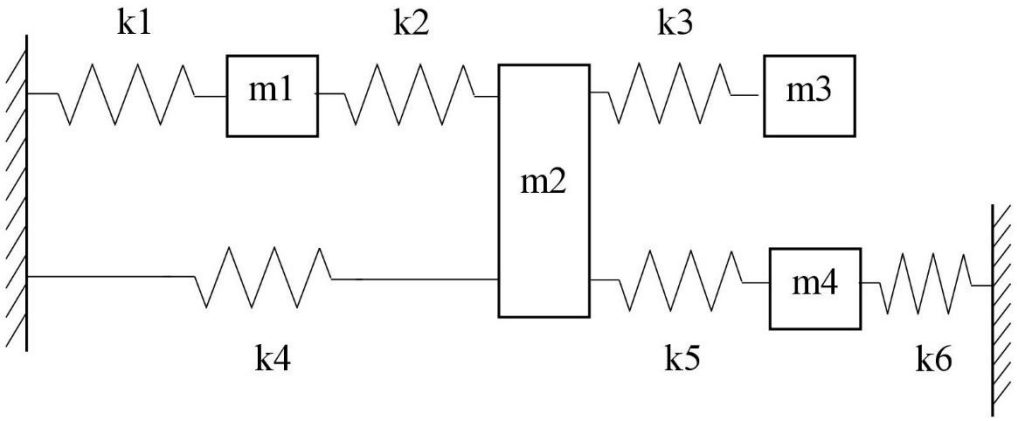

Figure 4-3 4-DoF mass-spring system.

Assume that the values of the following parameters are known accurately:

$$m1 = 5\text{kg}, \quad m2 = 10\text{kg}, \quad m3 = 5\text{kg}, \quad m4 = 5\text{kg}$$

$$k1 = 100\text{N/m}, \quad k4 = 60\text{N/m}, \quad k6 = 150\text{N/m}$$

$k2$, $k3$ and $k4$ are uncertain parameters to be determined and their initial estimations are:

$$k2 = 50\text{N/m}, \quad k3 = 50\text{N/m}, \quad k5 = 50\text{N/m}$$

while their real values are

$$k2 = 70\text{N/m}, \quad k3 = 120\text{N/m}, \quad k5 = 90\text{N/m}$$

The comparison between the natural frequencies of the system using the initial parameters and the real values is shown in

Table 4-1 Natural frequencies (Hz) of the system.

Mode	Initial	Real
1	0.38	0.45
2	0.70	0.89
3	0.91	1.0
4	1.0	1.2

The updating is done by 4 ways classified by the methods and data used, which are referred to as 'Sen1', 'Sen2', 'GA1' and 'GA2', respectively. In the beginning, based on these frequencies, the objective function of this model updating problem can be constructed as

$$\min \qquad f = \sum_{i=1}^{4} \left(\frac{f_i^{\mathrm{a}} - f_i^{\mathrm{e}}}{f_i^{\mathrm{e}}} \right)^2 \tag{4.16}$$

where superscript 'a' represents the analytical value and superscript 'e' represents the real value which is considered as experimental data. This optimization problem can be solved by both the sensitivity method and GA, which are referred to as 'Sen1' and 'GA1', respectively.

The mode shape data can also be utilized in model updating. The following equation is solved by the sensitivity method (referred to as 'Sen2').

$$\min \qquad f = \sum_{i=1}^{4} \sum_{j=1}^{4} \left(\varphi_{ij}^{\mathrm{a}} - \varphi_{ij}^{\mathrm{e}} \right)^2 \tag{4.17}$$

where i denotes the mode order and j denotes the entry of the mode shape vector (normalized by equation (4.9)). The mode shape data can also be used with natural frequency data in another form:

$$\min \qquad f = \sum_{i=1}^{4} \left(\left(\frac{f_i^{\mathrm{a}} - f_i^{\mathrm{e}}}{f_i^{\mathrm{e}}} \right)^2 + MAC_{ii} \right) \tag{4.18}$$

The value of *MAC* can be determined by equation (4.10). Then GA is used to solve this problem which is referred to as 'GA2'.

At first, it is assumed that all the data are measured perfectly without noise. The updating results of the 4 ways are shown in Figure 4-4 (a). It is clear that all of them

can obtain the real values of the three parameters correctly. However, it happens randomly that GA1 converges to a local solution. Thus, it is suggested to run the GA several times until getting a stable solution.

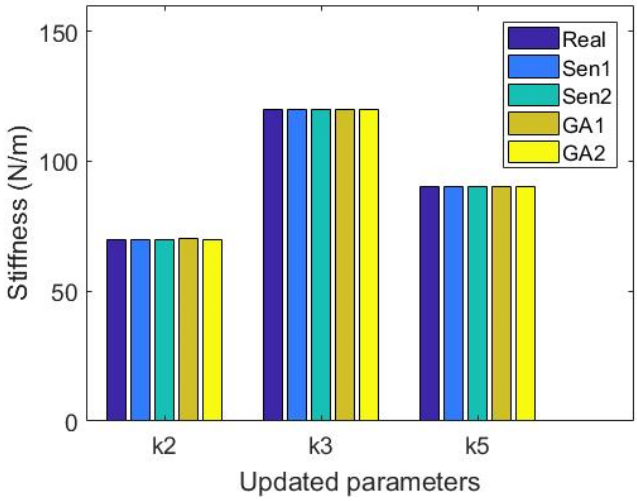

(a)

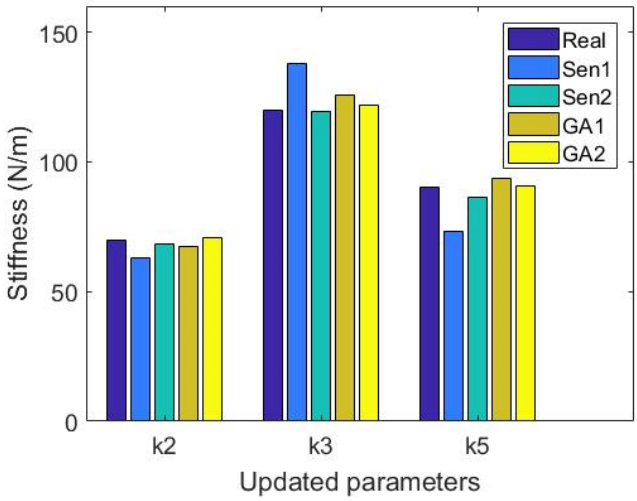

(b)

Figure 4-4 Updating results of the 4 ways: (a) Without noise; (b) Noise contaminated.

Then the white noise of 1% signal to noise ratio and 3% signal to noise ratio are added to the natural frequency and mode shape data respectively to simulate the actual test data, respectively. The updating results are shown in Figure 4-4 (b). Obviously, methods based only on natural frequencies (Sen1 and GA1) are more affected by the noise. Among them, Sen1 sometimes even does not converge, without introducing

regularization. On the other hand, although the noise added to the mode shape data is greater, Sen2 still produces good results. This is mainly because the mode shape data contains far more information than the frequency data. The result of GA2 is also great. It provides a way to use both frequency and mode shape data while their effects are similar. In addition, the use of MAC data can reduce the impact of some heavily polluted measurements in the mode shape data.

In this simulation, a simple conclusion is that the more test data used, the stronger the noise resistance. As described in Chapter 3, modal data are extracted from the FRF data, which means that the FRF data can provide the most vibration information. The model updating method utilizing FRF data is described in the next section.

4.4 Sensitivity-based methods using FRFs

FRF residues have been widely used to update FE models. They are a kind of original measurement information and have the advantages of rich data and no extraction errors, etc. However, like other sensitivity-based methods, an FRF-based identification method also needs to face the ill-conditioning problem which is even more serious since the sensitivity of the FRF in the vicinity of a resonance is much greater than elsewhere. Furthermore, for a given frequency measurement, directly using a theoretical FRF at a frequency may lead to a huge difference between the theoretical FRF and the corresponding experimental FRF which finally results in larger effects of measurement errors and damping. Hence in the solution process, correct selection of the appropriate frequency to get the theoretical FRF in every iteration in the sensitivity-based approach is an effective way to improve the robustness of an FRF-based algorithm. A primary tool for right frequency selection based on the correlation of FRFs is the Frequency Domain Assurance Criterion (FDAC). In this section, the theory of the FRF-based model updating method is described and then a new frequency selection method is presented (The main content of this section was published on reference [173]), which directly finds the frequency that minimizes the difference of the order of magnitude between the theoretical and experimental FRFs.

4.4.1 Basic theory

The essential purpose of the FRF based model updating method is to use the parameterized theoretical FRFs to approximate the measured ones. A brief description of the fundamental theory is given below [77] which begins with a simple equation:

$$\mathbf{H}_{\mathrm{a}}(\omega)-\mathbf{H}_{\mathrm{x}}(\omega)=\mathbf{H}_{\mathrm{a}}(\omega)-\mathbf{H}_{\mathrm{x}}(\omega). \tag{4.19}$$

where $\mathbf{H}_{\mathrm{a}}(\omega)$ and $\mathbf{H}_{\mathrm{x}}(\omega)$ are $n\times n$ theoretical and experimental FRF matrices at frequency ω, respectively. Equation (4.19) can be rewritten as

$$\mathbf{H}_{\mathrm{a}}(\omega)\left(\mathbf{H}_{\mathrm{x}}^{-1}(\omega)-\mathbf{H}_{\mathrm{a}}^{-1}(\omega)\right)\mathbf{H}_{\mathrm{x}}(\omega)=\mathbf{H}_{\mathrm{a}}(\omega)-\mathbf{H}_{\mathrm{x}}(\omega) \tag{4.20}$$

Replacing $\mathbf{H}^{-1}(\omega)$ by the dynamic stiffness matrix $\mathbf{Z}(\omega)$

$$\mathbf{H}_{\mathrm{a}}(\omega)\Delta\mathbf{Z}\mathbf{H}_{\mathrm{x}}(\omega)=\mathbf{H}_{\mathrm{a}}(\omega)-\mathbf{H}_{\mathrm{x}}(\omega) \tag{4.21}$$

where

$$\Delta\mathbf{Z}=\mathbf{Z}_{\mathrm{x}}(\omega)-\mathbf{Z}_{\mathrm{a}}(\omega)=-\omega^2\Delta\mathbf{M}+\mathrm{j}\omega\Delta\mathbf{C}+\Delta\mathbf{K} \tag{4.22}$$

The basic assumption here is that the damage causes a reduction of the mass, damping and stiffness matrices of the model at element level. So the difference of the 3 global matrices can be expressed as

$$\Delta\mathbf{M}=\sum_{i=1}^{n_{\mathrm{e}}}p_{\mathrm{m}i}\mathbf{M}_i^{\mathrm{e}},\quad \Delta\mathbf{C}=\sum_{i=1}^{n_{\mathrm{e}}}p_{\mathrm{c}i}\mathbf{C}_i^{\mathrm{e}},\quad \Delta\mathbf{K}=\sum_{i=1}^{n_{\mathrm{e}}}p_{\mathrm{k}i}\mathbf{K}_i^{\mathrm{e}} \tag{4.23}$$

where n_e is the number of updating elements, $\mathbf{M}_i^{\mathrm{e}}$, $\mathbf{C}_i^{\mathrm{e}}$ and $\mathbf{K}_i^{\mathrm{e}}$ are respective contributions of the ith clement to the global mass, damping and stiffness matrices and $p_{\mathrm{m}i}$, p_{ci} and $p_{\mathrm{k}i}$ are the corresponding scalar multipliers representing the proportional changes from their values in the intact state and are also regarded as updating parameters. Substituting equations (4.23) and (4.22) into (4.21) and assuming only one column vector $\mathbf{h}_{\mathrm{x}}(\omega)$ of the measured FRF matrix $\mathbf{H}_{\mathrm{x}}(\omega)$ is available, one obtains

$$\begin{bmatrix}\mathbf{S}_{\mathrm{m}}(\omega) & \mathbf{S}_{\mathrm{c}}(\omega) & \mathbf{S}_{\mathrm{k}}(\omega)\end{bmatrix}\begin{Bmatrix}\mathbf{p}_{\mathrm{m}}\\ \mathbf{p}_{\mathrm{c}}\\ \mathbf{p}_{\mathrm{k}}\end{Bmatrix}=\mathbf{h}_{\mathrm{a}}(\omega)-\mathbf{h}_{\mathrm{x}}(\omega) \tag{4.24}$$

where $\mathbf{S}_{\mathrm{m}}(\omega)$, $\mathbf{S}_{\mathrm{c}}(\omega)$ and $\mathbf{S}_{\mathrm{k}}(\omega)$ are the sensitivity matrices with $\mathbf{n}_e$ submatrices arranged in a row and $\mathbf{p}_{\mathrm{m}}$, $\mathbf{p}_{\mathrm{c}}$ and $\mathbf{p}_{\mathrm{k}}$ are the column vectors of the corresponding updating parameters. The ith submatrix of the 3 sensitivity matrices is calculated as

$$\begin{aligned}\mathbf{S}_{\mathrm{m}}^{i}(\omega) &= -\omega^{2}\mathbf{H}_{\mathrm{a}}(\omega)\mathbf{M}_{i}^{\mathrm{e}}\mathbf{h}_{\mathrm{x}}(\omega)\\ \mathbf{S}_{\mathrm{c}}^{i}(\omega) &= \mathrm{j}\omega\mathbf{H}_{\mathrm{x}}(\omega)\mathbf{C}_{i}^{\mathrm{e}}\mathbf{h}_{\mathrm{x}}(\omega)\\ \mathbf{S}_{\mathrm{k}}^{i}(\omega) &= \mathbf{H}_{\mathrm{a}}(\omega)\mathbf{K}_{i}^{\mathrm{e}}\mathbf{h}_{x}(\omega)\end{aligned} \tag{4.25}$$

Equation (4.24) is the final form of most FRF based methods. However, as mentioned before, choosing good theoretical frequencies different from their counterparts can improve the robustness of the method. To achieve this, equation (4.24) and (4.25) are rebuilt where two different frequencies are considered: $\boldsymbol{\omega}_a$ as the analytical frequency and $\boldsymbol{\omega}_x$ as the experimental frequency. Equation (4.24) now becomes

$$\left[\mathbf{S}_{\mathrm{m}}(\omega_{\mathrm{a}},\omega_{\mathrm{x}})\quad \mathbf{S}_{c}(\omega_{\mathrm{a}},\omega_{\mathrm{x}})\quad \mathbf{S}_{\mathrm{k}}(\omega_{\mathrm{a}},\omega_{\mathrm{x}})\right]\begin{Bmatrix}\mathbf{P}_{\mathrm{m}}\\ \mathbf{P}_{\mathrm{c}}\\ \mathbf{P}_{\mathrm{k}}\end{Bmatrix} = \mathbf{h}_{\mathrm{a}}(\omega_{\mathrm{a}}) - \mathbf{h}_{\mathrm{x}}(\omega_{\mathrm{x}}) - \mathbf{e}_{\omega}(\omega_{\mathrm{a}},\omega_{\mathrm{x}}) \tag{4.26}$$

and

$$\begin{aligned}\mathbf{S}_{\mathrm{m}}^{i}(\omega_{\mathrm{a}},\omega_{\mathrm{x}}) &= -\omega_{\mathrm{x}}^{2}\mathbf{H}_{\mathrm{a}}(\omega_{\mathrm{a}})\mathbf{M}_{i}^{\mathrm{e}}\mathbf{h}_{\mathrm{x}}(\omega_{\mathrm{x}})\\ \mathbf{S}_{\mathrm{c}}^{i}(\omega_{\mathrm{a}},\omega_{\mathrm{x}}) &= \mathrm{j}\omega_{\mathrm{x}}\mathbf{H}_{\mathrm{a}}(\omega_{\mathrm{a}})\mathbf{C}_{i}^{\mathrm{e}}\mathbf{h}_{\mathrm{x}}(\omega_{\mathrm{x}})\\ \mathbf{S}_{\mathrm{k}}^{i}(\omega_{\mathrm{a}},\omega_{\mathrm{x}}) &= \mathbf{H}_{\mathrm{a}}(\omega_{\mathrm{a}})\mathbf{K}_{i}^{\mathrm{e}}\mathbf{h}_{\mathrm{x}}(\omega_{\mathrm{x}})\end{aligned} \tag{4.27}$$

$$\mathbf{e}_{\omega}(\omega_{\mathrm{a}},\omega_{\mathrm{x}}) = (-\omega_{\mathrm{x}}^{2}+\omega_{\mathrm{a}}^{2})\mathbf{H}_{\mathrm{a}}(\omega_{\mathrm{a}})\mathbf{M}\mathbf{h}_{\mathrm{x}}(\omega_{\mathrm{x}}) + \mathrm{j}(\omega_{\mathrm{x}}-\omega_{\mathrm{a}})\mathbf{H}_{\mathrm{a}}(\omega_{\mathrm{a}})\mathbf{C}\mathbf{h}_{\mathrm{x}}(\omega_{\mathrm{x}}) \tag{4.28}$$

where the additional item $\mathbf{e}_{\omega}(\omega_{\mathrm{a}},\omega_{\mathrm{x}})$ comes from equation (4.22) representing the difference of theoretical dynamic stiffness matrices between the two frequencies

By now the relationship between the difference of the FRFs and the updating parameters has been established. The next task is to find the best corresponding theoretical frequencies for every experimental frequency. A well-known method for doing this is the FDAC method [81] which matches the measured frequency with the theoretical frequency whose FDAC value is the greatest. The FDAC value can be regarded as the correlation of the two FRFs and its expression is

$$FDAC(\omega_{\mathrm{a}},\omega_{\mathrm{x}}) = \frac{\{\mathbf{h}_{\mathrm{a}}(\omega_{\mathrm{a}})\}^{\mathrm{T}}\{\mathbf{h}_{\mathrm{x}}(\omega_{\mathrm{x}})\}}{\left|\{\mathbf{h}_{\mathrm{a}}(\omega_{\mathrm{a}})\}\right|\left|\{\mathbf{h}_{\mathrm{x}}(\omega_{\mathrm{x}})\}\right|} \tag{4.29}$$

The experimental FRF can be considered as the shift of theoretical FRF caused by the change of the updating parameters. The key point of FDAC method is to find the

corresponding theoretical frequency to the experimental one. However, this method requires searching for the whole frequency range, which is very time-consuming.

Since the main idea of this method is to avoid a big difference of the theoretical and experimental FRFs, a new index is proposed to find the theoretical frequency with a minimum order of magnitude difference (MOMD) from the measured frequency and is expressed as:

$$MOMD(\omega_{\mathrm{a}},\omega_{\mathrm{x}})=\sum_{i=1}^{n}\left|\log_{10}(\mathbf{momd}_{\mathrm{i}})\right|$$

$$\mathbf{momd}_i=\begin{cases}\left|\dfrac{\{\mathbf{h}_{\mathrm{a}}(\omega_{\mathrm{a}})\}_i}{\{\mathbf{h}_{\mathrm{x}}(\omega_{\mathrm{x}})\}_i}\right|, \{\mathbf{h}_{\mathrm{a}}(\omega_{\mathrm{a}})\}_i\cdot\{\mathbf{h}_{\mathrm{x}}(\omega_{\mathrm{x}})\}_i\geq 0 \\ \left|\dfrac{\{\mathbf{h}_{\mathrm{a}}(\omega_{\mathrm{a}})\}_i-\{\mathbf{h}_{\mathrm{x}}(\omega_{\mathrm{x}})\}_i}{\min\left(\left|\{\mathbf{h}_{\mathrm{a}}(\omega_{\mathrm{a}})\}_i\right|,\left|\{\mathbf{h}_{\mathrm{x}}(\omega_{\mathrm{x}})\}_i\right|\right)}\right|, \{\mathbf{h}_{\mathrm{a}}(\omega_{\mathrm{a}})\}_i\cdot\{\mathbf{h}_{\mathrm{x}}(\omega_{\mathrm{x}})\}_i<0\end{cases} \tag{4.30}$$

where $\mathbf{momd}_i$ represents the degree of closeness of every pair of elements in the two vectors.

$\mathbf{momd}_i$ has different expressions to reduce the influence of anti-phase vector with the same modulus value. The closer its value is to 1, the smaller *MOMD* is. After calculating all the *MOMD* values in a certain interval around the measured frequencies, the one with smallest *MOMD* value is chosen as the theoretical frequency. By using the MOMD index, the robustness of the algorithm has been improved significantly, which is verified in the next section. For simplicity, the FRF based model updating methods without and with different frequency matching techniques under comparison are referred to as the original method, the MOMD method and the FDAC method, respectively.

To deal with the problem that in practice usually not all DoFs are measurable and incomplete measured data cannot be directly substituted into equations (4.26), (4.27) and (4.28), a dynamic reduction method is considered which generates the slave DoFs by the master DoFs if a harmonic excitation is applied at the master DoFs. The transformation is given as

$$\begin{bmatrix}\mathbf{x}_{\mathrm{m}}\\ \mathbf{x}_{\mathrm{s}}\end{bmatrix}=\begin{bmatrix}\mathrm{I}\\ -\left(-\omega^2\mathbf{M}_{\mathrm{ss}}+\mathrm{j}\omega\mathbf{C}_{\mathrm{ss}}+\mathbf{K}_{\mathrm{ss}}\right)^{-1}\left(-\omega^2\mathbf{M}_{\mathrm{sm}}+\mathrm{j}\omega\mathbf{C}_{\mathrm{sm}}+\mathbf{K}_{\mathrm{sm}}\right)\end{bmatrix}\left[\mathbf{x}_{\mathrm{m}}\right]=\mathbf{T}_{\mathrm{d}}\mathbf{x}_{\mathrm{m}} \tag{4.31}$$

where subscripts m and s stand for the master and slave DoFs, respectively, and displacement vector $\mathbf{x}$ and mass, damping and stiffness matrices $\mathbf{M}$, $\mathbf{C}$ and $\mathbf{K}$ are divided into sub vectors and sub matrices relating to these DoFs. By suitably dividing the measured DoFs into the master DoFs and the slave DoFs, the theoretical model is reduced by

$$\mathbf{M}_r = \mathbf{T}_d^T \mathbf{M} \mathbf{T}_d, \quad \mathbf{C}_r = \mathbf{T}_d^T \mathbf{C} \mathbf{T}_d, \quad \mathbf{K}_r = \mathbf{T}_d^T \mathbf{K} \mathbf{T}_d \tag{4.32}$$

where $\mathbf{M}_r$, $\mathbf{C}_r$ and $\mathbf{K}_r$ are the reduced mass, damping and stiffness matrices.

It should be noted that the fewer the measured DoFs there are, the less information the experimental FRF data contains and the more model errors the theoretical model produces, which causes the updating procedure to diverge. Thus, the method which updates parameters correctly with fewer measured DoFs is considered to be more robust.

4.4.2 Case study using simulated FRF data

A six-bay truss structure with 25 rods of identical cross-section and 21 DoFs as shown in Figure 4-5, adapted from [78], is used in simulation. The structure is modelled with 2D truss elements. The properties of the structure are Young's modulus of 200GPa, mass density of $7800\,\mathrm{kg/m^3}$ and cross section area of $1800\,\mathrm{mm^2}$. The DoFs are arranged in the order of the node numbers and for each node the horizontal displacement is placed ahead of the vertical displacement.

In this study, two damage scenarios listed in Table 4-2 are considered to gauge the performance of the proposed method. Both damage scenarios are represented by the reduction factor of the mass and stiffness matrices of some elements and for the sake of simplicity, the 'experimental' FRF data from only the first column of the FRF matrices directly obtained by the finite element simulation, are used to update the original intact structure.

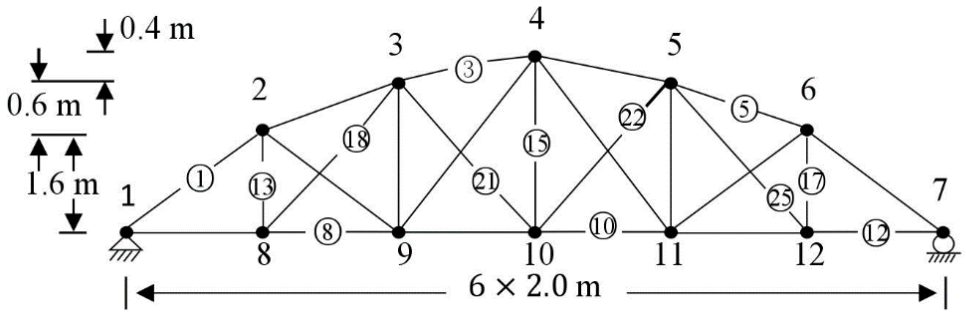

Figure 4-5 Geometry of a truss model.

Table 4-2 Damage scenarios of the truss structure.

Scenario 1			Scenario 2		
Element no.	M (%)	K (%)	Element no.	M (%)	K (%)
7	15	20	7	50	70
12	30	40	12	60	80
21	25	32	21	40	60

First, scenario 1 which represents a moderate damage case is used to get experimental FRF data without noise. Figure 4-6 shows the results of damage identification using both the FDAC and the MOMD methods when all DoFs are measurable. It is clear that the FRF based model updating method is able to update so many parameters at the same time if enough and accurate test data are available.

Scenario 1 is also used to compare the identification performance of the three methods (plus the original method without frequency shift). The minimum number of the required measurable DoFs (MD) is considered a criterion. For the sake of fair comparison, for all the methods the measurable DoFs are removed gradually from the end of the DoF sequence and the experimental frequencies (whose FRFs are measured) are selected at a regular interval in the range of 0 to 900Hz controlled by the total number of measured frequency points, denoted by NF, which is from 20 to 60. Table 4-3 lists the results of this comparison, which shows that the MOMD method can get acceptable updating results using far fewer measured DoFs than the FDAC and the original method. The FDAC method is slightly better than the Original method as it has more acceptable NFs with the same MD. However, it takes the longest time to get the final solution of updating parameters.

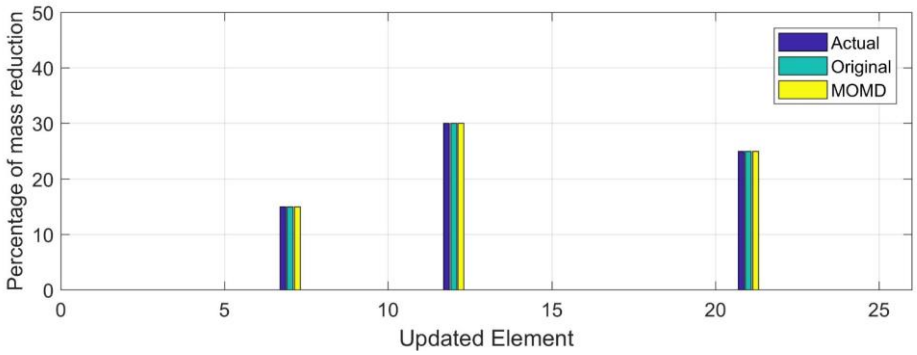

(a)

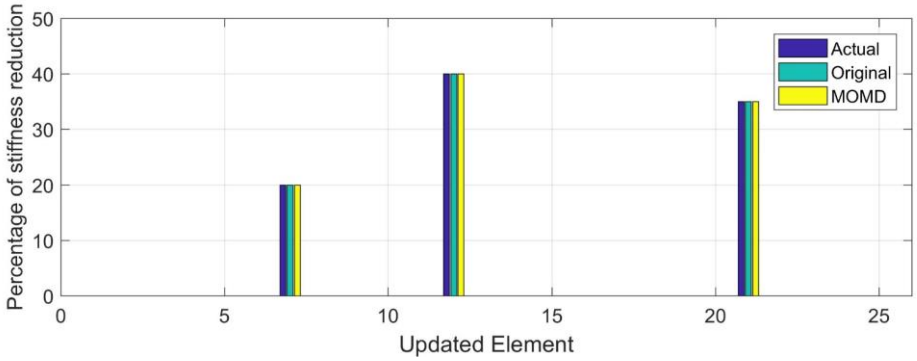

(b)

Figure 4-6 Actual and updating results for damage scenario 1 (top graph for mass and bottom graph for stiffness).

Table 4-3 Updating limits of the three methods.

Method	minimum of MD	Acceptable NF	Single operation time(s) (MD=15,NF=30)
Original	8	21, 24, 32, 38, 40, 58	1.75
MOMD	4	33, 59	4.26
FDAC	8	20, 22, 28, 37, 40, 41, 42, 44, 47, 48, 49, 57, 59	83.86

Secondly, scenario 2 which represents a more severe damage case than scenario 1 is used to compare the performance of the three methods in this extreme circumstance. This time the experimental FRF data is contaminated by 1% white Gaussian white

noise which is introduced though function awgn in MATLAB. Other parameter values are the same as before. The numbers of measured DoFs are from 12 to 18; and the corresponding numbers of acceptable NF, for which an acceptable result can be obtained by the three FRF-based methods are illustrated in Figure 4-7. It is clear that for each number of measured DoFs the MOMD method is more likely to achieve convergence than the original method.

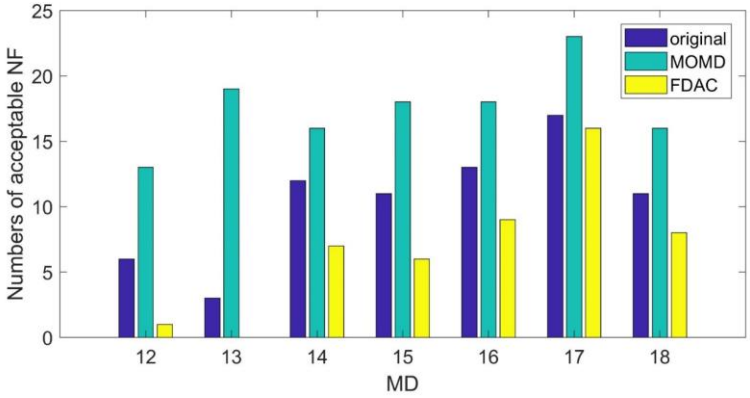

Figure 4-7 Numbers of acceptable NF for the three methods with different numbers of measured DoFs.

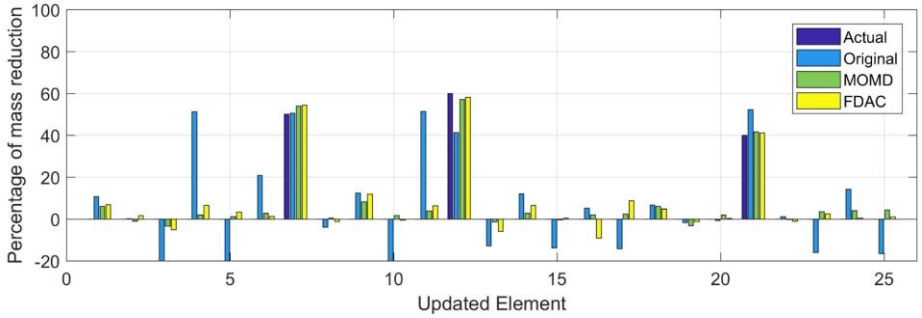

(a)

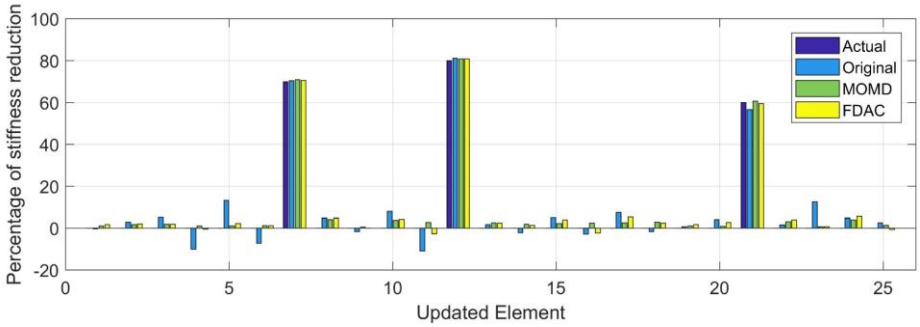

(b)

Figure 4-8 Actual and updating results for damage scenario 2 with 3% white Gaussian noise polluted data (top graph for mass and bottom graph for stiffness).

Then, the proportion of white Gaussian noise is increased to 3% to compare the noise robustness of the three methods. The MD and NF are set to 17 and 30 respectively, by which an acceptable updating results can be obtained by all methods. After enough iterations, the results are considered convergent solutions as shown in Figure 4-8, which illustrate that although all methods are able to identify the damage, the MOMD method makes the best predictions.

In this section, the FRF-based model updating method is shown and a new frequency matching technique is proposed which can be used for the FRF based model updating method. With a small additional amount of computational time, a best theoretical frequency whose FRF has the minimum order of magnitude difference from the experimental one is selected in the vicinity of the related experimental frequency. The results of the simulated truss structure show that the MOMD method makes a big improvement in the performance of convergence over conventional FRF-based identification methods.

4.5 Conclusions

In this section, several common model updating methods are described in detail. Both the sensitivity-based and the GA-based updating theory have played a guiding and supporting roles in the contents of the following chapters. It can be seen that the updating result is susceptible to noise interference. Therefore, it should be ensured that the number of reference responses is sufficiently more than the number of updating parameters to improve robustness.

The FRF-based updating method is slightly different from the modal data-based updating method. A complete column of FRF test data is used in calculating the sensitivity matrix as shown in equation (4.26). This requires that each degree of freedom of a structure must be measured. If this is not possible, the theoretical model will need to be condensed or the experimental data will be expanded, which will introduce certain errors. In a specific updating process, matching the theoretical FRF with the experimental data can improve the convergence. A MOMD method is proposed for its performance due to the traditional FDAC method. In the specific

updating process, the best updating results can be obtained by manually selecting the FRF data of the appropriate frequencies.

Chapter 5 - Modal Strain Energy Based Model Updating Method for Damage Identification on Beam-like Structures

5.1 Introduction

Modal strain energy (MSE) is a sensitive dynamic characteristic for non-destructive damage identification. In the past decades, it has been widely used in damage index methods for localization of damage. However, this kind of methods often make misjudgement, especially for beam- and plate-like structures, because their angular displacements usually cannot be measured directly which play an important role in calculating element model strain energy. In this chapter, using Gaussian smoothing technique and a laser scanning vibrometer, a new MSE-based model updating method is proposed for damage assessment of beam-like structures.

5.2 Background

In civil engineering, damage identification (DI) is always a popular topic that seeks to detect defects in structures at an early stage. Thus, proper maintenance can be implemented in time to avoid a catastrophic loss of life and property. Vibration-based DI, as a global DI technique, has drawn great attention in the past decades.

Theoretically, natural frequencies, mode shapes, the derivatives of mode shapes and their combinations can all be used in vibration-based DI. Reviews of this research field were presented by Doebling, et al. [9] and Fan and Qiao [5]. It can be concluded that mode shapes are more sensitive to local damage than natural frequencies but less than their derivatives. Among the mode shape derivatives, the performances of methods based on mode shape curvature [37], flexibility [30], flexibility curvature [174] and modal strain energy (MSE) [45] were compared by Alvandi and Cremona [175] where the MSE based method showed the best performance. However, it is intuitive that MSE is very sensitive to noise as well as damage, which limits its application to some extent.

MSE can be calculated by the FE method using stiffness matrix and mode shapes. Shi and Law [47] presented a damage localization method which directly used the change ratio of element MSE as a damage index. The theoretical FE model was used as a baseline model and the MSE of the damaged model was calculated from measured mode shape data. A two-story steel plane frame structure was used for experimental verification. Similarly, Shi et al. [48, 49] also proposed their own damage quantification methods. Moradipour et al. [51, 52] improved the formula of calculating the MSE of the damaged model by using the reduced stiffness matrix.

Although MSE has been shown to be a sensitive damage factor, most damage index methods mentioned above have a serious problem: misjudgement. In many papers, even for simulated cases, the damage indices of some undamaged elements were not close to zero while the threshold for detecting damage was usually based on experience or prior knowledge rather than sound science. When noisy data were used, a false alarm was likely, which would reduce confidence in the damage severity assessment based on this indicator.

Compared with precise localization, the ability of MSE based damage index to locate the most possible damage region is more convincing. In many studies, this index was developed as a step-1 method which was used as an effective tool to reduce the damage searching range. Then damage evaluation was done by other methods based on modal data such as frequencies and modes. The evolutionary algorithm based methods like tug-of-war optimization [108], cyclical parthenogenesis algorithm [109] and particle swarm optimization [100] benefitted most from the reduced searching range.

This researcher believes that MSE has the potential to identify damage independently. However, the damage index methods cannot make the most use of the information MSE provides, as most of them utilize the MSE of each element separately. Conversely, model updating method, as an important branch of the DI field, can take advantage of all the measured MSE data at the same time.

However, there is no report in the open literature on model updating method using MSE alone with reliable experimental verification. Jaishi and Ren [176] used global

MSE (MSE of a whole mode) for model updating. The global MSE was then combined with frequency for better performance. The method was not specially designed for DI as it focused on the overall dynamic characteristics of the structure. Cha and Buyukozturk [177] detected damage by minimizing each element MSE. However, the main novelty was the proposed multi-objective optimization approach and the method was applied on only a simulated steel frame structure. Yan and Ren [178] derived a formula to calculate the sensitivity of element MSE by which it was more intuitive to see the influence of damage on each element MSE. Yan, et al. [179] also proposed an element MSE sensitivity based damage index method for damage detection, which showed good performance on DI of three simulated models. This method was close to model updating but it was not experimentally validated.

In reality, generally angular displacements of beam- and plate-like structures are difficult to measure. If measurements of only translational displacements at FE nodes are available, the measured MSE calculated by the two methods, curvature [45] and FE model [47], will be unacceptable for model updating even if an interpolating method [43] or a Guyan reduction method [180] is used. Relatively accurate test data of the damaged structure is a prerequisite for this kind of method. The author recommend to use a finer mesh of measurement points than the FE mesh when element MSE is calculated in terms of curvature [171] and to use strain mode shape measured by strain gauges to calculate element MSE [181, 182], when the FE method is adopted.

In this chapter, a new MSE based model updating method for beam-like structures is presented based on Yan's method. There is a subtle but important improvement to the original formula. Besides, a weighting matrix and a penalty function are incorporated for practical applications. Benefiting from advanced instrumentation such as a scanning laser vibrometer, some modes are measured on more points than the number of the FE nodes and the associated MSEs are calculated. An image filtering technique, Gaussian smoothing [183] is also adopted to reduce the influence of noise. The proposed method is a baseline free method and can localize and quantify cracks in beams accurately in both simulation and experiment.

5.3 Basic theory

In this section, the details of the MSE based model updating method are presented, including the formulas, the updating procedure and the data processing of measurements. It should be noted that the proposed method is valid for crack-like damage.

5.3.1 Sensitivity of element modal strain energy

The eigenvalue problem of a structure with *m* elements and *n* degrees of freedom is

$$\mathbf{K}\boldsymbol{\varphi}_r = \lambda_r \mathbf{M}\boldsymbol{\varphi}_r \tag{5.1}$$

where $\mathbf{K}$ and $\mathbf{M}$ are the global stiffness and mass matrices, respectively; λ_r and $\boldsymbol{\varphi}_r$ are the *r*th eigenvalue and eigenvector of the structure. The global stiffness and mass matrices are the sums of the local ones of individual elements, which can be expressed as

$$\begin{aligned} \mathbf{K} &= \sum_{j=1}^{m} \mathbf{K}_j \\ \mathbf{M} &= \sum_{j=1}^{m} \mathbf{M}_j \end{aligned} \tag{5.2}$$

When the FE method is applied, the MSE of the *j*th element of the *r*th mode can be easily calculated by

$$MSE_{jr} = \frac{1}{2}\boldsymbol{\varphi}_r^{\mathrm{T}} \mathbf{K}_j \boldsymbol{\varphi}_r \tag{5.3}$$

where $\boldsymbol{\varphi}_r$ is normalized by

$$\boldsymbol{\varphi}_r^{\mathrm{T}} \mathbf{M}\boldsymbol{\varphi}_r = 1 \tag{5.4}$$

After the required theoretical MSEs are obtained, they will be tuned to the experimental ones by updating selected parameters. Traditional model updating methods can be roughly divided into two categories: sensitivity and evolutional based methods. The former is chosen as it will save much computing time when a large number of updating parameters are used.

To apply the sensitivity based method, the first-order derivative of element MSE with respect to each updating parameter must be calculated by

$$\frac{\partial MSE_{jr}}{\partial p} = \frac{\partial \boldsymbol{\varphi}_r^{\mathrm{T}}}{\partial p}\mathbf{K}_j\boldsymbol{\varphi}_r + \frac{1}{2}\boldsymbol{\varphi}_r^{\mathrm{T}}\frac{\partial \mathbf{K}_j}{\partial p}\boldsymbol{\varphi}_r \tag{5.5}$$

To calculate the first-order derivatives of mass normalized mode shapes, different methods were compared by Lee and Jung [66], and a method was proposed by them:

$$\begin{Bmatrix} \dfrac{\partial \boldsymbol{\varphi}_r}{\partial p} \\ \dfrac{\partial \lambda_r}{\partial p} \end{Bmatrix} = \begin{bmatrix} \mathbf{K} - \lambda_r\mathbf{M} & -\mathbf{M}\boldsymbol{\varphi}_r \\ \boldsymbol{\varphi}_r^{\mathrm{T}}\mathbf{M} & 0 \end{bmatrix}^{-1} \begin{Bmatrix} -(\dfrac{\partial \mathbf{K}}{\partial p} - \lambda_r\dfrac{\partial \mathbf{M}}{\partial p})\boldsymbol{\varphi}_r \\ \dfrac{1}{2}\boldsymbol{\varphi}_r^{\mathrm{T}}\dfrac{\partial \mathbf{M}}{\partial p}\boldsymbol{\varphi}_r \end{Bmatrix} \tag{5.6}$$

For damage detection, it is assumed that damage will cause a decrease in the stiffness of certain elements while the mass of these elements will stay the same. In this chapter, the remaining stiffness as a proportion of each element's original stiffness is taken as the updating parameter whose value is limited within [0, 1]. Then, the *j*th (*j* = 1, 2, …, *m*) element stiffness matrices of the damaged structure can be represented by

$$\mathbf{K}_j^{\mathrm{d}} = p_j\mathbf{K}_j \tag{5.7}$$

By this assumption, the sensitivities of the damaged global/local stiffness and mass matrices to the *i*th updating parameter are given as

$$\begin{gathered} \frac{\partial \mathbf{K}^{\mathrm{d}}}{\partial p_i} = \frac{\partial \mathbf{K}_i^{\mathrm{d}}}{\partial p_i} = \mathbf{K}_i, \quad \frac{\partial \mathbf{K}_j^{\mathrm{d}}}{\partial p_i} = 0, \quad i \neq j \\ \frac{\partial \mathbf{M}^{\mathrm{d}}}{\partial p_i} = 0 \end{gathered} \tag{5.8}$$

The sensitivity of *j*th element MSE of the *r*th mode to the *i*th parameter is expressed by

$$\frac{\partial MSE_{jr}}{\partial p_i} = S_{ijr} \tag{5.9}$$

where S_{ijr} is calculated from equations (5.5), (5.6) and (5.8). Please note that when using equation (5.5) and (5.6), $\mathbf{K}$ and $\mathbf{K}_j$ should be replaced by $\mathbf{K}^{\mathrm{d}}$ and $\mathbf{K}_j^{\mathrm{d}}$, respectively.

5.3.2 Calculation of residuals

The aim of model updating is to minimize the residuals between the selected MSEs of the theoretical model and the damaged structure. It can be written as an optimization problem whose objective function is

$$f(\mathbf{p}) = \boldsymbol{\varepsilon}_{\mathbf{mse}}^{\mathrm{T}} \boldsymbol{\varepsilon}_{\mathbf{mse}}, \quad 0 < p_i \le 1, \quad i = 1, 2, ..., m$$
$$\boldsymbol{\varepsilon}_{\mathbf{mse}} = \mathbf{MSEd} - \mathbf{MSEa}(\mathbf{p}) \tag{5.10}$$

where **MSEa**(**p**) is the theoretical element MSE vector of the current updating parameters and **MSEd** is the measured element MSE vector from the damaged structure.

This optimization problem is solved by the sensitivity based method which is also regarded as the iteration based method. In each iteration, the parameters are updated to minimize the objection function by the following equation:

$$\boldsymbol{\Delta}\mathbf{MSEa} = \mathbf{S}_{\mathbf{mse}} \boldsymbol{\Delta}\mathbf{p} = \boldsymbol{\varepsilon}_{\mathbf{mse}} = \mathbf{MSEd} - \mathbf{MSEa}(\mathbf{p}_k) \tag{5.11}$$
$$\mathbf{p}_{k+1} = \mathbf{p}_k + \boldsymbol{\Delta}\mathbf{p}$$

where k represents the kth iteration. $\mathbf{S}_{\mathbf{mse}}$ is a matrix of S_{ijr} for the corresponding parameter and element MSE, calculated from equation (5.9). As for the residual part, the theoretical element MSE is easy to be obtained while the **MSEd** must be calculated from the measured mode shapes. In Yan et al.'s method [179], the element MSE of the damaged structure is calculated by

$$MSEd_{jr} = \frac{1}{2} \boldsymbol{\varphi}_r^{\mathrm{d}\,\mathrm{T}} \mathbf{K}_j^{\mathrm{d}} \boldsymbol{\varphi}_r^{\mathrm{d}} = p_j \frac{1}{2} \boldsymbol{\varphi}_r^{\mathrm{d}\,\mathrm{T}} \mathbf{K}_j \boldsymbol{\varphi}_r^{\mathrm{d}} \tag{5.12}$$

where $\boldsymbol{\varphi}_r^{\mathrm{d}}$ is the measured mode shape of the rth mode and $\mathbf{K}_j^{\mathrm{d}}$ is the damaged element stiffness matrix which contains the updating parameter to be determined. Thus, the $\mathbf{S}_{\mathbf{mse}}$ and $\boldsymbol{\varepsilon}_{\mathbf{mse}}$ have to be adjusted in their work. That method works for simulated examples. However, when experimental measurements are used, the authors recommend the following equation which is further discussed in section 5.4.

$$MSEd_{jr} = \frac{1}{2} \boldsymbol{\varphi}_r^{\mathrm{d}\,\mathrm{T}} \mathbf{K}_j \boldsymbol{\varphi}_r^{\mathrm{d}} \tag{5.13}$$

Rather than using the FE method, in this research, the curvature based method is used for more accurate calculations, whose formula is

$$MSEd_{jr} = \frac{1}{2} \int_{x_j}^{x_{j+1}} EI^* (v_{xx})^2 \mathrm{d}x = EI \frac{1}{2} \int_{x_j}^{x_{j+1}} (v_{xx})^2 \mathrm{d}x \tag{5.14}$$

where v_{xx} is the mode shape curvature, and EI is the bending stiffness. By assuming that the real stiffness EI^* is affected by the damage slightly, EI is considered unchanged and the damage is only reflected by the curvature change. With much more

measurement points than the FE nodes, the angular displacements and the curvatures are obtained by the measured displacements as

$$v_{x,i} = \frac{v_{i+1} - v_i}{h}, \quad v_{xx,i} = \frac{v_{x,i+1} - v_{x,i}}{h} \tag{5.15}$$

where i represents the ith measurement point and h is the distance between 2 measurement points.

5.3.3 Data processing

In equation (5.15) the finite difference method is used to calculate the mode shape curvature. A smaller h will produce more accurate v_{xx} theoretically while it will amplify the noise influence at the same time. In order to reduce the noise effect, Gaussian smoothing [183], also referred to as Gaussian blur or Gaussian filter, is introduced to process the data to get more precise curvature from measured displacements. This technique is originally used to 'blur' images which will remove noise but inevitably some useful information. It is very suitable for denoising measured MSE as the curvature of the damage structure is supposed to be fairly smooth without noise and integration is less affected by such 'blur'.

The Gaussian filtering of the response of a point outputs the weighted average of the responses at that point and its neighbours. The weighting of each point is calculated by the Gaussian distribution

$$G(x) = \frac{1}{\sqrt{2\pi}\sigma} \mathrm{e}^{-\frac{x^2}{2\sigma^2}} \tag{5.16}$$

where σ is the standard deviation of the distribution, x is the distance between the afore-mentioned reference point and one of all the other points within this neighbourhood. This distribution is illustrated in Figure 5-1.

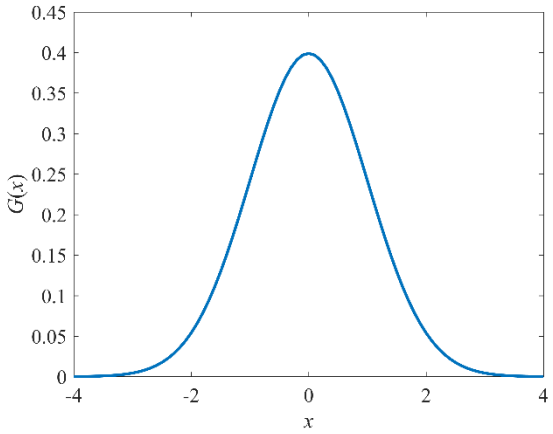

Figure 5-1 1-D Gaussian distribution with σ=1.

The weightings should also be normalized to make sure that their sum is 1. Then the measured data are filtered by this vector through convolution operation. The noise-induced fluctuation is decreased and its great performance is shown in section 5.5.

After reliable curvature measurements are obtained, an interpolation method is used to get a better integration result in equation (5.14). In each element, the integration region is divided into subregions whose meshes are finer than the measurement mesh, and in each subregion the curvature is assumed to be constant. The values of these parts equal to their left points which are determined by the nearest 3 measurement points through the following curve fitting equation

$$v_{xx}(x) = c_0 + c_1 x + c_2 x^2 \tag{5.17}$$

Moreover, the experimental translational displacement and angular displacement data at the FE nodes are also obtained through the interpolation, which allows the whole displacement data to be mass normalized initially as the FE mode shapes

$$\mathbf{dis}_r = \mathbf{dis}_r * 1/(\boldsymbol{\varphi}_r^{\mathrm{d}\,\mathrm{T}} \mathbf{M} \boldsymbol{\varphi}_r^{\mathrm{d}}) \tag{5.18}$$

where $\mathbf{dis}_r$ is the measured displacement vector of the *r*th mode.

It is easy to prove that the theoretical model will give the same mode shape result even if a different *E* is used for the whole structure. Thus, the initial values of *E* and ρ do not need to be very accurate as each of them has the same effect on all the element MSE respectively and only damage will change element MSE if the mode shapes are normalized to the same mass matrix. This means that there is no need to have test data

of the intact structure and MSE based model updating is a baseline free damage identification method.

5.3.4 Model updating procedure

Besides efficient data processing to make MSE measurements more reliable, the objective function in model updating can be improved through introducing weightings. A different weighting for each measurement and a penalty function are added in equation (5.10). The new objection function is defined as

$$\begin{aligned} f(\mathbf{p}) &= \boldsymbol{\varepsilon}^{\mathrm{T}}\mathbf{W}_{\mathbf{mse}}\boldsymbol{\varepsilon}^{\mathrm{T}} + w_g g(\mathbf{p}), \quad 0 < p_i \le 1, \quad i = 1,2,...,m \\ \boldsymbol{\varepsilon}^{\mathrm{T}} &= \mathbf{MSEd} - \mathbf{MSEa}(\mathbf{p}) \\ g(\mathbf{p}) &= \sum_{i=1}^{m} \left(\frac{1}{a(p_i - b)}\right)^2 \end{aligned} \tag{5.19}$$

$\mathbf{W}_{\mathbf{mse}}$ is the weighting matrix to make MSE of different modes have a similar influence. It is a diagonal matrix whose elements are calculated by

$$W_{mse,i,i} = \frac{1}{(\mathrm{mean}(\mathbf{MSEd}_r))^2} \tag{5.20}$$

where W_{mseii} represents the weighting of the *i*th residual which belongs to the *r*th mode. $\mathrm{mean}(\mathbf{MSEd}_r)$ is the average value of all the measured element MSEs of the *r*th mode.

w_g in equation (5.19) is the weighting of the penalty function which is used to adjust the influence of the two parts in the objective function and is set to 20 in the following sections.

The proposed MSE based model updating method is mainly used for DI. Theoretically, there is no reason for the value of any of the updating parameters to become greater than 1. So it is reasonable to add a penalty function $g(\mathbf{p})$ to stop the procedure from producing meaningless results. In the penalty function, the upper bound is set as *b* whose value should be slightly more than 1 to allow $p_i = 1$. *a* is a very large value to ensure that the penalty function has little influence when $p_i \le 1$. In this chapter, *a* and *b* are set to 10000 and 1.05, respectively.

The sensitivity of the penalty function is also shown and the new objective function is minimised with respect to $\mathbf{p}$ though the following equations

$$\begin{cases} S_{gii} = \dfrac{-1}{a(p_i - b)^2}, & i = 1, 2, \ldots m \\ S_{gij} = 0, & i \neq j \\ \varepsilon_{gi} = \dfrac{-1}{a(p_i - b)}, & i = 1, 2, \ldots m \end{cases} \tag{5.21}$$

$$\mathbf{\Delta p} = (\mathbf{S}^{\mathrm{T}}\mathbf{W}\mathbf{S})^{-1}\mathbf{S}^{\mathrm{T}}\mathbf{W}\mathbf{r} \tag{5.22}$$

$$\begin{cases} \mathbf{S} = \begin{bmatrix} \mathbf{S}_{\mathbf{mse}} \\ \mathbf{S}_{\mathbf{g}} \end{bmatrix} \\ \mathbf{W} = \begin{bmatrix} \mathbf{W}_{\mathbf{mse}} & \\ & \mathbf{W}_{\mathbf{g}} \end{bmatrix} \\ \mathbf{r} = \begin{Bmatrix} \boldsymbol{\varepsilon}_{\mathbf{mse}} \\ \boldsymbol{\varepsilon}_{\mathbf{p}} \end{Bmatrix} \end{cases}$$

The above equations are easy to understand and hence are not explained in detail here. As mentioned before, many iterations will be needed to get a converged solution. Also, in each iteration the step length of parameter change should also be limited by sl so that

$$\begin{cases} \mathbf{\Delta p} = \mathbf{\Delta p}, & \max(\mathbf{\Delta p}) < sl \\ \mathbf{\Delta p} = \mathbf{\Delta p}\dfrac{sl}{\max(\mathbf{\Delta p})}, & \max(\mathbf{\Delta p}) \geq sl \end{cases} \tag{5.23}$$

Control of the step length is very important because the problem is nonlinear and the sensitivity matrix is only valid in a small range of **p** (and thus must be updated in iterations). The value of sl should be much smaller than b-1 to prevent any parameter from exceeding the upper bound b in equation (5.19). sl used in this chapter is set to 0.01.

Finally, the procedure of the proposed method is summarized as follows:

- **Step 1**: Select the elements to be updated and modes to be used in the procedure.
- **Step 2**: Calculate the required **MSEd** in equation (5.14) from the measured data and the data processing technique.

- **Step 3**: In each iteration, calculate the current sensitivity matrix $\mathbf{S}_j$, the weighting matrix $\mathbf{W}$ and the residual vector $\mathbf{r}_j$ by the input $\mathbf{p}_j$ and **MSEd** in equation (5.22). Initially, $\mathbf{p}_0 = \mathbf{1}$.
- **Step 4**: Solve the least square solution $\mathbf{\Delta p}$ in equation (5.22).
- **Step 5**: Ensure that the step length satisfies equation (5.23). Then check if $\|\mathbf{\Delta p}\|_2 < c$ (c is a given tolerance), the updating procedure converges; otherwise set $\mathbf{p}_{j+1} = \mathbf{p}_j + \mathbf{\Delta p}$ and go to Step 3.

After model updating, the location and severity of damage are exposed as the proportional loss of each element's stiffness by the updated parameters. The severity evaluated by model updating method has its own physical meaning, which is better than the damage index method.

5.4 Numerical simulation

In this section, a simply supported beam, similar to the numerical example used in reference [179], is used to verify the proposed method. The beam is divided into 15 elements and its geometrical data are shown in Figure 5-2. The material properties are set as 32GPa in Young's modulus, 2500 kg/m^3 in mass density and 0.3 in Passion's ratio (which can represent reinforced concrete).

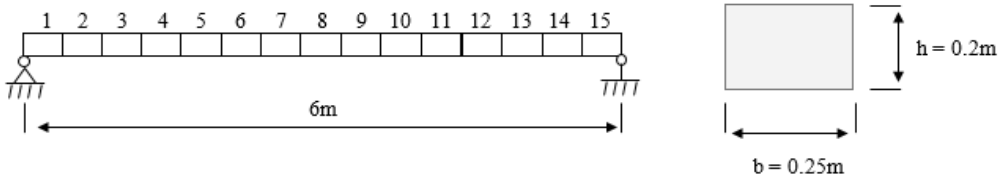

Figure 5-2 Simulate simply supported beam and its geometry.

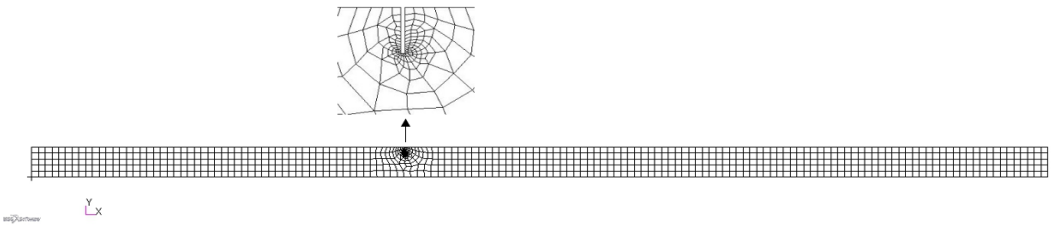

Figure 5-3 Beam model with damage of a crack built in Patran.

The theoretical model of the beam in Figure 5-2 is built in Matlab using Euler-Bernoulli beam elements whose updating parameters defined in equation (5.7) are updated to detect damage of another model with the same dimensions and material but with a crack. This damaged model is built in Patran using 2D quadrilateral shell elements (CQUAD4) whose *z*-direction deflections of all nodes are fixed to 0 to allow only in-plane vibration. The crack locates at 2.2m from the left, which is at the centre of the 6th element of the theoretical model, and the depth of the crack is 0.05m from the top. As shown in Figure 5-3, a much finer mesh, especially at the tip of the crack, is applied on the beam in the commercial software while the mesh seed of the bottom line of the model is exactly 0.08m. Vibration data of this damaged model solved by Nastran are used as 'measured' data.

Initially, the 'measured' data are used to obtain the element MSEs of the model built in Matlab in the damaged state and the 1st mode element MSEs of 4 different sources are compared in Figure 5-4(a). The 4 sources are referred to as 'curvature method', 'real result', 'intact model' and 'FE1 method', respectively, and are defined below.

The 'curvature method' refers to the element MSEs computed from equation (5.14) and (5.15) using the 'measured' translation displacements of the nodes on the bottom line of the damaged model (Figure 5-3). This is also the suggested way in this chapter.

The 'real result' refers to the element MSEs computed directly from the detailed FE model (as shown in Figure 5-3) in Nastran. The element MSEs of the shell elements in the corresponding region of each beam element are added up to get its MSE in the damaged state.

The ‘intact model’ refers to the element MSEs of the theoretical model (Figure 5-2) when all the elements are undamaged.

The ‘FE1 method’ refers to the calculated element MSEs from equation (5.13). The translational displacement and angular displacement data at the FE nodes that are obtained after the ‘curvature method’ are now used.

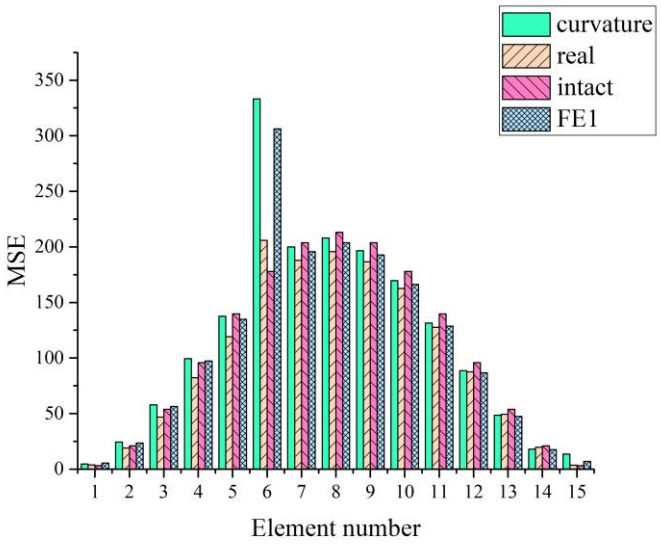

(a)

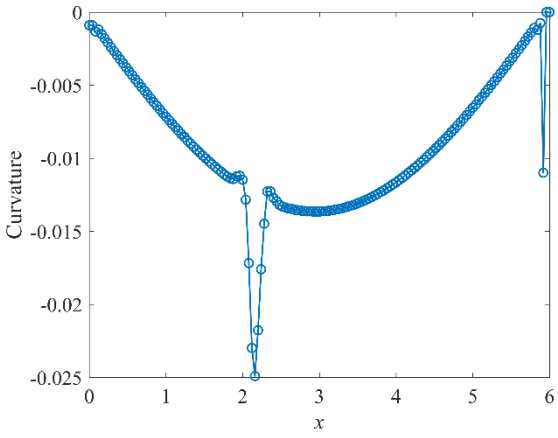

(b)

Figure 5-4 MSE calculation: (a) Comparison of element MSEs of 1st mode from different sources; (b) Curvature of the 1st mode.

From Figure 5-4(a), it is clear that the largest difference in element MSEs exists in element 6 which is just the element with crack in the damaged model. So element

MSEs are capable of reflecting damage. There are slight computation errors of MSEs by the curvature method at the undamaged elements compared with the real ones, and this error is much larger at the damaged element. The reason should be that the real stiffness EI^* of the beam is considerably reduced at the crack location but is assumed to be unchanged in equation (5.14). Usually, the absolute value of the mode shape curvature is largest in such a region as shown in Figure 5-4(b). Thus, it can be concluded that the curvature method produces a much larger element MSE of the damaged element than the real one, which is regarded as a merit for DI in this research as this method can expose the damage area.

The FE1 method gives similar results to the curvature method, as it also uses the undamaged stiffness matrix to calculate element MSEs. This method can be used instead of the curvature method if the measured translational displacements and angular displacements are reliable and sufficient in number. However, there is a higher possibility for FE1 method to produce large errors as it uses fewer measured data.

The difference between element MSEs of the real result and the intact model shows the influence of stiffness loss in element 6. This influence is illustrated in more detail in Figure 5-5 where the element MSEs of the theoretical model under different input of p_6 are shown. As damage increases in element 6, the MSE of the damaged element increases while the MSEs of the other elements decrease monotonously. Therefore, MSE is a reliable indicator in the sensitivity-based model updating method.

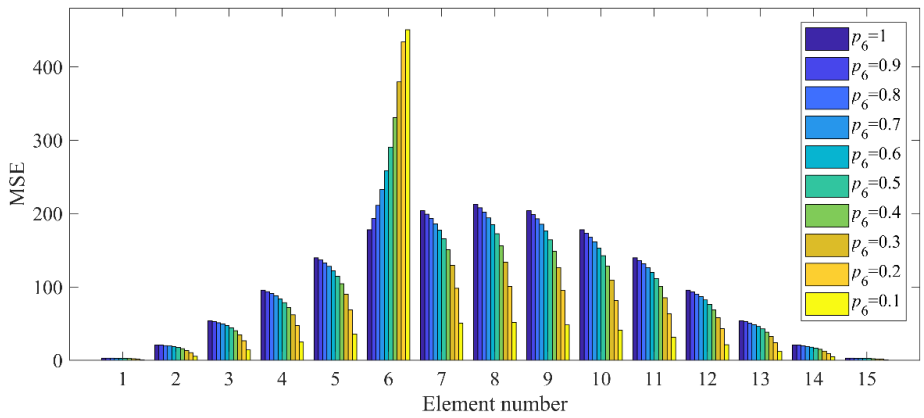

Figure 5-5 Element MSEs of 1st mode calculated by theoretical model with different values.

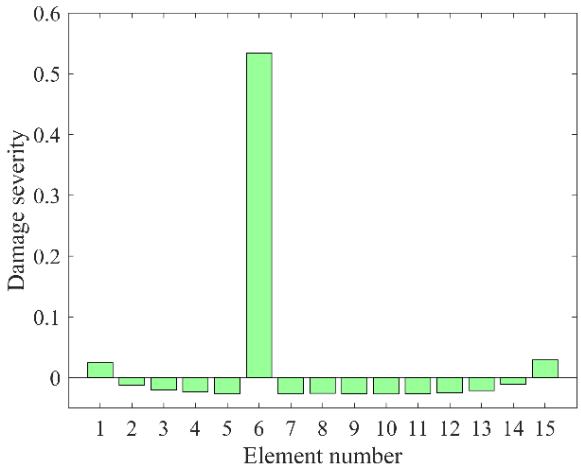

(a)

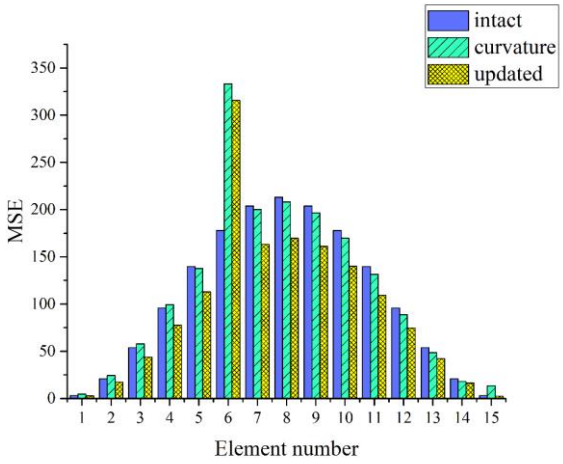

(b)

Figure 5-6 Updating results of the data from curvature method: (a) Damage severity represented by $\mathbf{1}-\mathbf{p}_{\mathrm{d}}$; (b) MSE comparison.

The proposed model updating procedure is applied based on the element MSEs from the curvature method. In this simulation, only the data of the 1st mode are used as enough information is available from them without measurement noise. The updated parameter vector, $\mathbf{p}_{\mathrm{d}}$, is shown in Figure 5-6(a) in terms of $\mathbf{1}-\mathbf{p}_{\mathrm{d}}$ to represent the severity of the damage. It is clear that the MSE based model updating method can accurately locate the damage.

The MSEs of the updated model are compared with the ones from the intact model and the curvature method in Figure 5-6(b), which shows that the updated model's MSE of

the damaged element is close to the MSE from the curvature method. However, as mentioned before, the curvature method overestimates that MSE, which amplifies damage severity and the differences between MSEs of other undamaged elements as p_6 decreases. The updating procedure tends to increase all the parameter values (the stiffness) of these undamaged elements, which would cause a reduction in those differences. However, this increase would be constrained by the penalty function. That is why in Figure 5-6(a), there is a small decrease in the values of damage severity of most undamaged elements. It should be noted that although in this simulation the measurement noise is absent, there are still modelling errors and numerical errors in the 'measured' data. Thus, the errors in the final values of the updating parameters are considered acceptable.

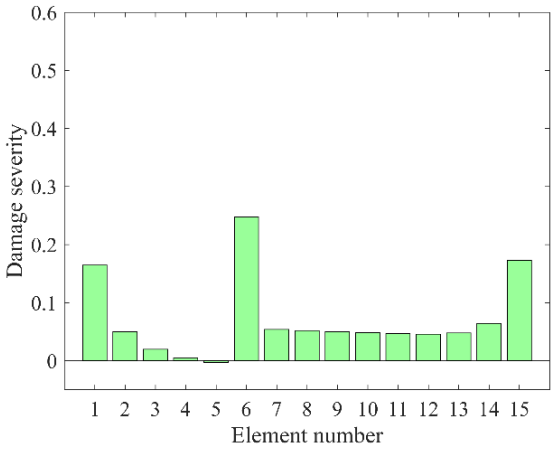

(a)

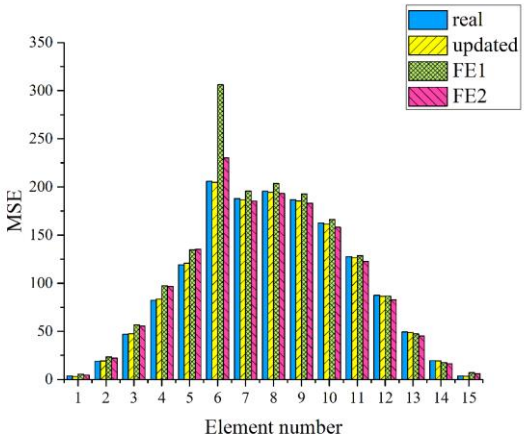

(b)

Figure 5-7 Updating results of the data from real result: (a) Updated parameters change from 1; (b) MSE comparison.

As a comparison, the updating result based on the element MSEs of the real result is also presented. The updated MSEs are very close to the real ones, as shown in Figure 5-7(b). However, the DI result shown in Figure 5-7(a) is not good enough. Even though the largest damage is located in element 6, there are obvious false alarms in elements 1 and 15. Moreover, there exist considerable errors in the updating result of elements 7 to 14. This time the MSE of the damaged element is not overestimated; but, the effects of the modelling error and integration error in the updating procedure have increased compared with the effects of the cracks. Also, the evaluated damage severity of the damaged element becomes lower than that predicted by the curvature method, which causes the errors of other elements to increase, as shown when Figure 5-6(a) and Figure 5-7(a) are compared. The updated parameters may produce close theoretical element MSEs to the ones of the real result, while their changes, $\mathbf{1}-\mathbf{p}_{\mathrm{d}}$, cannot reflect damage well. Of course, some extra efforts could be made to improve this DI result. However, it is preferred to use the curvature method directly for simplicity and the exposure of damage.

The updated parameters are also used to calculate the 'measured' element MSEs from equation (5.12), using damaged stiffness matrix and 'measured' mode shape data, which is referred to as 'FE2 method' shown in Figure 5-7(b). It can be seen that overall the MSEs of the FE2 method are closer to the real ones than FE1 while there is still a considerable error in the damaged element. Therefore, there is no guarantee that the result of using data from the FE2 method will be better than the curvature method and FE1 method in this simulation, let alone a few challenges that need to be overcome before using this method as the damage is not known in advance.

In this simulation, the proposed method shows good performance in DI. The effect of damage is amplified by using the curvature method to calculate the 'measured' MSEs, which helps to detect damage at an early stage. Although the method actually overestimates the severity of the damage, the evaluation can still be used to reveal the severities of different damage, especially for the different severities of damage at the same location. The method also shows a good resistance to modelling errors and numerical errors. The influence of measurement noise together with the performance of the Gaussian smoothing technique is analysed in the next section.

5.5 Experimental setup and results

In this section, the proposed method is validated by experimental measurements of a cantilever beam. The beam is made of aluminium having dimensions of $0.64\times0.02\times0.02\text{m}^3$ and is fixed between two metal blocks with 4 bolts to apply a sufficient preload to implement clamping. Damage is introduced as 2 small cracks cut at specified locations. Details of the cracks are listed in Table 5-1 and 99 measurement points are distributed along the beam as shown in Figure 5-8(b). A PSV-500 scanning laser vibrometer is used to set up the measurement mesh and acquire the velocity responses at these points. This device can perform non-contact measurements with high precision and can greatly save test time when there are a large number of points which need to be measured repeatedly.

The whole experimental setup (shown in Figure 5-8(b)) also involves a shaker (LDS V406) fixed at the free end of the beam, a force sensor inserted between the shaker and the beam to measure the input force, and an amplifier to boost input signals from the PSV-500 system. In practice, the mode shapes are measured in 2 steps. Firstly, a pseudorandom excitation in the frequency range of 0-2000 Hz is generated by the PSV-500 system and the natural frequencies of the beam are estimated from the measured FRF peaks. Secondly, sinusoidal excitation signals near the natural frequencies are generated to ensure that they are strong and stable signals and the measured responses are regarded as the mode shapes of the corresponding frequencies. In this test, the measured natural frequencies and the frequencies of excitation used are listed in Table 5-2.

Table 5-1 Information of crack configurations.

Cracks	Location (m)	Corresponding element	Depth (m)	Width(m)
Crack 1	0.014	4	0.006	0.001
Crack 2	0.034	9	0.006	0.001

Table 5-2 Natural frequencies of the damaged beam and the used driving frequencies of the shaker.

Modes	Natural frequencies (Hz)	Driving Frequencies (Hz)
1	36.3	33
2	229.4	230
3	640.0	635
4	1241.9	1254

(a)

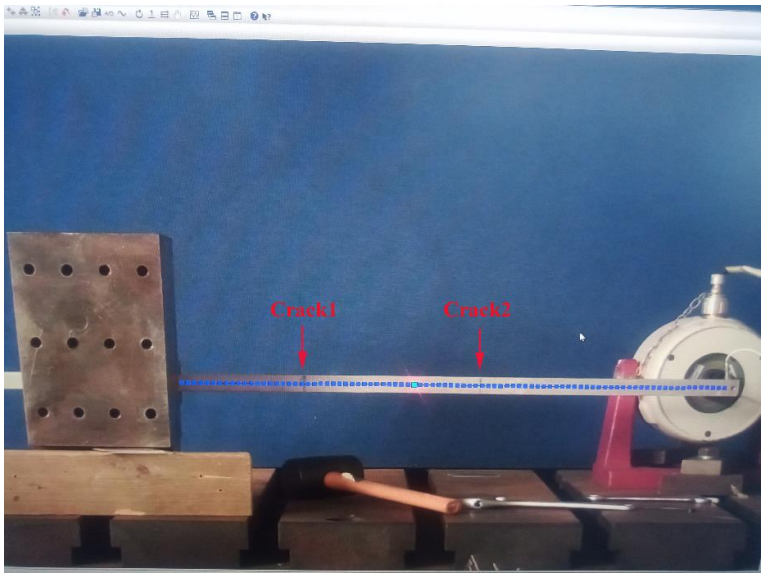

(b)

Figure 5-8 Photos of test on a cantilever beam: (a) Experimental setup; (b) Measurement points set up by PSV-500 system.

As this method is a baseline free method, common aluminium material properties are used: 69 GPa in Young's modulus, 2700 kg/m^3 in mass density and 0.33 in Passion's ratio. An FE model similar to the one shown in Figure 5-2 is built with fixed-free boundary conditions (the beam is divided into 16 elements). Then, the measured mode shape data are normalized and element MSEs of different modes are calculated based on this theoretical model.

Even though the measured mode shape data at each point are an average of 60 responses at the same location, it is not precise enough, as the mesh is too fine. Hence Gaussian smooth technique is adopted. In this research, the technique is applied before each finite difference calculation is performed (equation (5.15)), using the 'fspecial' and 'imfliter' functions of MATLAB. For different measured mode shape data, the input function parameters are carefully chosen to reduce fluctuation in the data. The curvatures of mode 1 calculated with and without smoothing are shown in Figure 5-9. It is clear that the calculation of curvature is significantly improved by applying Gaussian smoothing technique. Also, the MSEs can reflect the damage better than the curvature, as the effect of noise is reduced by the integration in equation (5.14).

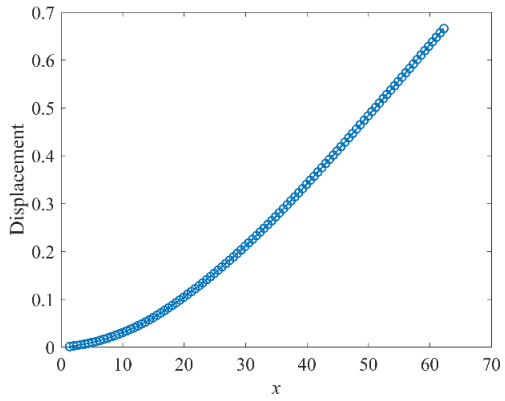

(a) Measured mode shape displacement.

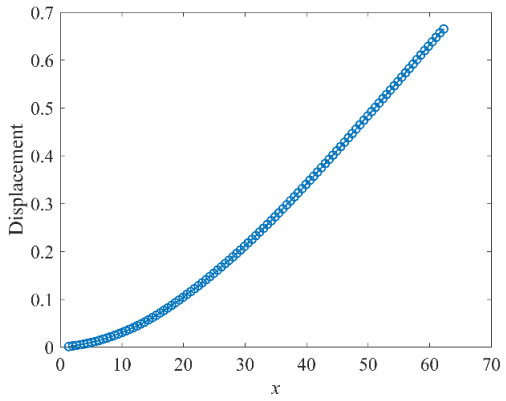

(b) Smoothed displacement.

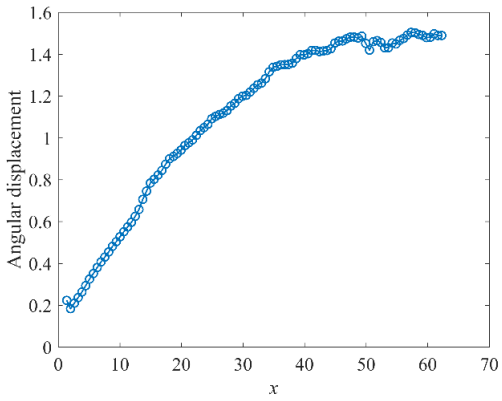

(c) Angular displacement calculated from (a).

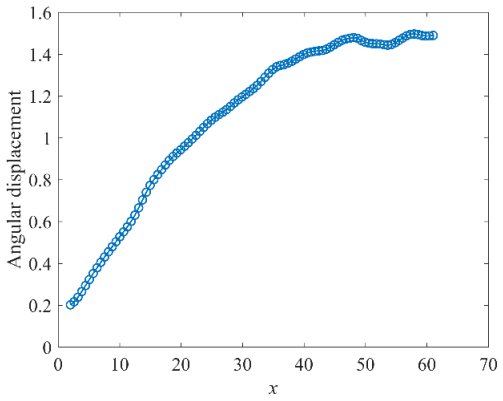

(d) Smoothed angular displacement calculated from (b).

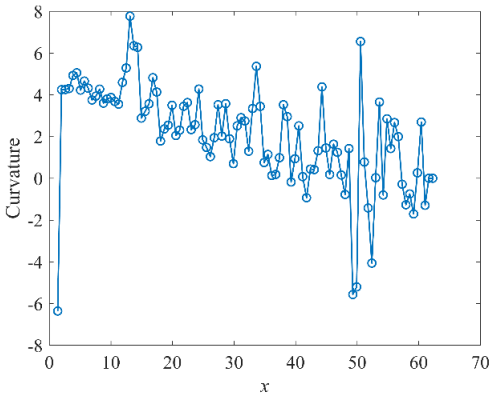

(e) Curvature calculated from (c).

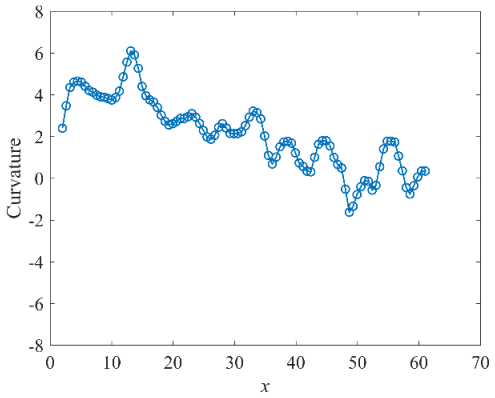

(f) Curvature calculated from (d).

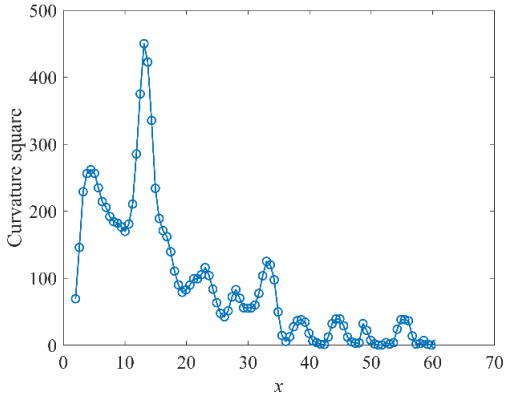

(g) Normalized curvature square from (b), (d) and (f).

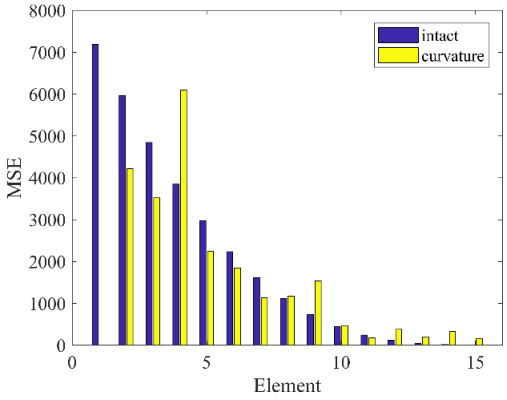

(h) MSE calculated by curvature method compared with that of the intact theoretical model.

Figure 5-9 MSE calculation based on the experimental data.

However, in the practical application, the MSEs of elements 1 and 16 cannot be calculated correctly by the curvature method. The first reason is that it is hard to obtain

measurement data near the two ends of the beam due to the presence of the clamp and the shaker. Additionally, the measured mode shape values at those points near the two ends cannot be smoothed properly as there are not enough left/right points for averaging. In Figure 5-9(g), it is obvious that the first several points of the MSE are incorrect, as they should form a downward trend since the MSE of element 1 should be the largest in the 1st mode. In this chapter, only the calculation of MSEs of elements 2 to 15 is guaranteed to be accurate, so parameters 2 to 15 are selected in updating. This limitation is caused by insufficient measurement capability rather than the updating method itself.

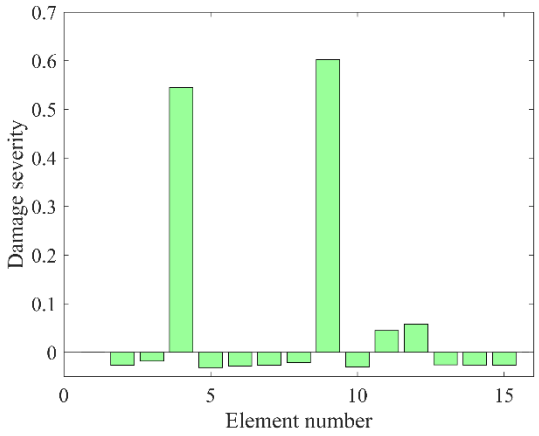

Figure 5-10 Updating results of the experimental data shown by reduced proportion.

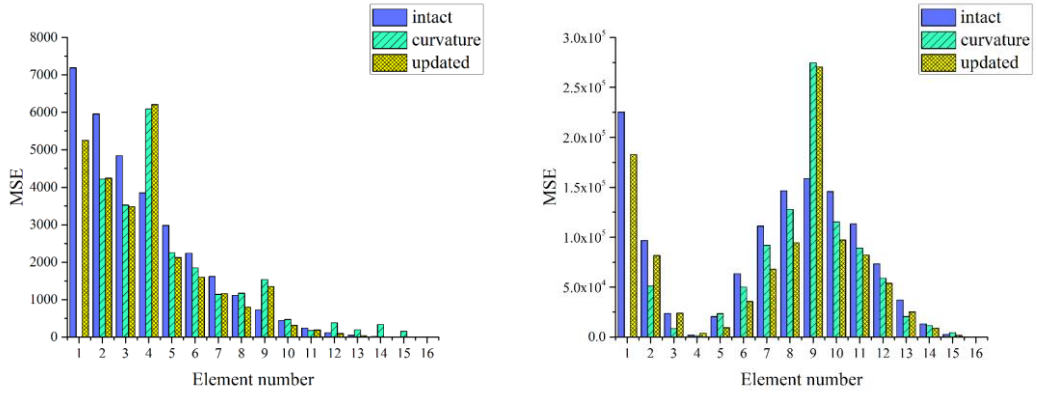

(a) (b)

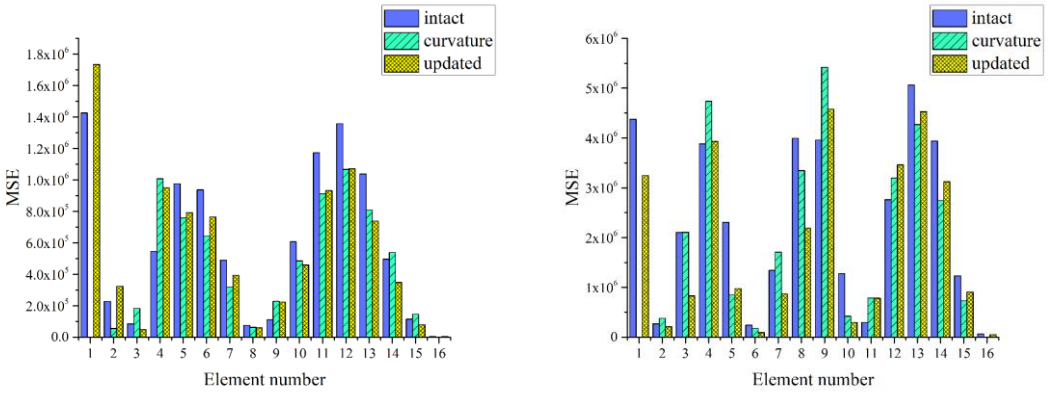

(c) (d)

Figure 5-11 Comparison of MSE of different modes between the intact model, calculated by the curvature method and the updated model: (a) Mode 1; (b) Mode 2; (c) Mode 3; (d) Mode 4.

The MSEs of the first 4 modes are used in the model updating procedure shown in Figure 5-11 and the updating result is shown in Figure 5-10. Cracks are correctly located at elements 4 and 9 with quite accurate evaluation of relative severity. The MSEs of the updated model are also compared with those of the intact model and the measured ones. It can be seen that there are many obvious differences between some element MSEs of the updated model and the measured ones. However, based on the reasonable objective function proposed in this chapter, the effect of measurement noise and modelling errors is reduced to a very low level. Thus, this method is verified as an effective and robust multi-damage identification method for beam-like structures.

It should be noted that an element MSE cannot reflect damage if its value is small. For example, it is hard to see the difference between MSE of element 4 of mode 2 of the intact model and the measured one in Figure 5-11(b). That is why measurements of 4 modes are used to get a good result, or some false positives will be seen in the elements near the free end. Nonetheless, the damage in elements 4 and 9 can always be detected. In contrast, the precise updating result of element 16 can hardly be obtained even though its MSE measurement is available, as its value is close to 0 for all modes. As far as DI is concerned, parts of the structure like element 16 can be ignored since their damage usually does not affect the function of the structure. As for parts of structures

like element 1, it can be detected by using extra tools to measure its MSE or using a local damage detection technique.

5.6 Influence of damping

In reality, the existence of damping is inevitable. It will cause the measurement result of the mode shape to become a complex vector. Since damping is not the focus of this thesis, in the previous section, the magnitude of measured complex mode shape data are used as normal modes, and the effect of damping is simply classified as that of noise. In this section, a numerical simulation is used to demonstrate the effect of damping itself on the proposed method.

Damping is a mathematical approximation used to reflect the energy dissipation of materials. Two types of damping are generally used for linear-elastic materials: viscous and structural. The structural damping force is proportional to displacement. In Patran's simulation, the structural damping coefficient can be added directly from the material property settings, which will cause the calculated natural frequencies to increase. However, structural damping has little influence on the mode shapes. The imaginary part of the complex modes can be ignored and the measured MSE do not change in the simulation.

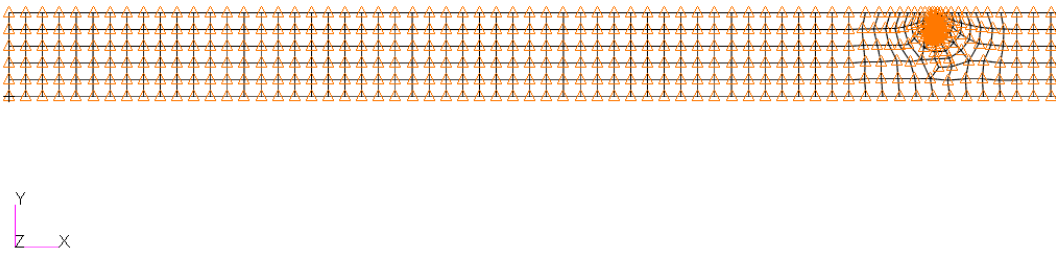

Figure 5-12 Beam with grounded viscous dampers (view of part of the beam that covers the crack).

The viscous damping force is proportional to velocity. It can decrease the natural frequencies and raise the proportion of the imaginary part of the complex modes. But viscous damping cannot be set directly in the material property. Instead, each node of the beam used in Section 5.4 is connected to a grounded viscous damper (only Y-

direction is restricted) as shown in Figure 5-12. In this way, the viscous damping from the grounded damper will mainly affect the first mode of the beam. This effect is regarded similar to that caused by the material viscous damping.

The damping coefficient (dc) is required to be an input for all the dampers. 4 cases are compared in which the dc has been set to 0, 5, 20, 50, respectively. The corresponding modal damping ratios are as 0, 0.703, 0.2814, 0.7096, respectively, calculated by the following equation (ω_d and ω_n are obtained from Nastran .f06 file):

$$\omega_d = \sqrt{1-\xi^2}\,\omega_n \tag{5.24}$$

where ξ is the modal damping ratios, ω_n is the undamped natural frequency and ω_d is the damped natural frequency.

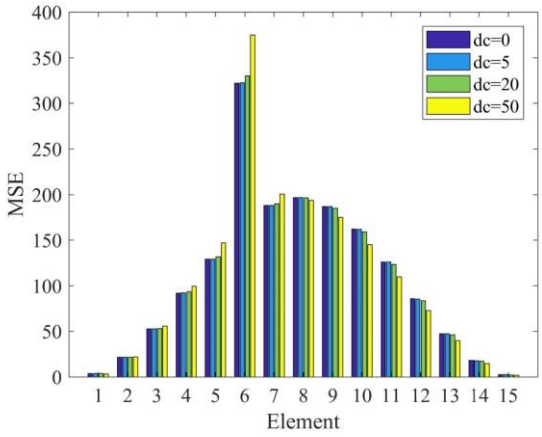

Figure 5-13 The 1st mode MSE calculation results comparison.

Based on the magnitude of the complex mode shape data, the 1st mode MSE calculation results of the 4 cases are calculated by equation (5.14). As shown in Figure 5-13, when the value of dc is below 20, the 1st mode MSE data of the damped beam are almost the same with the undamped beam (dc=0), which means the viscous damping will not affect the damage identification result if the modal damping ratio is less than 0.3.

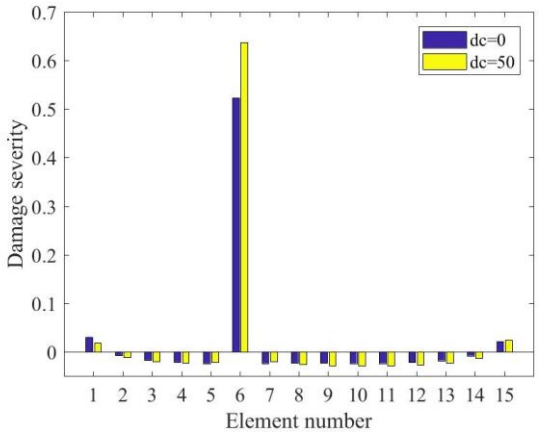

Figure 5-14 Updating results of the 2 cases.

Besides, in the extreme case (dc=50), the influence of the viscous damping is obvious. For example, the 1st complex mode shape of a random node is -4.4e-2 - 3.3e-4i. Although the MSE data calculated in this case have big differences from the other cases, the damage identification result of this case is still acceptable as shown in Figure 5-14, which is a strong proof of the robustness of the proposed method.

The effect of material damping on real structure is more complicated. However, through the analysis of this section and the experiment in Section 5.5, it can be concluded that for the low-damping materials commonly used in engineering, the method proposed in this chapter is not much affected by the damping and is feasible for damage identification.

5.7 Conclusion

In this study, a modal strain energy (MSE) based model updating method is proposed for damage identification. This method is a baseline free method which can locate and quantify multiple damages at the same time. Measured element MSEs are calculated from curvatures, and Gaussian smoothing technique is introduced to get reliable curvature data based on modal displacement measurements. Cases of a simulated simply supported beam and an experimental cantilever beam are used to validate the effectiveness of this method. The results show that this method can identify damage correctly and is robust to the measurement noise from the test of using a scanning laser vibrometer. The proposed method is recommended for structures with low-damping

materials and should perform even better if a more advanced MSE testing technique is available.

Chapter 6 - A Kriging model-based finite element model updating method for damage detection.

6.1 Introduction

Model updating is an effective means of damage identification and surrogate modelling has attracted considerable attention for saving computational cost in finite element (FE) model updating especially for large-scale structures. This chapter presents a new surrogate model-based model updating method taking advantage of the measured FRFs. The Frequency Domain Assurance Criterion (FDAC) is used to build the objective function whose nonlinear response surface is constructed as a Kriging model. Then, the efficient global optimization (EGO) algorithm is introduced to get the model updating results. The proposed method has good accuracy and robustness, which are verified by a numerical simulation of a cantilever and experimental test of a laboratory three-story structure. The main content of this chapter was published in reference [184].

6.2 Background

In early research, the sensitivity-based and evolutionary algorithm-based model updating methods had achieved great success. However, one of the main limitations of model updating methods in engineering applications is computational efficiency. In theory, the denser the FE mesh is, the more accurate prediction of the structural response is — a dense FE mesh improves the reliability of the model updating results. However, a very fine FE mesh will result in a considerable increase in the computational time of a single theoretical model response. If the model updating procedure requires a considerable number of iterations to converge, the required computation time will be long and even become unacceptable, especially when running FE analyses of complicated structures.

In this context, the surrogate model (also called the response surface method), as a quick alternative to computer experiments (FE analysis), has attracted the attention of many researchers. The core idea of a surrogate model is to replace the FE analysis

model with a much more simplified model for the relationship between the parameters and the response. After confirming the accuracy of the surrogate model, the response of the original model is calculated directly through this model to achieve the purpose of a quick solution.

At present, the surrogate model-based global optimization has been extended to nonlinear optimization problems [185]. There have been many applications of surrogate models in place of the finite element models. Ren and Chen [114], and Fang and Perera [8], Fang and Perera [113] use the response surface method for model updating and damage identification. The polynomial of a particular order is used to fit the relationship between the parameters and the responses. In most cases, the first and second-order polynomials are the two most commonly used models:

$$\begin{aligned} y &= f(x_1, x_2, \cdots, x_n) + \varepsilon = \beta_0 + \sum_{i-1}^{n} \beta_i x_i + \sum_{i<j} \sum_{j=2}^{n} \beta_{ij} x_i x_j + \varepsilon \\ y &= f(x_1, x_2, \cdots, x_n) + \varepsilon = \beta_0 + \sum_{i-1}^{n} \beta_i x_i + \sum_{i-1}^{n} \beta_{ii} x_i^2 + \sum_{i<j} \sum_{j=2}^{n} \beta_{ij} x_i x_j + \varepsilon \end{aligned} \tag{6.1}$$

where y is an output response, x_i is one of n input parameters (usually the updating parameters), ε denotes the unconsidered residual between the real value and the mathematical expression. The least-squares method is used to determine the coefficients (β_i) of the polynomial based on reasonable initial sampling [2, 8, 113, 114, 186] (using D-optimal design or central composite design). A small number of sampling points can be effectively used to predict the response of the structure under different parameters. The second formula contains more quadratic terms about the updating parameters, so that it can better describe the gradient change of the response surface compared with the first formula. In practical applications, the order of the polynomial selected should be judged based on the approximate shape of the response surface.

Furthermore, as a special response surface construction method similar to the Gaussian basis function [118], the Kriging model has received more and more attention in recent years [119]. Khodaparast, et al. [187] used a Kriging model to establish the relationship between the positional parameters of two beams and the frequency of the whole structure, for fast interval model updating to define the uncertain range of the

parameters. Liu, et al. [120] proposed a 2-level model updating method based on Kriging predictor for large complex structures.

Most of the methods mentioned above have chosen the frequency as the output response of the surrogate model. This is mainly because the response surface of a frequency has a relatively gentle shape with respect to different system parameters. Especially when a polynomial is used as the mathematical construct of a surrogate model, the frequency is not sensitive to the cross terms of the polynomial. So an accurate response surface can be built from a small number of sample points. On the other hand, the FRF can provide more structural vibration information than the frequency and its use as the response in surrogate modelling is worth investigating, which has rarely been attempted.

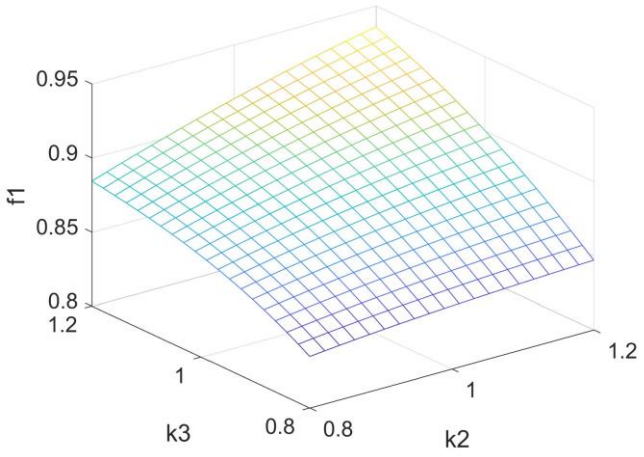

(a)

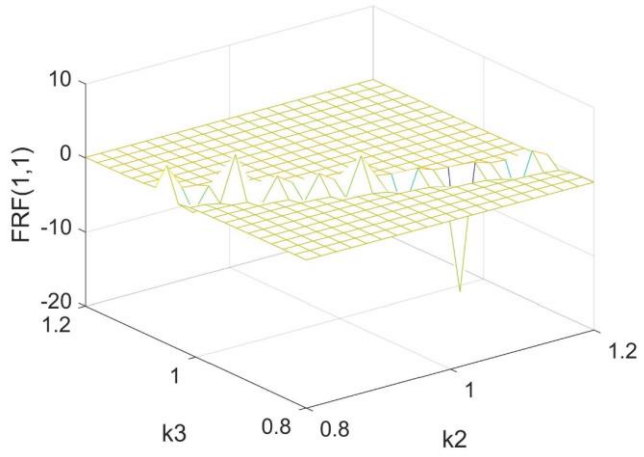

(b)

Figure 6-1 Real response surface of (a) First order frequency; (b) FRF(1,1).

This is mainly because the response surfaces of the FRF data are difficult to be built. Figure 6-1 shows the real response surface of the first-order frequency and a specified FRF (FRF(1,1) at frequency 0.45) of the model in section 4.3 while the 2 variables are the coefficients (changing from 0.8 to 1.2) of the k_2 and k_3 whose default values are $70\mathrm{N/m}$ and $120\mathrm{N/m}$, respectively. It is obvious that it is easy to use mathematical tools to approximate the frequency response surface while the FRF response surface can hardly be simulated.

Therefore, in this chapter, a new strategy is proposed to utilize those responses that change sharply with the updating parameter in the response surface-based model updating method. When dealing with the FRF data, a Kriging model with good simulation performance of a nonlinear response surface is constructed to establish the relationship between the updating parameters and the residual of the FDAC value, and a model updating method is used based on the Kriging model for damage identification. The EGO algorithm is introduced to realize fast convergence of the updating procedure. The proposed method is applied to a simulated example of a cantilever beam with 3 weakened elements and a laboratory three-story frame structure to verify its effectiveness.

6.3 Kriging based model updating method

In this section, the theory of the Kriging based model updating method is presented. Generally, it requires two steps to build a precise Kriging model. The first step is to build a Kriging model through initial sample points generated by design of experiments (DOE). The second step is to add a new sample point by a specified infill criterion and rebuild the Kriging model until the precision of the prediction value meets the requirements.

In this chapter, the Latin hypercube sampling (LHS) method is used to produce initial sample points, the number of which is usually 10 times the dimension. The infill criterion is described in section 6.3.3.

6.3.1 Construction of Kriging Model

A Kriging model is a surrogate model based on a stochastic process. It was originally put forward in geostatistics and made its way into engineering design following the work of Sacks, et al. [188]. For a given set of sample data (input), $\mathbf{X}=\left\{\mathbf{x}_1,\mathbf{x}_2,\cdots,\mathbf{x}_{\mathrm{n}}\right\}^{\mathrm{T}}$, and the observed responses (output), $\mathbf{Y}=\left\{y_1,y_2,\cdots,y_{\mathrm{n}}\right\}^{\mathrm{T}}$, the expression of the Kriging model that reflects the relationship between them is :

$$y(\mathbf{x}_i)=\mathbf{f}^{\mathrm{T}}(\mathbf{x}_i)\boldsymbol{\beta}+z(\mathbf{x}_i),\quad i=1,2,\cdots,n \tag{6.2}$$

where $\mathbf{f}(\mathbf{x}_i)$ is a polynomial vector of the sample $\mathbf{x}_i$, $\boldsymbol{\beta}$ is the vector of the linear regression coefficients to be estimated and $z(\mathbf{x}_i)$ represents errors and is assumed to be a stochastic process that follows a normal distribution of $N(0,\sigma^2)$ with a zero mean and standard deviation σ.

It should be noted that the basic assumption of the Kriging model is that the same input will lead to an identical output. Therefore, the deviation between the output response and the polynomial regression part is only due to the modelling error itself, regardless of the measurement error and other random factors. This method does not depend on the simulated precision of the polynomial part to the response surface, but focuses on constructing the appropriate surrogate model by effective filling of the stochastic process part, which makes it more suitable for dealing with nonlinearity. Thus, the polynomial part is often taken as a constant in some other references.

To estimate the stochastic process $z(\mathbf{x})$, Kriging assumes that the true response surface is continuous, and any two points will trend to have the same value as the distance in between approaches zero and it is the same for $z(\mathbf{x})$ of two points. Thus, the correlation between $z(\mathbf{x})$ of any two sample points can be expressed as a function of their spatial distance. The most widely used Gaussian correlation model is adopted here:

$$R(z(\mathbf{x}_i),z(\mathbf{x}_j))=\exp\left(-\sum_{k=1}^{m}\theta_k\left|x_i^k-x_j^k\right|^2\right) \tag{6.3}$$

where x_i^k and x_j^k are the kth components of the two sample points $\mathbf{x}_i$ and $\mathbf{x}_j$, m denotes the number of design variables, θ_k controls the decay rate of correlation on different

dimensions. And then the matrix of correlation functions between sample points is obtained as

$$\mathbf{R}=\begin{bmatrix} R(\mathbf{x}_1,\mathbf{x}_1) & \cdots & R(\mathbf{x}_1,\mathbf{x}_n) \\ \vdots & \ddots & \vdots \\ R(\mathbf{x}_n,\mathbf{x}_1) & \cdots & R(\mathbf{x}_n,\mathbf{x}_n) \end{bmatrix} \tag{6.4}$$

Then the likelihood function of the sample point can be written as:

$$L=\frac{1}{\left(2\pi\sigma^2\right)^{m/2}\left|\mathbf{R}\right|^{1/2}}\exp\left[-\frac{\left(\mathbf{Y}-\mathbf{F}\boldsymbol{\beta}\right)^{\mathrm{T}}\mathbf{R}^{-1}\left(\mathbf{Y}-\mathbf{F}\boldsymbol{\beta}\right)}{2\sigma^2}\right] \tag{6.5}$$

where $\mathbf{F}$ is a matrix of vector $\mathbf{f}(\mathbf{x})$ for each sample point. $|\mathbf{R}|$ is the determinant of $\mathbf{R}$ which is a function of θ_k. According to the maximum likelihood function method, one can get:

$$\begin{aligned} \hat{\boldsymbol{\beta}} &= (\mathbf{F}^{\mathrm{T}}\mathbf{R}^{-1}\mathbf{F})^{-1}\mathbf{F}^{\mathrm{T}}\mathbf{R}^{-1}\mathbf{Y} \\ \hat{\sigma}^2 &= \frac{\left(\mathbf{Y}-\mathbf{F}\boldsymbol{\beta}\right)^{\mathrm{T}}\mathbf{R}^{-1}\left(\mathbf{Y}-\mathbf{F}\boldsymbol{\beta}\right)}{n} \end{aligned} \tag{6.6}$$

Based on this, the logarithmic form of the maximum likelihood function can be written as:

$$\ln(L)\approx-\frac{m}{2}\ln(\hat{\sigma}^2)-\frac{1}{2}\ln\left|\mathbf{R}\right| \tag{6.7}$$

The maximum value of the function above is solved by the genetic algorithm to determine the value of the decay rate θ_k on different dimensions.

At this point, a Kriging model linking the sample point and the response is constructed. The next step is to predict the value of new points. For any point $\mathbf{x}_0$, following the principle that the predicted value for the point continues to maximize the augmented likelihood function of both the sample point and the new point, the predicted response value can be obtained by:

$$\hat{y}(\mathbf{x}_0)=\mathbf{f}^{\mathrm{T}}(\mathbf{x}_0)\hat{\boldsymbol{\beta}}+\mathbf{r}^{\mathrm{T}}(\mathbf{x}_0)\mathbf{R}^{-1}(\mathbf{Y}-\mathbf{F}\hat{\boldsymbol{\beta}}) \tag{6.8}$$

and the mean squared error of the predictor can also be calculated to estimate the accuracy of the predicted value, which is denoted by $\hat{s}^2(\mathbf{x})$:

$$\hat{s}^2(\mathbf{x})=\sigma^2\left[1-\left\{\mathbf{f}^{\mathrm{T}}(\mathbf{x}),\mathbf{r}^{\mathrm{T}}(\mathbf{x})\right\}\begin{bmatrix}0 & \mathbf{F}^{\mathrm{T}}\\ \mathbf{F} & \mathbf{R}\end{bmatrix}^{-1}\begin{Bmatrix}\mathbf{f}(\mathbf{x})\\ \mathbf{r}(\mathbf{x})\end{Bmatrix}\right] \tag{6.9}$$

where $\mathbf{r}^{\mathrm{T}}(\mathbf{x}_0)$ is a row vector of correlation function between the new point and each sample point:

$$\mathbf{r}^{\mathrm{T}}(\mathbf{x}_0) = \left[R(\mathbf{x}_0, \mathbf{x}_1), \cdots, R(\mathbf{x}_0, \mathbf{x}_n)\right] \tag{6.10}$$

It is worth noting that when the value of the *i*th sample point is predicted, since $\mathbf{r}^{\mathrm{T}}(\mathbf{x}_i)\mathbf{R}^{-1}$ equals the *i*th order unit vector (whose elements are all zero except the *i*th element which is one), equation (6.8) becomes:

$$\hat{y}(\mathbf{x}_i) = \mathbf{f}^{\mathrm{T}}(\mathbf{x}_i)\hat{\boldsymbol{\beta}} + y_i - \mathbf{f}^{\mathrm{T}}(\mathbf{x}_i)\hat{\boldsymbol{\beta}} = y_i \tag{6.11}$$

which shows that Kriging model predicts the real response value at the sample point. That is why it can be considered an interpolation technique. Interested readers can refer to references [116, 189] for a more detailed presentation of the theory, and to reference [188] for a more detailed formulation based on the idea of the best linear unbiased predictor.

6.3.2 Kriging model in model updating

Model updating technique is to make the theoretical model, usually the FE model, produce a response as closely as possible to the experimental data. The traditional sensitivity-based model updating method uses the sensitivity matrix to correlate the updating parameters with the residuals of the response, which is the first derivative of the response residual with respect to the updating parameters, and then iteratively solves the associated optimization by the (weighted) least-squares method. However, this method usually requires the knowledge of all the degrees of freedom (DoFs) of the FE model. When some DoFs cannot be measured, the model condensation technique shall be used and if the number of measured response points is much smaller than the number of the model degrees of freedom, this method will fail to give a unique solution.

Model updating can be essentially considered an optimization problem which can be formulated in the following form:

$$\min f(\mathbf{x}), \text{ s.t. } \quad lb_j < x_j < ub_j, \quad j = 1, 2, \cdots, n \tag{6.12}$$

where $f(\mathbf{x})$ is the objective function and usually the response residual between theoretical prediction and experimental data, design variable x_j is the *j*th parameter of

the structure to be updated, lb_j and ub_j are the lower and upper bound of x_j, respectively.

By solving this optimization problem, design variable vector $\mathbf{x}$ which minimizes the objective function (response residual) gives the right updating parameter values. Besides using the sensitivity method which can also be regarded as the steepest descent method, the artificial intelligence algorithm is also convenient. In this chapter, the widely used genetic algorithm (GA) is selected again. The advantage of this method is that it is easy to update some special parameters of which the sensitivity matrices are difficult to calculate and to specify the interval of parameters to prevent them from convergence to meaningless results.

Of course, due to the strong complementarity among the updating parameters, the optimization problem of model updating is a typical multi-peak problem. The algorithm can easily cause convergence to a local optimal solution if the number of updating parameters is large. In addition, the core problem of this approach is that a huge number of objective function values at different sets of design variables are required by the GA to find the global minimum. If the computation time taken to evaluate a single value of the objective functional from the theoretical model is long, the total duration of solution by the algorithm may be unacceptable. That is why a Kriging model is required here to calculate the objective function instead of the original FE model.

There are two ways to use the Kriging model to improve the computational efficiency in the model updating procedure. Firstly, the response of the FE model is used as the output response. A precise Kriging model is constructed for every response to totally replace the FE analysis in the subsequent model updating procedure. However, this kind of usage is mainly for the frequency as response and for a few updating parameters. When it comes to FRF, for Kriging model construction, not only many measured responses are required, but also many sample points are required since the true response surface of the FRF is much more complicated than that of the frequency.

These are the main reasons why in this chapter the second way is taken in which the value of the objective function of the optimization is directly used as the output response of the Kriging model. In so doing, only one Kriging model is required to be built and the EGO algorithm is adopted to obtain the model updating results, which is described in the next subsection.

However, it is unwise to set the residual of FRF between the theoretical and experimental FRF models as the objective function, because there is easily a big difference in magnitude between the two FRFs at a specified frequency and in this case, their residual may overwhelm the influence of the smaller residuals at other frequencies.

Hence Frequency Domain Assurance Criterion, proposed by Pascual [80, 81] to compare the correlation between two FRFs, is introduced to be the objective function:

$$f = \sum_{i=1}^{n} w_i (1 - |FDAC(\omega_i)|) \tag{6.13}$$

where n is the number of selected frequencies, ω_i is the ith frequency, and w_i is the weighting.

The revised FDAC given in [77] is adopted:

$$FDAC(\omega) = \frac{\begin{Bmatrix} \mathbf{h}_{\mathrm{a}}^{\mathrm{R}}(\omega) \\ \mathbf{h}_{\mathrm{a}}^{\mathrm{I}}(\omega) \end{Bmatrix}^{\mathrm{T}} \begin{Bmatrix} \mathbf{h}_{\mathrm{x}}^{\mathrm{R}}(\omega) \\ \mathbf{h}_{\mathrm{x}}^{\mathrm{I}}(\omega) \end{Bmatrix}}{\left\| \begin{Bmatrix} \mathbf{h}_{\mathrm{a}}^{\mathrm{R}}(\omega) \\ \mathbf{h}_{\mathrm{a}}^{\mathrm{I}}(\omega) \end{Bmatrix} \right\| \left\| \begin{Bmatrix} \mathbf{h}_{\mathrm{x}}^{\mathrm{R}}(\omega) \\ \mathbf{h}_{\mathrm{x}}^{\mathrm{I}}(\omega) \end{Bmatrix} \right\|} \tag{6.14}$$

where $\mathbf{h}$ is a specified column of the FRF matrix, $\boldsymbol{\omega}$ is the frequency, subscripts “a” and “x” are corresponding to the theoretical and experimental data respectively and superscripts “R” and “I” denote the real part and imaginary part of the FRF vector $\mathbf{h}$, respectively. It follows from equation (6.14) that FDAC values are limited to the interval [-1, 1], regardless of the modulus value difference between two vectors.

There are 2 more main advantages of the proposed objective function:

1. It contains more physical meanings during the model updating procedure, which can improve the reliability of the updating results.
2. The shape of the response surface becomes more gentle, which reduces the fitting difficulty of the Kriging model.

Moreover, unlike the sensitivity-based method, it is not necessary to use FRFs of all the DoFs to calculate the FDAC value. The consistency of several sets of FRF curves is sufficient to ensure correct updating results, which allows elimination of the measured data with low signal to noise ratio.

6.3.3 Efficient Global Optimization

The EGO algorithm was proposed by Jones, et al. [189] as an effective method using response surfaces for global optimization. In that method a Kriging model was constructed between the design variables and the objective function of the optimization problem and only the accuracy of the location where the minimum value might exist was of interest. By only adding sample points in these effective areas, the purpose of solving the optimization problem using only a small number of sample points is achieved.

After constructing the Kriging model by the initial sample points, it is easy to get the prediction and its mean squared error of any point by equation (6.8) and equation (6.9). The EGO algorithm treats the uncertainty in the prediction as a Gaussian probability density function with the predicted value as mean value and the mean squared value as variance, as shown in Figure 6-2. When finding a new point to be added in the sample points, the algorithm does not simply select the point with the minimum value of the current Kriging model, but rather selects the point with the maximum value of the expected improvement (ei) relative to the minimum value of the current responses at all the sample points. Based on the Gaussian probability density function, *ei* is calculated by:

$$
\begin{aligned}
&I(\mathbf{x}) = y_{\min} - y(\mathbf{x}) \\
&ei(\mathbf{x}) = E[I(\mathbf{x})] = \int_0^{\infty} I(\mathbf{x}) \cdot \left\{ \frac{1}{\sqrt{2\pi}\hat{s}^2(\mathbf{x})} \exp\left[-\frac{(y_{\min} - I(\mathbf{x}) - \hat{y}(\mathbf{x}))^2}{2\hat{s}^2(\mathbf{x})} \right] \right\} dI \\
&= (y_{\min} - \hat{y}(\mathbf{x}))[\frac{1}{2} + \frac{1}{2}\mathrm{erf}(\frac{(y_{\min} - \hat{y}(\mathbf{x}))}{\hat{s}(\mathbf{x})\sqrt{2}})] \\
&+ \hat{s}(\mathbf{x}) \frac{1}{\sqrt{2\pi}} \exp[-\frac{(y_{\min} - \hat{y}(\mathbf{x}))^2}{2\hat{s}^2(\mathbf{x})}]
\end{aligned}
\tag{6.15}
$$

where $y_{\min}$ is the minimum response value of the sample points, $I(\mathbf{x})$ is the improvement of the minimum value by adding a new point, $\mathrm{erf}(\cdot)$ is the cumulative distribution function, and $EI(\mathbf{x})$ is the expectation of that improvement. Usually the smaller the predicted value of the unknown point is, the larger the MSE is, and the larger the value of EI is, as shown in Figure 6-2 (a) in which the right axis is only for the expected improvement. The calculation of expected improvement at x=0.7 is illustrated in Figure 6-2 (b). Only the red region is valid for *EI* calculation which is controlled by $y_{\min}$.

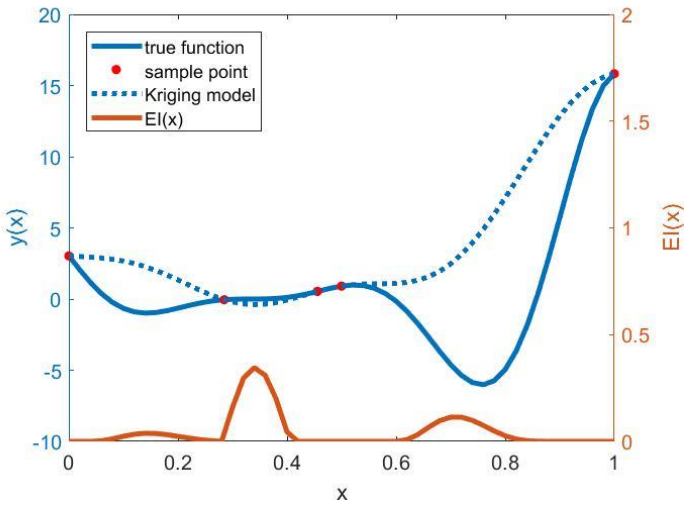

(a)

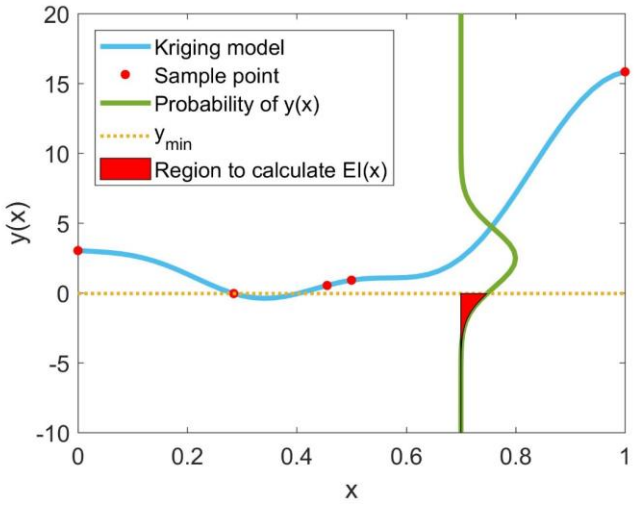

(b)

Figure 6-2 (a) The expected improvement of a one-variable function calculated by the Kriging model constructed through five sample points; (b) A graphical interpretation of the expected improvement at x=0.7.

Thus, the infill criterion of the EGO algorithm not only finds the minimum value of the Kriging model (local search) but also explores the region with high mean squared error (global search). After adding enough sample points, the Kriging model will be accurate in the region where the minimum of the objective function exits and the global optimization problem is solved efficiently. In this thesis, the solution for the location of the maximum expectation is also done by GA. And the stopping criterion is set as:

$$\max(EI(\mathbf{x})) \le \varepsilon_1 \tag{6.16}$$

where ε_1 is a small positive number that controls the precision and the convergence speed of the algorithm.

However, a shortcoming of the EGO algorithm in this study is that its precision of the local minimum value is not particularly high since it puts a certain amount of effort into the global search. Thus it can be considered a step to find the area in which the global minimum exists and a supplementary process is implemented which keeps adding the point with the minimum value of the Kriging model as a new sample point until the following criterion is reached:

$$\left\|\mathbf{x}_{\text{new}} - \mathbf{x}_{\text{min}}\right\| \le \varepsilon_2 \tag{6.17}$$

where $\|\cdot\|$ is the Euclidean distance between the new sample point $\mathbf{x}_{new}$ and $\mathbf{x}_{min}$ whose output response is minimum among current sample points, and the small positive number ε_2 denotes the tolerance for termination of iteration.

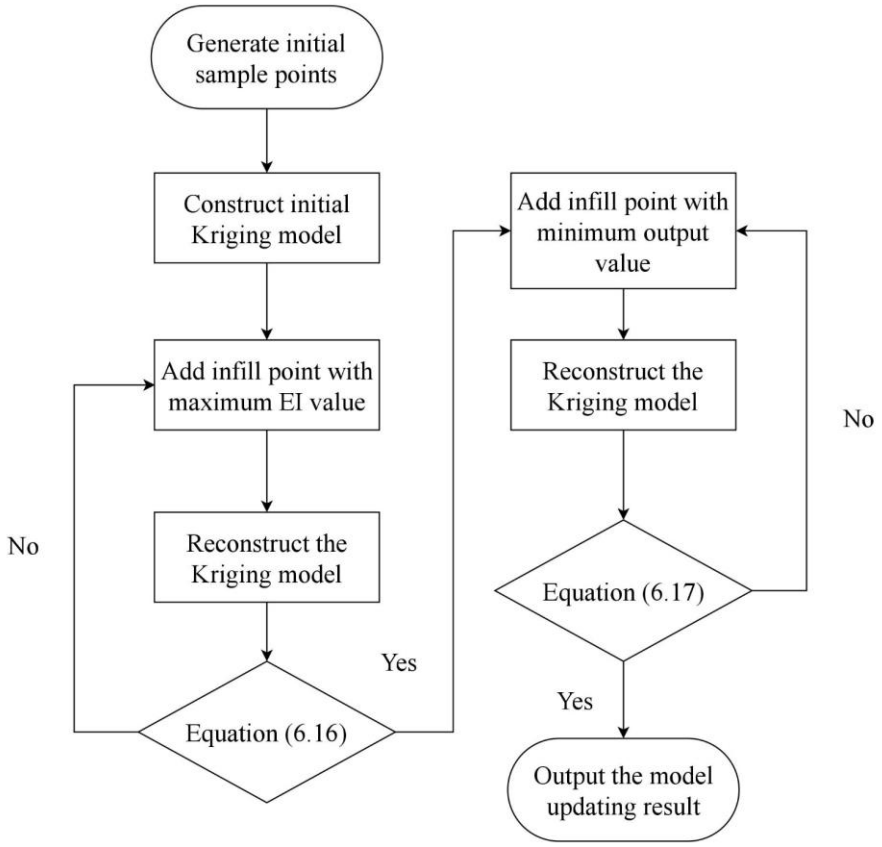

Figure 6-3 Flow chart of the proposed model updating method.

Based on all methods mentioned above in section 6.3, the flow chart of the complete model updating procedure is presented in Figure 6-3 and can be described as follows:

- **Step 1**: Generate initial sample points of the updating parameters by DOE.
- **Step 2**: Run the FE analysis program to calculate the objective function (equation (6.13)) output vector of the sample points and construct the initial Kriging Model.
- **Step 3**: Find the point with the maximum expected improvement value of the current Kriging model and add it into the set of sample points.
- **Step 4**: Calculate the true response of the new sample point and reconstruct the Kriging model by the new set of sample points and their response.

- **Step 5**: Check whether the first termination criterion (equation (6.16)) is satisfied. If it is, go to step 6. Otherwise, go back to step 3 and continue adding new points.
- **Step 6**: Find the point with the minimum value of the current Kriging model and continue to add it into the set of sample points, calculate the true response output and reconstruct the Kriging model.
- **Step 7**: Check whether the second termination criteria (equation (6.17)) is satisfied. If it is, then stop updating the Kriging model and the sample corresponding to the minimum value in the output vector is used as the right updating result. Otherwise, go back to step 4 and continue adding new points.

The method described in this section successfully uses the FRF data and the Kriging model for model updating. In fact, this method can be summarized as a new solution strategy of the response surface-based model updating method, which can be easily extended to other responses. Figure 6-4 shows the basic process of the whole strategy. Its core idea is to transform the problem of how to construct complex response surface using surrogate model into the problem of how to construct an objective function with smooth response surface in the neighbourhood of the optimal solution. The difficulty is undoubtedly greatly reduced compared with the initial problem. By applying this strategy, not only can the response types of the response surface-based model updating method be enriched, but also the total amount of data involved in the updating can be significantly increased, because no matter how many responses are used, only one response surface about the objective function needs to be constructed, rather than constructing a response surface for each response as in the traditional method. A response surface is constructed. However, subjective judgment and trial-and-error method are still the main methods to evaluate the availability of objective function, which means that some preparatory work should be done before reliable model updating.

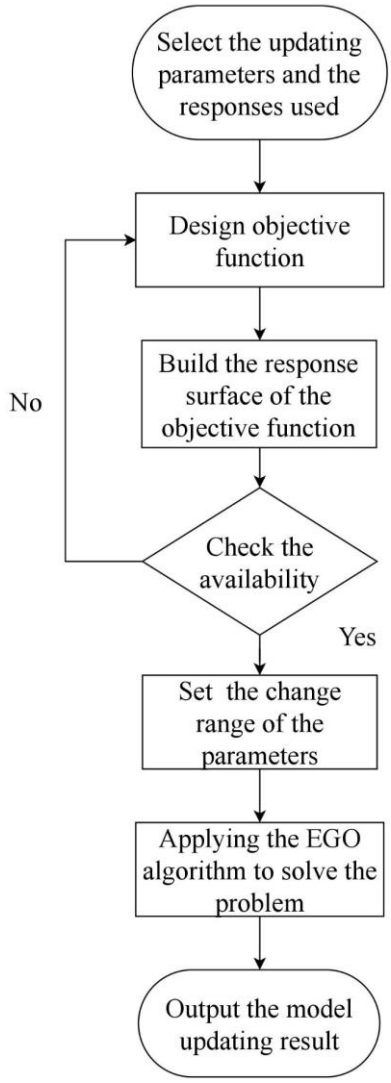

Figure 6-4 Flow chart of the proposed updating strategy.

6.4 Numerical example

The proposed model updating method is first verified through a simulated numerical example of a cantilever beam of rectangular cross-section divided into 9 elements as shown in Figure 6-5. The properties of the beam are 0.9 m in length, 200 GPa in Young's modulus, $7670 kg/m^3$ in mass density, and 6 mm and 50 mm in height and width respectively.

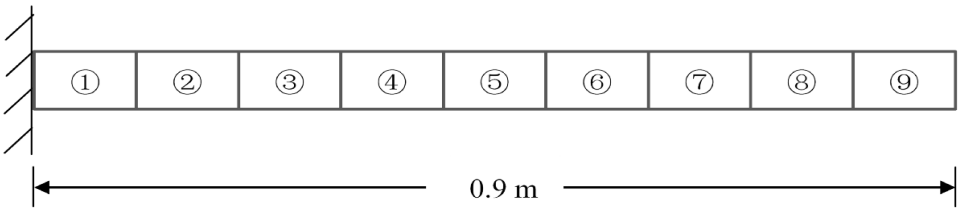

Figure 6-5 The cantilever beam used for numerical simulation.

9 Euler-Bernoulli beam elements are used and each node has two degrees of freedom of transverse displacement and rotation. It is assumed that the damage of the structure results in stiffness reduction in element 2 by 20%, in element 4 by 25% and in element 5 by 10%. The natural frequencies of the undamaged model and the damage model are shown in Table 6-1.

Table 6-1 Natural frequencies of the theoretical and damaged model of the cantilever (unit: Hz).

Mode no.	Undamaged model	Damaged model
1	6.11	5.81
2	38.29	36.87
3	107.26	104.95
5	210.41	203.89
5	348.63	332.91
6	522.95	506.21
7	734.98	712.38
8	985.66	952.78
9	1261.5	1216.71

The stiffness coefficients of all elements are used as the updating parameters and their change interval is set to [0.7, 1]. The number of the frequencies selected for FRF should be more than the number of the updating parameters to reduce the effect of noise and excellent frequency selection away from resonance and anti-resonance can effectively improve the reliability and convergence speed of the algorithm. However, to check the robustness of the algorithm, the frequency range of the FRF is simply set from 20 Hz to 800 Hz at every 50 Hz.

90 samples are obtained by LHS as the initial sample population and the Kriging model-based model updating is carried out with the stopping criterion of ε_1=10^{-10} in equation (6.16) and criterion of ε_2=10^{-4} in equation (6.17). At the same time, the model updating based on GA directly is also implemented as a benchmark to compare the results of the two methods. These two methods are hereinafter referred to as Kriging method and GA method respectively. The GA used in this thesis is the ga function of MATLAB 2017 whose FunctionTolerance value is set to 10^{-9} as the stopping criterion. For details, please consult Matlab help menu.

In this example, the Kriging model is constructed after 358 iterations. As the dimension of the parameter is high, only the stiffness coefficients of element 1 and 2 are taken as variables while the stiffness coefficients of the other elements are set to 1 to demonstrate the similarity between the response surface predicted by the Kriging model and the real response surface as shown in Figure 6-6. It can be seen that when there are many parameters to be updated, the prediction error of the objective function of the Kriging model is large at the location away from the minimum.

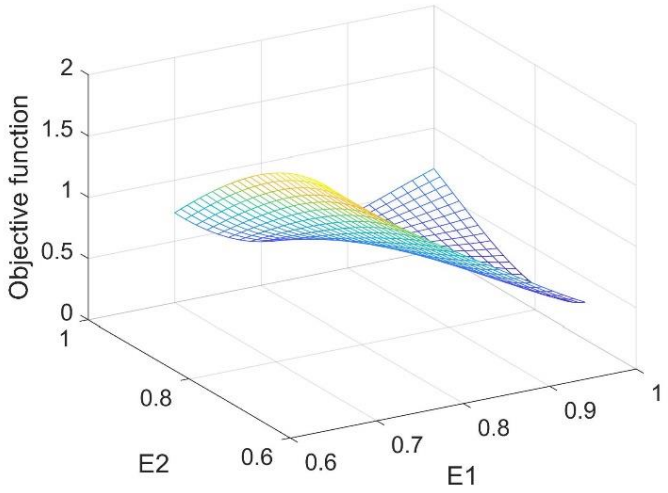

(a)

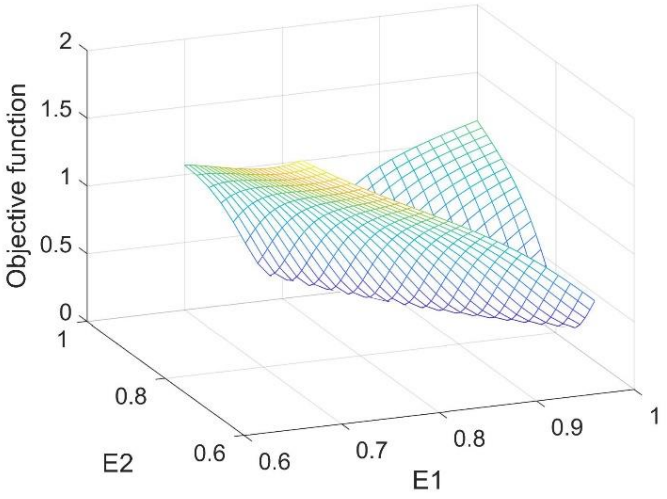

(b)

Figure 6-6 The response surface of the objective function when only two parameters are variable: (a) The Kriging model prediction; (b) Real response surface.

Furthermore, the complexity of the real response surface when all the parameters are design variables can be envisaged through Figure 6-6 (b). Even building that 2-D surface requires a considerable number of sample points. That is why the EGO algorithm is adopted to save the computational cost. The final updating results are shown in Figure 6-7. For the sake of comparison, a conventional way of using FRF in the Kriging based model updating is also applied, in which the amplitude of FRF is used to construct the objective function, which is referred to as the AF approach in the chapter.

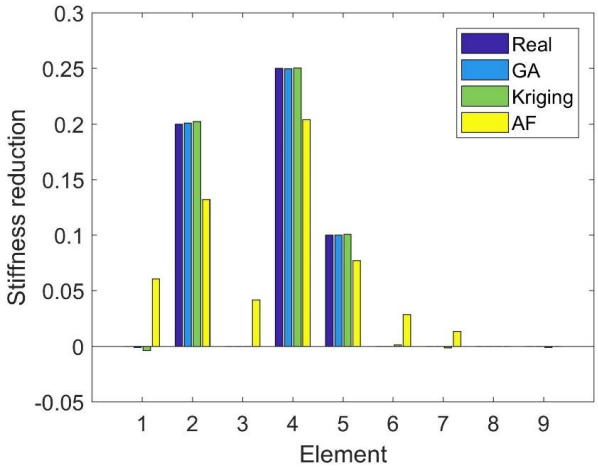

Figure 6-7 The updating results of the Kriging method, GA method and AF approach compared with the ‘real’ damage.

As illustrated in Figure 6-7, the proposed Kriging method can effectively identify the stiffness reduction caused by damage in this numerical simulation experiment. A great improvement has been made by introducing the FDAC in the objective function as the AF approach contains obvious errors. Actually, the AF approach can hardly get correct results as using the FRF to construct the objective function directly will lead to a too complicated response surface for Kriging to build and this method will not be mentioned in the next case. On the other hand, although the Kriging method contains slightly higher errors in results compared with the GA method directly, it needs a far fewer number of running the FE program than the latter, as shown in Table 6-2, which is the core purpose of this method.

Table 6-2 The required number of running the FE program of the Kriging method, and the GA method (which is repeated 3 times).

	Kriging	**GA**
1	448	119600
2	380	92600
3	421	161000

6.5 Experimental study

In this section, the experimental data [190] of a three-story building structure made of aluminium tested at Los Alamos National Laboratory(LANL) shown in Figure 6-8 is used to verify the effectiveness and the practicability of the proposed approach. The test-bed structure consists of 4 plates and 12 columns assembled by bolted joints and was installed on rails that allow sliding in only one direction. Also, a centre column suspended from the top floor and an adjustable bumper mounted on the 2nd floor were used to simulate the nonlinear behaviour of damage.

An electrodynamic shaker was used to provide a band-limited random lateral excitation (20-150 Hz) to the base floor along the centreline of the structure and a force transducer was connected to the tip of the stinger to measure the input force. At the same time, four accelerometers were attached at the centreline of each floor on the

opposite side from the excitation to measure the dynamic response of the system. The analogue sensor signals were discretized into 8192 data points sampled at 3.125ms intervals corresponding to a sampling frequency of 320 Hz.

Force- and acceleration-time histories for 17 different structural state conditions were collected. However, only 9 of them are utilized as the others are concerned with nonlinearity which is not within the scope of this article. The 9 different states can be divided into 3 categories: the baseline structure, the increase of the mass and the reduction of the stiffness. The change of mass was realized by adding a 1.2kg concentrated mass to the aluminium plates while the reduction of stiffness was introduced by replacing the corresponding column with another one with half the cross-section thickness in the direction of shaking. Each state was tested separately and the detailed state conditions [191] are shown in Table 6-3.

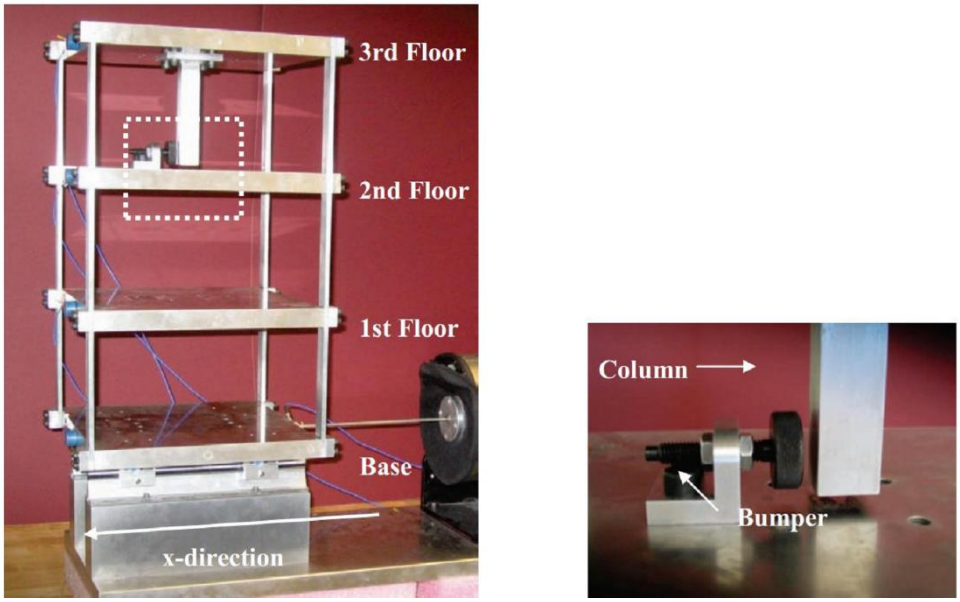

Figure 6-8 Overview of the three-story structure (Source: Courtesy of [190]).

Table 6-3 Summary of structural state conditions.

State	Condition	Description
State 1	Baseline condition	-
State 2	19.1% base mass increment	1.2 kg additional mass on the base
State 3	19.1% 1st-story mass increment	1.2 kg additional mass on the 1st story

State 4	21.8% 1st-story stiffness reduction	Replace one column (1st story)
State 5	43.7% 1st-story stiffness reduction	Replace two column (1st story)
State 6	21.8% 2nd-story stiffness reduction	Replace one columns (2nd story)
State 7	43.7% 2nd-story stiffness reduction	Replace two column (2nd story)
State 8	21.8% 3rd-story stiffness reduction	Replace one columns (3rd story)
State 9	43.7% 3rd-story stiffness reduction	Replace two column (3rd story)

As recommended in [190], the structure is modelled as four lumped masses for the floors shown in Figure 6-9. All the mass and stiffness values are selected as the updating parameters except k_0 since the friction between the rails and the structure is negligible. Besides, the damping matrix is introduced based on the proportional damping assumption which can also be affected by the mass factors.

At first, the Baseline condition is used to update the theoretical model to get the original undamaged model. The FRF of the first floor after the updating procedure compared with the experimental data is illustrated in detail in Figure 6-10. It can be seen clearly that the model after updating shows good agreement with the experimental data. However, there is considerable noise in the imaginary part of the experimental FRF especially near the anti-resonance points and modelling error in the theoretical FRF around the same points. Moreover, there is also a big difference between the real parts of the two FRF values near 22Hz which should not be selected as the frequency points of the objective function since such a big difference cannot be eliminated by model updating.

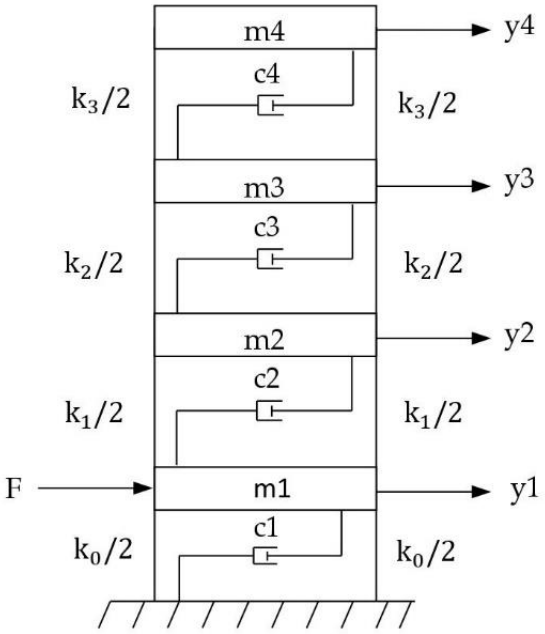

Figure 6-9 Theoretical model for the test structure.

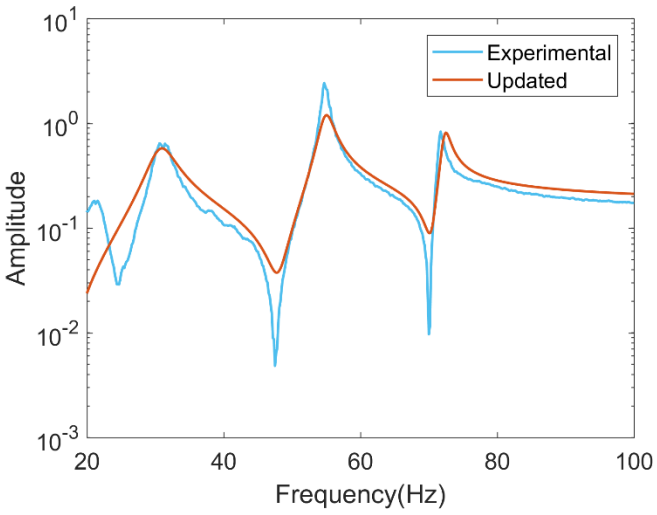

(a)

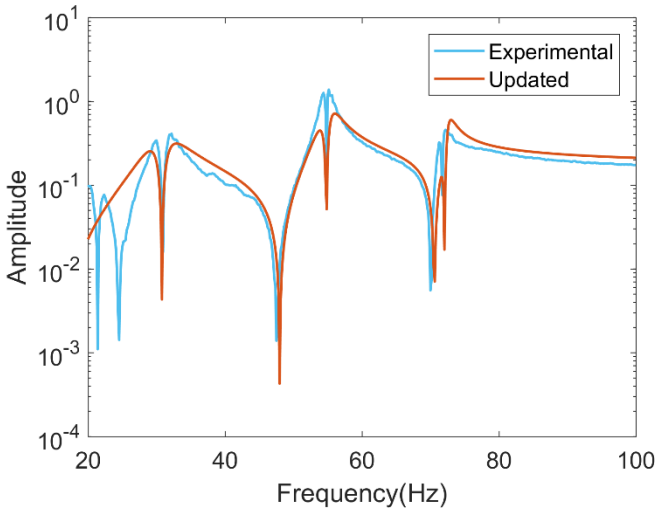

(b)

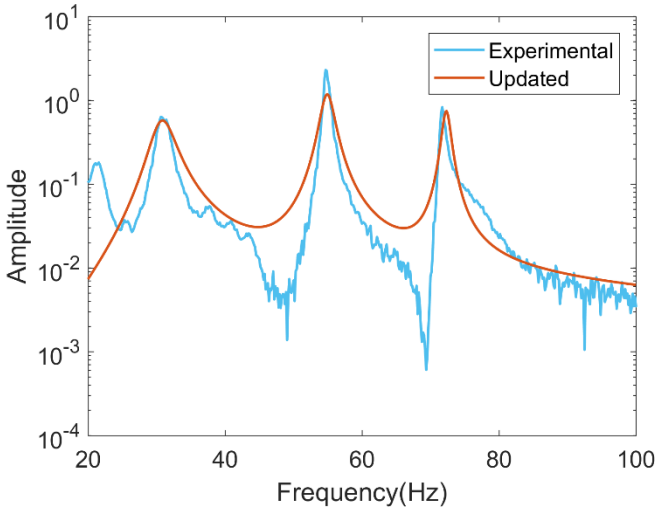

(c)

Figure 6-10 The FRF of the first floor of the real structure and the updated model: (a) Absolute value of $H(1,1)$; (b) Absolute value of the real part of $H(1,1)$; (c) Absolute value of the imaginary part of $H(1,1)$.

Then the two methods are applied to the undamaged model obtained using the experimental data of the other states. The intervals of the mass and stiffness parameter ratios are set to $[0.98, 1.5]$ and $[0.4, 1.0]$, respectively. This setting is based on the pre-knowledge of the structure's change and prevents all parameters from becoming larger at the same time or smaller at the same time, which would make little change in the value of the objective function.

Unlike the numerical simulation mentioned in section 3, in this case, setting a larger parameter range is beneficial in getting the right updating parameter values. However, this may lead to selected frequencies to become close to a theoretical resonant frequency, which would result in a sharply increased objective function value, as illustrated in Figure 6-11.

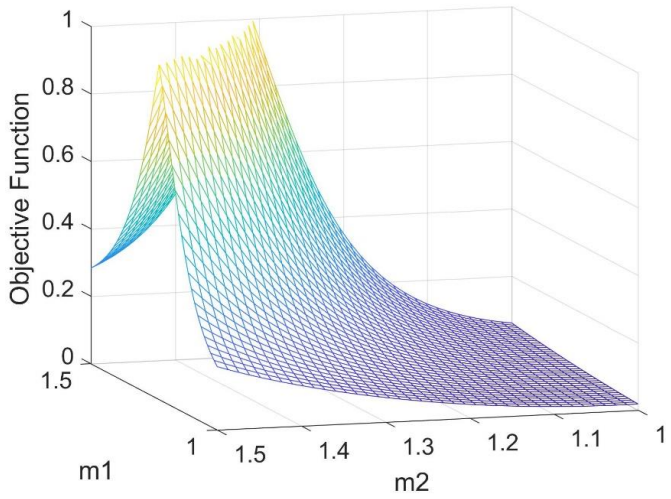

Figure 6-11 The objective function of 50Hz when only m1 and m2 are variable using experimental data of state 1.

Since the experimental data has considerable noise, the number of selected frequency points for model updating should be much higher than the number of updating parameters to reduce the effects of noise and damping. If such an increase appears in too many frequency points, there will be severe fluctuations in the response surface of the final objective function formed at these frequency points, which are undesirable and useless in identification.

It is not difficult to relate this increase to the sharp decline of the real parts of the FRFs near the natural frequency as shown in Figure 6-10. In contrast, the imaginary parts of the FRFs show better correlation near the natural frequency. Thus if the selected frequencies are near the natural frequencies shown in the experimental data, 3 Hz on either side of a peak of the real part of the experimental FRFs is used as a criterion; in

this case, the imaginary part of the FRFs only is chosen to calculate the FDAC to get a smooth response surface.

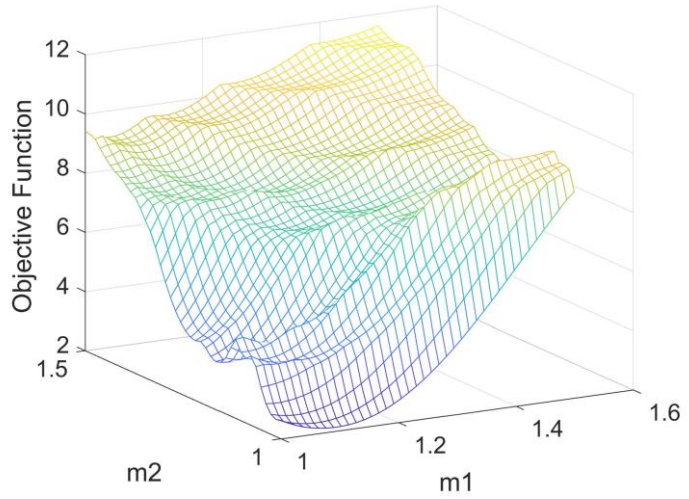

(a)

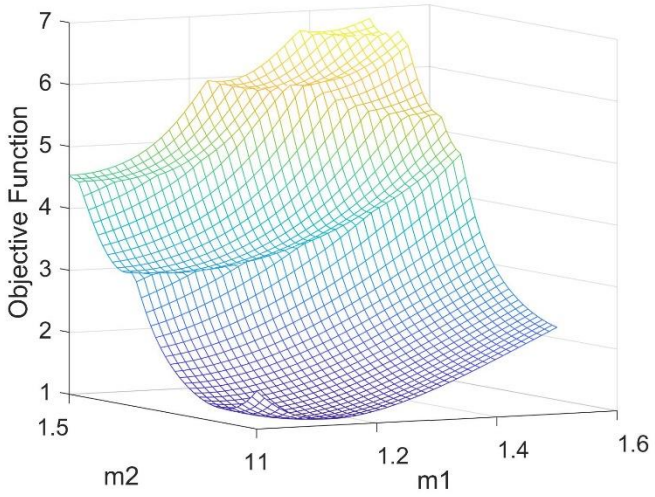

(b)

Figure 6-12 The response surface of the objective function when only m1 and m2 are variable: (a) Before improvement; (b) After improvement.

This measure turns out to reduce the complexity of the frequency response surface. This improvement is shown in Figure 6-12. It is clear that the response surface is much smoother than before, after such a special treatment which saves a great deal of computation time in constructing the Kriging model because the fluctuating portion of

the response surface is largely reduced. It should be noted that both the Kriging method and the GA method benefit from the improvement that their computing times decrease significantly.

Finally, the updating results of each state by the two methods are shown in Figure 6-13.

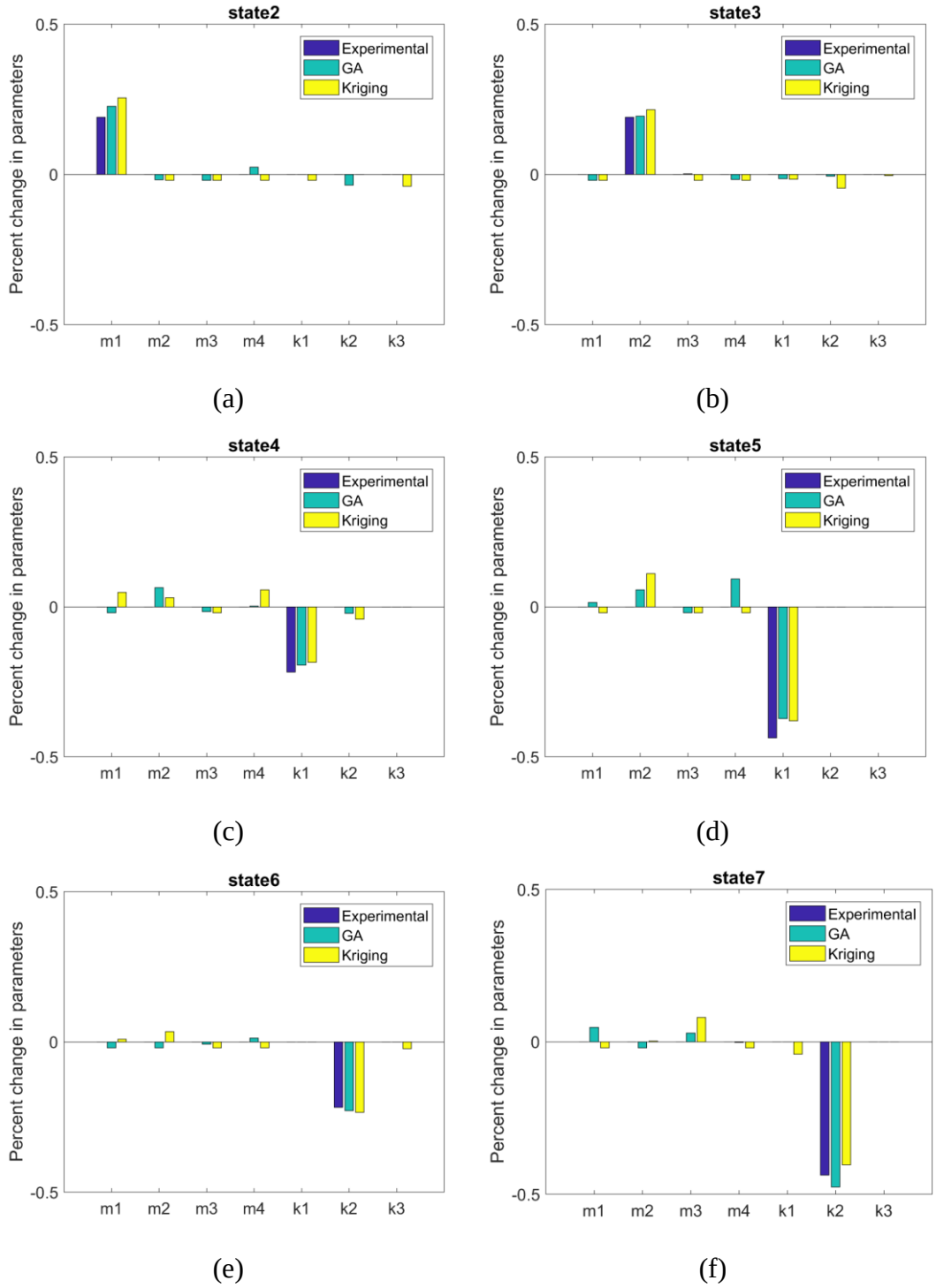

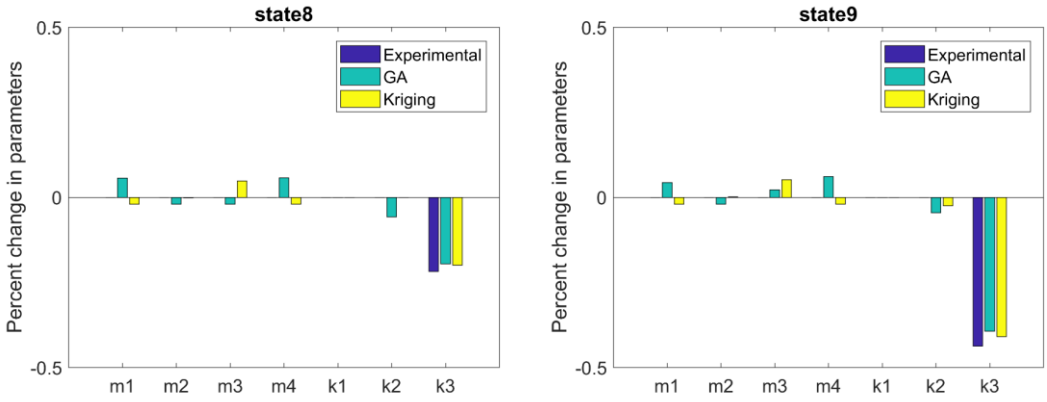

(g) (h)

Figure 6-13 Updating results of the different states of the two methods compared with the real value.

It is clear that the updating results of both methods match the experimental values quite well. The parameter that has experienced the largest change can be clearly identified with small false alarms in other parameters due to the measurement noise and the modelling error in the theoretical model. The successful application in identifying these states is sufficient to demonstrate the superiority of using FDAC value to build the objective function and the Kriging method shows similar updating results to those by the GA method, which means the proposed Kriging method has the advantage of a typical good surrogate model and ensures high updating accuracy at the same time.

Additionally, the required numbers of the finite element runs for all states by the two methods are listed in Table 6-4. Again the Kriging method shows a great improvement over the GA method. It should be noted that the proposed method can also converge very quickly if a point near the global minimum is selected as one of the initial sample points.

Table 6-4 The required number of running the FE programs of the Kriging method and the GA method for different states.

State	Kriging	GA
State 1	95	101200
State 2	122	55200

State 3	187	84600
State 4	226	125800
State 5	268	65600
State 6	201	69200
State 7	152	119200
State 8	160	140200

6.6 Conclusions

In this chapter, a new surrogate model-based model updating method using frequency response function (FRF) is proposed. Although FRF contains the most vibration information, its response surface is difficult to construct directly and the Frequency Domain Assurance Criterion (FDAC) is adopted to build the objective function rather than the residual of every single FRF. As a combination of three parts, the residual of FDAC for the objective function and the Kriging model for constructing the response surface and the efficient global optimization (EGO) for solving the optimization problem, this method is found through a simulated example and a real experiment to have the following merits: (1) it does not need to calculate the sensitivity of the parameters, (2) it has similar accuracy as the direct use of GA but requires much fewer runs of the finite element analysis, and (3) it has strong robustness in the face of measurement noise and modelling errors which are always present and cannot be ignored.

Chapter 7 - Finite element modelling and damage detection of seam weld

7.1 Introduction

Seam welds are widely used in assembled structures for connecting components. However, the dynamic effects of a seam weld are often difficult to characterize in numerical models for several reasons: (1) it is often not wise to build a fine mesh on the seam line which will add considerable computational cost for a structure with many welds, (2) the mechanical properties of weld materials are not well known; (3) sometimes some geometric information about welds is not known beforehand. In this chapter, the FE model of a welding connection joint is developed by employing CSEAM element in Nastran and its feasibility for representing a seam weld is investigated. Based on this result, a damage detection method by updating the properties of the built CSEAM elements is also proposed for welding quality assurance. The damage takes the form of a gap in the weld which causes a sharp change of model strain energy (MSE) at the edges of the gap for certain vibration modes. Specifically, the MSE shape is used as the objective function. A Kriging model is introduced for efficiency and simulation of a T-shaped welded plate structure to demonstrate the effectiveness of this method. The work in this chapter is based on chapter 5 and 6, and some parts of this chapter, mainly in the background and theory, were published in reference [192].

7.2 Background

Assembled structures are widely used in civil and mechanical engineering. Different structural members are produced independently and then connected together by special joining techniques. The joint formed has an important influence on the overall dynamical characteristics of the structure. Thus the accurate representation of the joints in the Finite Element (FE) models has significant research value [193].

Welding is one of the most commonly used joining techniques, whose FE modelling has drawn great attention in the past decades [194]. At the early stage, special elements

are designed for connection, like partly rigid beam element used in frame structures [160-162]. Then, with the development of computer-aided engineering software, many useful connectors are available in structural analysis software packages to represent welded joints in the FE model, like RBE2, ACM2 and CWELD [195]. The last one is specially designed for spot weld modelling in Nastran [151] and has been widely used and studied by many researchers. References [152, 153] show that after reliable model updating, CWELD elements can successfully represent the laser spot weld joints in a top-hat structure. Further research by Abu Husain et al. about damage identification [154] and uncertainty analysis [155] on that kind of structure also benefited from the superiority of the CWELD element.

Unlike the mature application of spot weld modelling, a seam weld which creates a weld seam line to connect parts together has not attracted much research, even though it is also widely used. Most research about FE modelling of seam welded joints does not focus on reflecting the dynamical characteristics, but on their deformation [156], rotational stiffness [159], fatigue capacity [196, 197] and residual stresses [140]. In the field of structural dynamics, Zahari et al. [163, 164] studied the modelling of friction stir weld joints. But their model is simplistic and thus cannot be used generally. Chee [157] and Rahman [158] presented common finite element modelling of T-shaped structures connected by fillet welds and their focus was on the impact of the types of elements used in plates. The joint part modelled by a shell or a solid element is not flexible enough to represent damage in a weld. In most cases, a seam weld provides a firm connection. But it may still suffer from cracks, underfill, burn through, incomplete fusion, welders' faults and so on. Therefore, an effective modelling method of seam welded joints that can properly reflect the weld properties and can be further applied in damage identification of the welding part is required in modern industry.

Besides different joint modelling methods, model updating is applied in most of the publications mentioned above. In actual applications, geometric and material properties of the welding part are often assumed but they may slowly vary over time or their accurate values are not known beforehand. One remedy is to update these models based on suitable responses. After that, the welding part is regarded as properly modelled.

In this chapter, the CSEAM element of Nastran is adopted to model the seam weld joint of a T-shaped plate structure. The advantages and disadvantages of this element are discussed and its application in damage identification is shown through an FE simulation and experiment. In both of them, the damage is in the form of an unwelded gap in the weld seam line and model updating method based on MSE is applied to detect the gap. The resulting optimization problem is solved by a genetic algorithm while the Kriging model based model updating method described in chapter 6 is added for computational efficiency.

7.3 Seam welded joint modelling

7.3.1 General seam welded joint modelling methods

The simplest way to join two plates of a T-shaped structure together in FE modelling is to delete extra overlapping points at the connection parts, as shown in Figure 7-1 (a) with the yellow line (connection between the two plates) denoting the place where nodes are merged. Thus, the two parts are assumed to be melt together representing the weld is firm enough. But in this case, the joint of the model is not adjustable and cannot be used for further calibration.

A smarter approach is to include extra shell or solid elements and delete overlapping points between them and the two plates as shown in Figure 7-1 (b). In this way, the properties of the weld can be changed through modifying the parameters of these elements. Model updating methods could be applied to make the model more accurate and reliable.

However, all of these methods mentioned above are limited by the mesh distribution of the two plates. They can hardly work with misalignment of the two meshes especially when the two element sizes are different. In order to solve more general problems involving seam welds, in this research the CSEAM element of Nastran is explored. This type of element is specially designed for modelling seam welds and can easily overcome the misalignment problem. Also as shown in Figure 7-1 (c), the

CSEAM element is good at connecting two plates with a certain distance, which is considered as thickness offset.

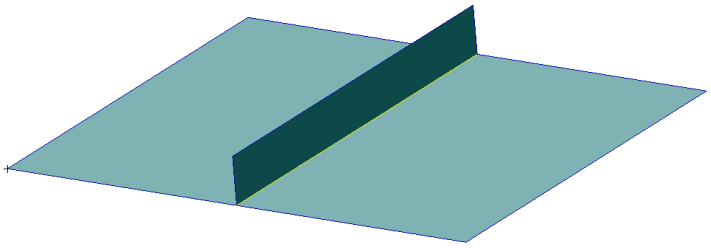

(a)

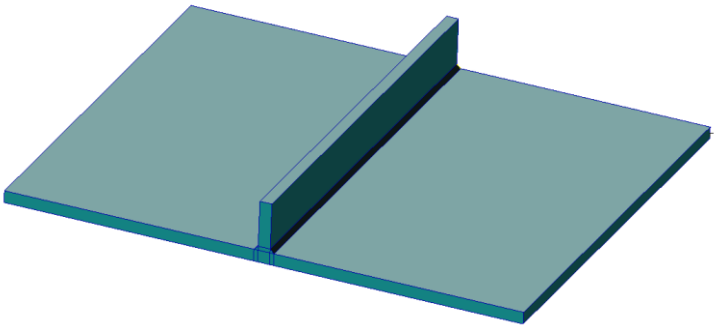

(b)

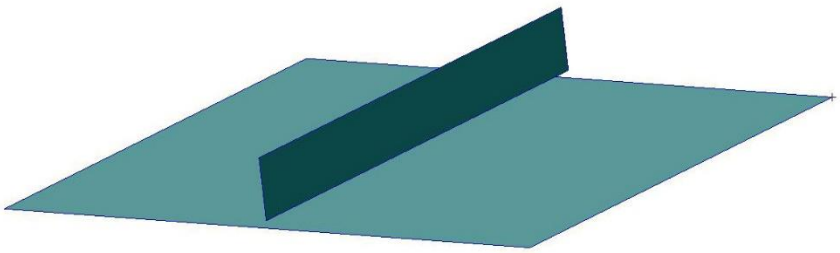

(c)

Figure 7-1 Three ways of modelling for comparison: (a) Shell elements with nodes overlapped; (b) Solid elements connected by solid elements; (c) Shell elements connected by CSEAM elements.

Here is a specific application of modelling a stiffened plate (simulation of the structure in reference [158]) as shown in Figure 7-1. This is a very common structure in industrial equipment and usually, the rib is welded on the plate with two welding seam on both side. The plate is made of aluminium with the following mechanical properties: 70GPa in Young's modulus, 0.33 in Poison ratio and 2796 kg/m^3 in mass density.

Table 7-1 Natural frequencies of the stiffened plate.

Mode	Test	Solid	Error	Shell	Error	CSEAM	Error
1	354	371	4.9%	365	3.2%	370	4.6%
2	451	453	0.5%	448	-0.5%	453	0.5%
3	781	795	1.8%	793	1.4%	792	1.8%
4		1009.2		1009		1013	
5		1061		1044		1067	

The element sizes of the three FE models are the same and their frequencies are compared with the test result as shown in Table 7-1. It is clear that all the frequencies of the three theoretical models are very similar. However, there is still a certain gap between them and the actual measured values, which means that model updating needs to be implemented to obtain more accurate FE models. This example is only used to show the effect of using CSEAM elements, and its specific working principle and modelling method will be introduced next.

7.3.2 CSEAM element modelling

Similar to CWELD designed for simulate spot weld, CSEAM is another connector element provided by Nastran. It is used to define a seam line to connect two surface patches. For welding, a weld seam can be created by selecting two surface patches by their property IDs (the simplest way) and specifying the width and the thickness of the seam. Compared with the RBE2 element, CSEAM element models the welding connection part directly. All the parameters of the material and size of the seam can be adjusted, which is very convenient for model updating.

Although the function of the CSEAM element seems great, one problem which limits its application is that this element can only be created in Nastran input file. By now no pre-processing software contains the menu of creating this element, so command line with the respective formats must be typed by hands into the Nastran input file. It is suggested to use Matlab or C++ to do this tedious work when there are many CSEAM elements to be created. Such inconvenience caused by this extra work is one disadvantage of this element. However, it is still worth to explore its performance in modelling seam welded joint.

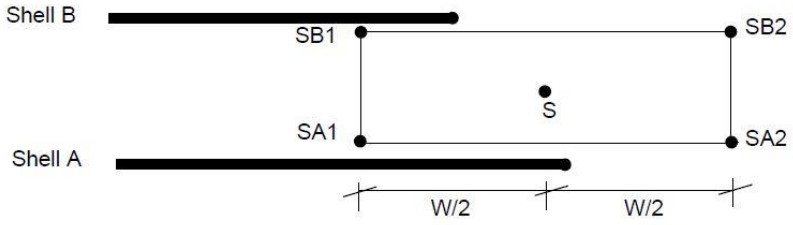

(a)

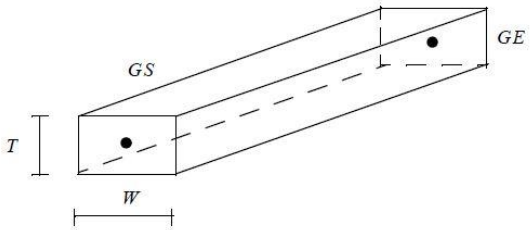

(b)

Figure 7-2 Illustration about the creation of CSEAM element: (a) Seam weld between two shell patches; (b) Dimensions of the seam element. (Source: reference [195] with permission from Nastran).

The full CSEAM input format and its detailed description are available in reference [195]. As shown in Figure 7-2, to create a CSEAM element the user needs to input the shell patches to be bonded, the coordinate of the start (GS) and end (GE) points, the material and the size (width and thickness) of the seam element. Then Nastran will build a hexahedron element automatically representing the seam based on the input. The information of the CSEAM element built finally can be found in .f06 and .pch file (see Appendices A1 and A2).

Here is a demonstration about how to do dynamic analysis with the use of CSEAM element. At first, four shell elements are created in Patran as shown in Figure 7-3 (a). Two CSEAM elements will be created between elements 1 and 4, between elements 3 and 2 (on the right side), which are two element pairs to be connected. Then, dynamic analysis is applied to this semi-finished structure and Patran will produce the input file of Nastran about this structure. Finally, after adding command line codes to create CSEAM elements between the two pairs (see appendix A), the input file is run in Nastran and the dynamic analysis is done.

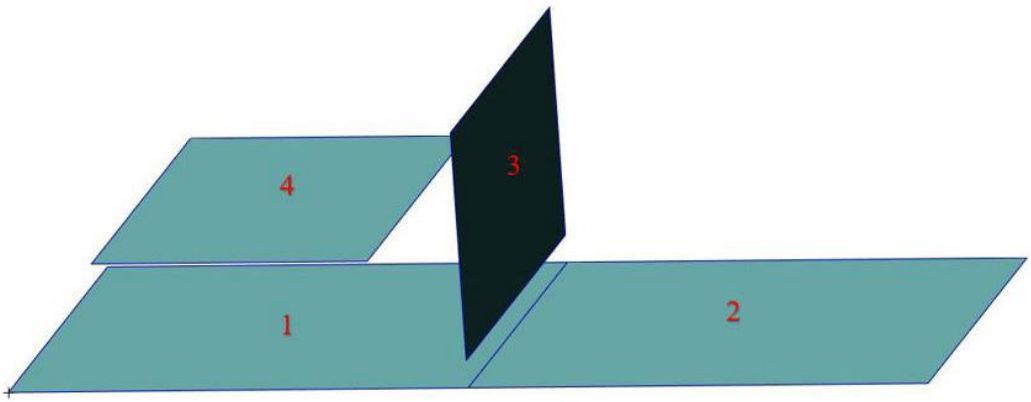

(a)

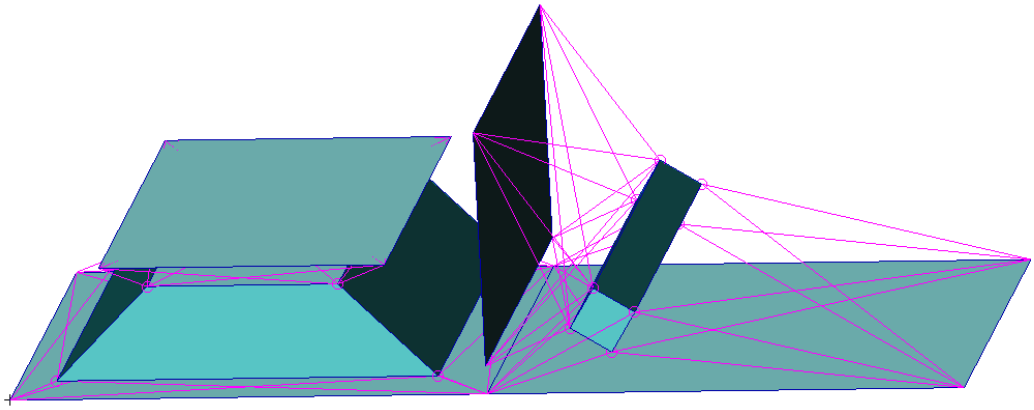

(b)

Figure 7-3 Demonstration about how CSEAM element is built in Nastran: (a) Semi-finished structure in Patran; (b) CSEAM elements built directly in Patran.

After the analysis is done, based on the information of the output files, the two CSEAM elements can be built directly in Patran as shown in Figure 7-3 (b). It is clear that two seam elements (hexahedron elements) are created between the two pairs of shell elements. Additionally, the nodes of the shell elements are linked with nodes of seam elements through the magenta lines. That is how the four shell elements are connected respectively.

These magenta lines represent RBE3 elements. RBE3 and RBE2 both belong to R-type elements in Nastran, which are used to describe the situation that the motion of a

DoF is dependent on the motion of at least one other DoF. Their difference is that an RBE2 element uses a rigid body to link the dependent and independent nodes while an RBE3 element forces the motion of the dependent node to be the weighted average of the motions of a set of independent nodes. An RBE3 element does not add additional stiffness to a structure and is a powerful tool for distributing applied loads and mass in a model [198].

The relationship between motions of nodes constructed by RBE3 elements is based on the user-input weighting factors and the geometry of these nodes. Figure 7-4 shows the theory behind this element in the view of how the force and moment are transferred from the reference point (dependent node) to the other points (independent nodes). In Figure 7-4 (a), the reference point is connected to all the other points through an RBE3 element with different weightings, respectively. The C.G. point is the centre of gravity of these points. The force applied on the reference point will be transferred to the C.G. point as force and moment. Then the force and moment will be distributed to the points connected to the reference point by the formula shown in Figure 7-4 (b).

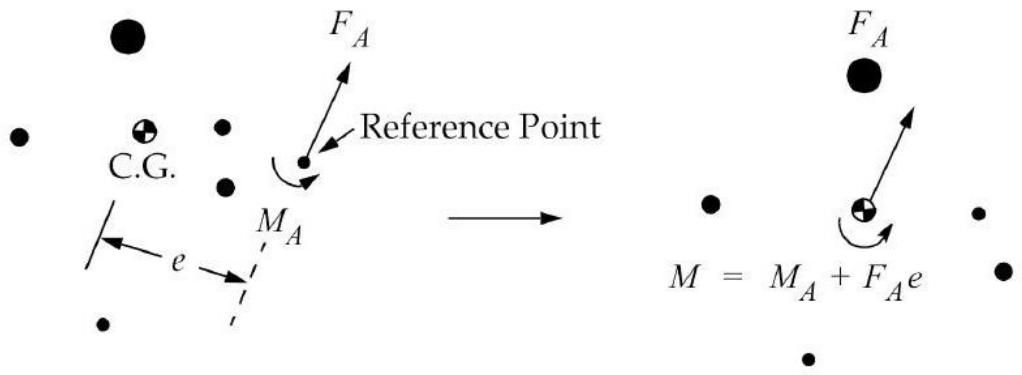

(a)

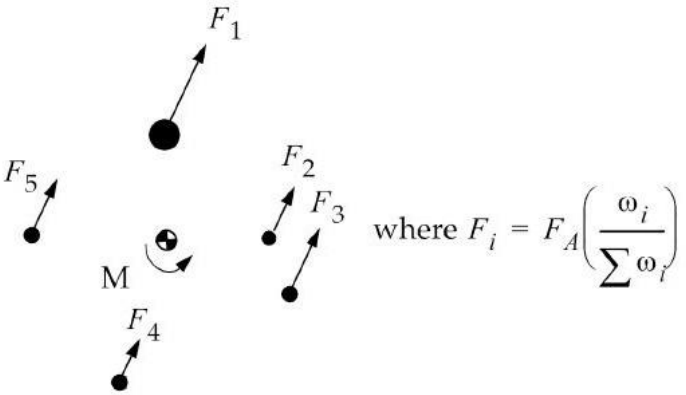

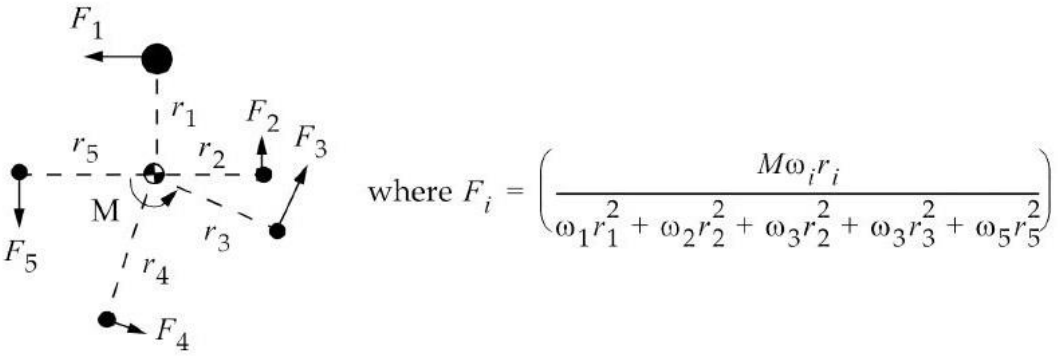

where:

F_i = force at DOF i

ω_i = weighting factor for DOF i

r_i = radius from the weighted center of gravity to point i

(b)

Figure 7-4 Force and moment transferred from the reference points to other points connected by RBE3: (a) From reference point to the centre of gravity; (b) From the centre of gravity to other points; (Source: reference [198] with permission from Nastran).

When a CSEAM element is built, each node of the seam element works as a reference point whose motion is determined by motions of 4 nodes of its corresponding shell element through an RBE3 element (see Figure 7-3 (b) where 4 magenta lines from a seam element node represent an RBE3 element). Thus, a great number of special motion constraints are added between these nodes, which finally results in the constraint between each shell element pair. The stiffness of the constraint depends

mainly on the Young's modulus of the seam element. If the stiffness meets the requirements, then the two shell elements can be considered to be connected by a seam welded joint.

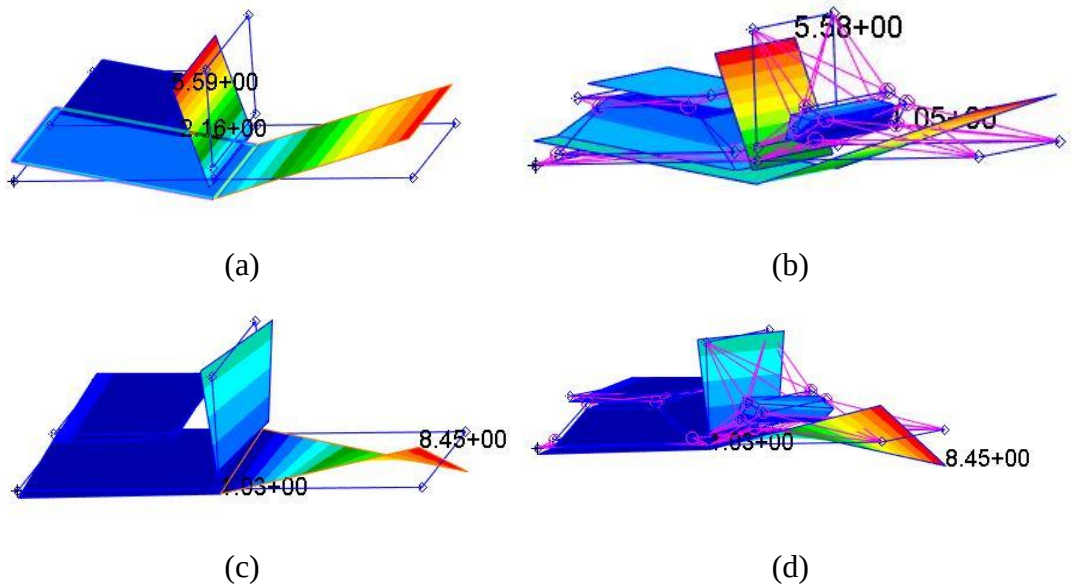

(a) (b)

(c) (d)

Figure 7-5 Mode shapes of the structures connected by CSEAM elements: (a) Mode 1 of the Semi-finished structure; (b) Mode 1 of the full structure; (c) Mode 2 of the Semi-finished structure; (d) Mode 2 of the full structure.

After applying dynamic analysis, the first two mode shapes of the two structures are shown in Figure 7-5. Here the semi-finished structure represents the case that CSEAM element are created by Nastran. Figure 7-5 (a) and (c) are obtained by reading the specific output file, which is generated after running the modified (CSEAM element added) input file by Nastran, into the semi-finished structure in Patran and this result is generally what can be gotten in the real application of the CSEAM element. The full structure represents the case that CSEAM elements are built directly in Patran and can only be achieved in simple cases for illustration when the number of CSEAM elements is very limited.

It is clear that the mode shapes of the shell elements of the two structures are almost exactly the same, which also happens to their frequencies. This verifies that CSEAM element is a combination of seam element and RBE3 elements created by Nastran to connect two surface patches. The advantage of the RBE3 element is that it does not

add additional stiffness to the structure itself. Also, as a weighted multi-point constraint (MPC) element, CSEAM element can be used to assemble components with different meshes. This advantage is very important as this allows the meshes of two plates to be adjusted freely to meet the actual needs.

The CSEAM element can be built by Nastran with a small amount of input information, which is very convenient compared to create such a complex element combination manually. However, it should be pointed out that the construction of CSEAM elements is not completely controllable. As shown in Figure 7-3 (b), the size information of the seam element inputted is the width and thickness of a rectangle while the cross sections of the two seam elements created are a trapezoid (left) and a rotated rectangle (right). This is because Nastran must follow several criteria to ensure the rationality of the constructed CSEAM element. Some of the criteria are shown as follows.

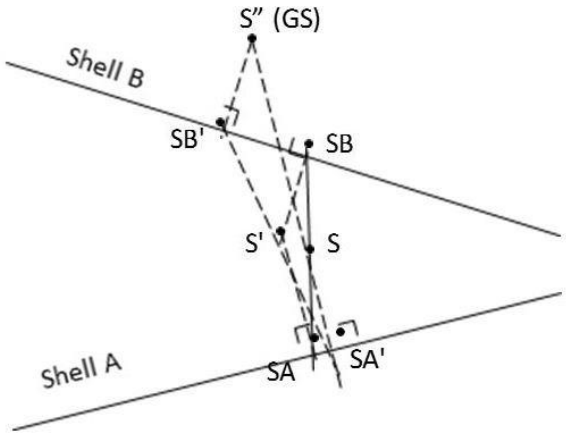

Figure 7-6 Illustration about modifying the location of start point GS (Provided by MSC Technique Support with permission to use).

In the beginning, Nastran modifies the location of GS and GE. As shown in Figure 7-6, if GS locates outside of the space between two shell patches, it will be relocated to the midpoint of the line connecting its projections on each shell patch. Then, the same thing happens again to ensure that GS finally locates midway between the two patches. Generally, if there is no big mistake in inputting the GS and GE, this relocation will only happen once. That is why the distance from GS to the two patches are actually half of what it is designed when the shell patches are vertical in Figure 7-3 (b) (the right CSEAM).

After the GS and GE are located, 4 auxiliary points of the cross section at start point GS, as shown in Figure 7-7, are constructed by equation (7.1), where *W* is the width and *T* is the thickness of the seam. They and the other 4 auxiliary points of GE are the 8 vertex points of the seam element to be created. Base on this theory, a seam element with rectangle cross section should be created between two parallel shell patches. But Nastran will make sure that each auxiliary point has a projection on its corresponding shell patch by adjusting the value of *W* and *T* automatically. This is why the cross section of the left seam element is a trapezoid.

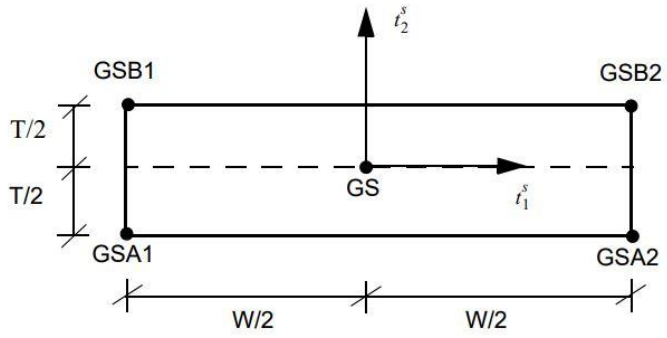

Figure 7-7 Seam element cross section at start point GS (Source: reference [150] with permission from Nastran).

$$
\begin{aligned}
x_{\mathrm{SA1}} &= x_{\mathrm{s}} - \frac{W}{2} t_1^{\mathrm{s}} - \frac{T}{2} t_2^{\mathrm{s}} \\
x_{\mathrm{SA2}} &= x_{\mathrm{s}} + \frac{W}{2} t_1^{\mathrm{s}} - \frac{T}{2} t_2^{\mathrm{s}} \\
x_{\mathrm{SB1}} &= x_{\mathrm{s}} - \frac{W}{2} t_1^{\mathrm{s}} + \frac{T}{2} t_2^{\mathrm{s}} \\
x_{\mathrm{SB2}} &= x_{\mathrm{s}} + \frac{W}{2} t_1^{\mathrm{s}} + \frac{T}{2} t_2^{\mathrm{s}}
\end{aligned}
\tag{7.1}
$$

The t_1^{s} and t_2^{s} are tangent vectors of the element coordinates at start point GS. Their coordinates can be gotten from Nastran output file .f06. And the description of how they are calculated from MSC Technical Support is shown as follows:

t_2^{s} is calculated based on the coordinate of GSA and GSB, the projection points from GS to patch A and patch B, respectively. If these two patches are not too close, then

$$t_2^s = x_{sb} - x_{sa} \tag{7.2}$$

where x_{sa} and x_{sb} are vectors from GS to its projection on the two shell patches. Otherwise, t_2^s have to be determined from shell normal vectors of patch A and patch B, *Na* and *Nb* based on the following equation:

$$\begin{aligned} &\text{if } Na \cdot Nb > 0,\ t_2^s = Na + Nb \\ &\text{Otherwise, } t_2^s = Na - Nb. \end{aligned} \tag{7.3}$$

As for t_1^s

$$\begin{aligned} &\text{if} \quad \left|Na \cdot t_2^s\right| < 0.9 \text{ and } \left|Nb \cdot t_2^s\right| < 0.9 \\ &\text{then} \quad t_1^s = Na - \left(t_2^s \cdot Na\right) \cdot t_2^s \\ &\text{Otherwise,} \quad t_1^s = e1 \cdot Na \\ &\\ &\text{Where} \quad e1 = x_{sc} - x_{ec} \\ &\qquad x_{sc} = \left(x_{sa} + x_{sb}\right)/2 \\ &\qquad x_{ec} = \left(x_{ea} + x_{eb}\right)/2 \end{aligned} \tag{7.4}$$

where x_{ea} and x_{eb} are vectors from GE to its projection on the two shell patches.

The word ‘close’ is vague. However, as these criteria are from MSC Technical Support which cannot be found in a Nastran reference book, how the weightings of the RBE3 elements in a CSEAM element be allocated is not known. Nevertheless, these criteria are still very helpful for understanding how a CSEAM element is created and further control of the position of CSEAM elements in the design phase as all of the information about the construction of CSEAM element can be listed in the Nastran output file.

At this point, the modelling of the CSEAM element has been introduced. It has the following advantages that make it very flexible to connect two plates.

- It can connect 2 shell elements and make their relative stiffness be adjustable.
- It adds the least computation cost compared with shell and solid elements.
- It can be used to connect 2 grids of different mesh sizes.
- Thickness offset is acceptable.

- No additional manual operation is required in pre-processing.
- Its location and size are also easy to be modified.

7.4 Theory of model updating of seam welded joint

When an FE model is built, the discrepancies between the measured and predicted responses, like natural frequencies and mode shapes, are unavoidable. An FE model can be improved by systematically adjusting the structural parameters to minimise these discrepancies.

In seam weld joint modelling, even though the welds are well produced, model updating should still be applied to reflect their real properties. Usually the stiffness of all the seam elements is selected as a design parameter and the minimisation is carried out via a residual-based objective function:

$$\min \sum_{i=1}^{m} w_i \left(\frac{f_i^{\mathrm{a}}}{f_i^{\mathrm{e}}} - 1 \right)^2 \tag{7.5}$$

where f_i^{a} and f_i^{e} are the predicted and measured frequencies of the *i*th mode, respectively. w_i indicates the weighting coefficient of the residual of that mode.

Measured frequencies are enough for updating the intact model. However, in this research, the focus is the damage identification of a weld structure. As mentioned before, the damage is introduced as a gap within the weld seam representing missing connection shown in Figure 7-8 (a) in section 7.5. This time the mode shape must be used to localize the gap.

Raw mode shape data are not very sensitive to damage. Many methods took advantage of their derivatives, for example, mode shape curvature, flexibility matrix and MSE were used and compared in reference [175]. In addition, one thing that must be considered is that welds are difficult to be measured directly, especially when using PSV-500 scanning laser vibrometer described in chapter 3. Compared with the vertical plate, the horizontal plate is more convenient to measure in the weld area (the response can be measured on the bottom surface of the horizontal plate). Therefore, it is

necessary to find a dynamic response that is sensitive to weld damage on the horizontal plate.

The MSE is adopted because there is a significant stress concentration (strain energy peak) caused by weld gaps for some specific modes in the simulation shown in section 7.5, which indicates that the element MSE of the horizontal plate can be used to identify the location of the gap. The theory of the MSE based methods and one improvement are given below:

The energy stored in the *j*th element at mode *i* before and after the occurrence of damage is defined as:

$$MSE_{ij} = \boldsymbol{\varphi}_i^{\mathrm{T}} \mathbf{K}_j \boldsymbol{\varphi}_i, \qquad MSE_{ij}^{\mathrm{d}} = \boldsymbol{\varphi}_i^{\mathrm{dT}} \mathbf{K}_j \boldsymbol{\varphi}_i^{\mathrm{d}} \tag{7.6}$$

where $\boldsymbol{\varphi}_i$ is the mode shape vector, $\mathbf{K}_j$ is the global stiffness matrix of the *j*th element. $(*)^{\mathrm{d}}$ represents the damaged states.

In traditional MSE methods, the elemental modal strain energy change ratio is used as a good indicator for damage localization and is defined as:

$$MSECR_{ij} = \frac{\left| MSE_{ij}^{\mathrm{d}} - MSE_{ij} \right|}{MSE_{ij}} \tag{7.7}$$

But in this case, all horizontal plate elements are themselves intact and are indirectly affected by damage of weld. This means that the above damage indicators cannot be used directly; otherwise it is likely to provide wrong results.

To solve this problem, in this chapter a new MSE-based model updating method is proposed for seam welded joint damage identification. This method utilizes the shape of MSEs of the horizontal plate shell elements connected by the weld joint to localize the gap. Assuming that the vertical plate is in bending, the MSE of the shell element of the horizontal plate will increase and decrease sharply across the seam line at the edges of the gap. If the theoretical model predicted MSEs are closest to the experimental ones, the model can be regarded as properly updated and the change of the design parameter shows the location of the gap. The objective function to maximise this MSE shape similarities is defined as:

$$\min f = -\frac{\mathbf{MSEa}^{\mathrm{T}} \cdot \mathbf{MSEe}}{|\mathbf{MSEa}| \cdot |\mathbf{MSEe}|} \tag{7.8}$$

where a '-' is added to turn the maximum problem into a minimum problem. **MSEa** and **MSEe** are theoretical and experimental MSE vectors of the shell elements along the weld seam line for a certain mode, respectively. Usually, one row of shell elements nearest and parallel to the weld is enough to localize a gap in the weld.

Genetic algorithm (GA) is applied to solve the optimization problem in equation (7.8) and (7.5). This is a typical model updating problem that needs to be solved with the response surface method, because the calculation of the theoretical dynamic response must rely on Nastran. The Kriging model based model updating strategy proposed in chapter 6 (Figure 6-4) can be directly used to utilize the two responses (natural frequencies and MSEs) and it is found that the response surfaces of both objective functions meet the requirement. The updating of the intact model is relative easy as only one parameter *E* is considered. Thus, only the procedure of the model updating for damage identification is briefly described based on the method presented in Figure 6-3.

- **Step 1**: Select the updating parameters and set their range
- **Step 2**: Solve the optimization problem by the EGO algorithm. Note that the initial samples are generated by factorial sampling as there are only 2 design variables.
- **Step 3**: Check whether the shape of the final response surface built by the Kriging model is smooth enough. If it is, them stop and output the updating result. Otherwise, go back to step 1 and set a smaller range of the updating parameters.

Although the response surface of equation (7.8) can be used to get quite a good updating result, it also has some wrinkles, and the updating result can be improved by performing a new updating in the vicinity of the current solution. Actually, in the judgment of step 3, step 1 is returned only once by default. The method can be regarded as a two-step method: first determine the approximate range of the optimal solution and then obtain a much improved solution.

As for the calculation of experimental MSE, the curvature-based calculation method in chapter 5 (equation (5.14)) is used in this chapter, which is extended to the two-dimensional plane (assuming that the normal does not stretch when deformed, and and the mid-plane of the plate is inextensible)as follows

$$MSE = \frac{1}{2}\iint D\left\{\left(\frac{\partial^2 w}{\partial x^2}+\frac{\partial^2 w}{\partial y^2}\right)^2 + 2(1-\upsilon)\left[\left(\frac{\partial^2 w}{\partial x \partial y}\right)^2 - \frac{\partial^2 w}{\partial x^2}\frac{\partial^2 w}{\partial y^2}\right]\right\} \tag{7.9}$$

$$D = \frac{Eh^3}{12(1-\upsilon^2)}$$

where h is the thickness of the plate, υ is the Poisson's ratio, and w is the out-of-plane displacement.

7.5 Numerical simulation

In this section, an FE simulation is used to test the performance and robustness of the presented method. As shown in Figure 7-8, two plates are connected together to simulate a tee weld joint configuration with free edge conditions.

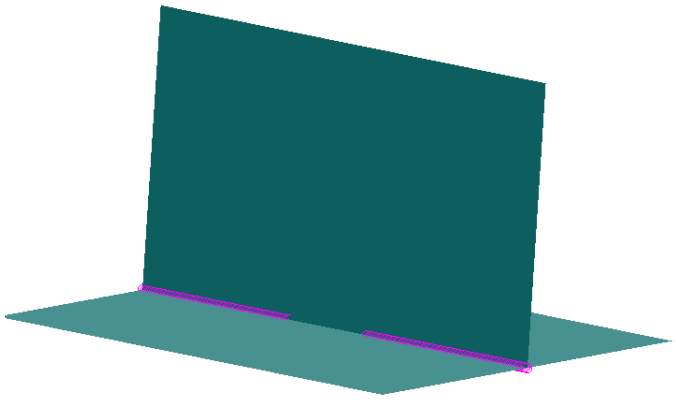

(a)

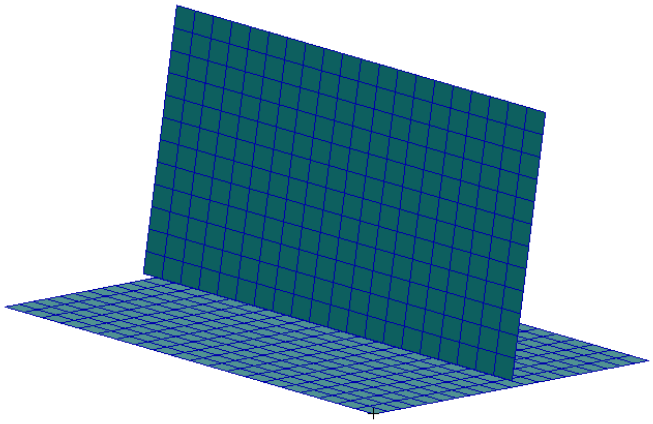

(b)

Figure 7-8 Illustrations of two T-shape models used in simulation by Patran: (a) Fine mesh with merged-node joint (b) General mesh with CSEAM element joint.

The sizes of the two plates are set to 200×200 mm (horizontal) and 200×120 mm (vertical) with 6 mm thickness. They share the same material properties: Young's modulus of 70 GPa, mass density of 2769 kg/m^3 and Poisson's ratio of 0.33. They are welded across the middle line of the horizontal plate. Two different models are constructed with shell elements (CQUAD4).

In the 1st model shown in Figure 7-8 (a), a very fine mesh (element size is set to 1mm) is distributed onto both plates. Their connected parts, edge and middle line, are overlapped. Welding connection is constructed by merging the 2 nodes at the same location as mentioned in Section 7.2. The magenta line shows the nodes that have been merged. Also, a gap is left in the middle of the weld seam representing the part of the welding fault (damage). The simulated responses of this model are regarded as experimental responses.

In the 2nd model shown in Figure 7-8 (b), the element size is set to 10mm for general use. There is a small distance between the two plates due to thickness of the horizontal plate. 20 CSEAM elements are created on both sides of the vertical plate to join the two plates together element by element, which cannot be seen in Patran. The material properties of these elements are set the same as the plates initially. Then their Young's modulus (E) is updated based on the first five frequencies of the 1st model without

damage by equation (7.5). The updated E is 28 GPa and the improvement in frequencies is shown in Table 7-2.

Table 7-2 Natural frequency improvement after updating.

Mode	1st model (Hz)	Original 2nd model (Hz)	Updated 2nd model (Hz)
1	401.3	442.1	398.9
2	459.8	463.1	456.3
3	642.6	668.0	651.2
4	680.3	694.5	656.9
5	897.5	920.7	909.8
Average error		3.9%	1.5%

Then, the proposed method is applied to identify the weld gap in the 1st model. The left edge point and length of the gap is chosen as updating parameters a and b, respectively. They both change from 0 to 20 with the constraint: $a+b \leq 20$ (unit: cm). As the gap represents the welding fault, the connection stiffness is 0 in the gap. During the updating process, E of each CSEAM element is multiplied by a factor which equals the proportion of its element length that is not covered by the gap represented by a and b.

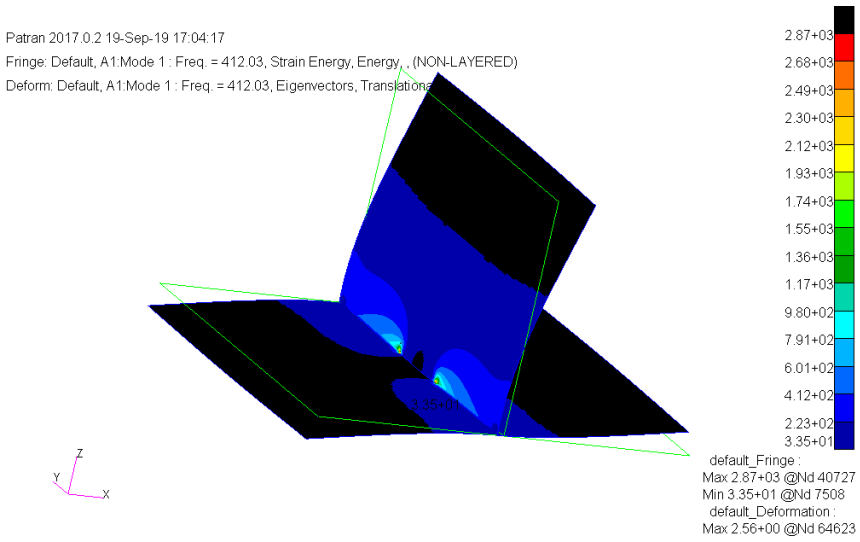

(a)

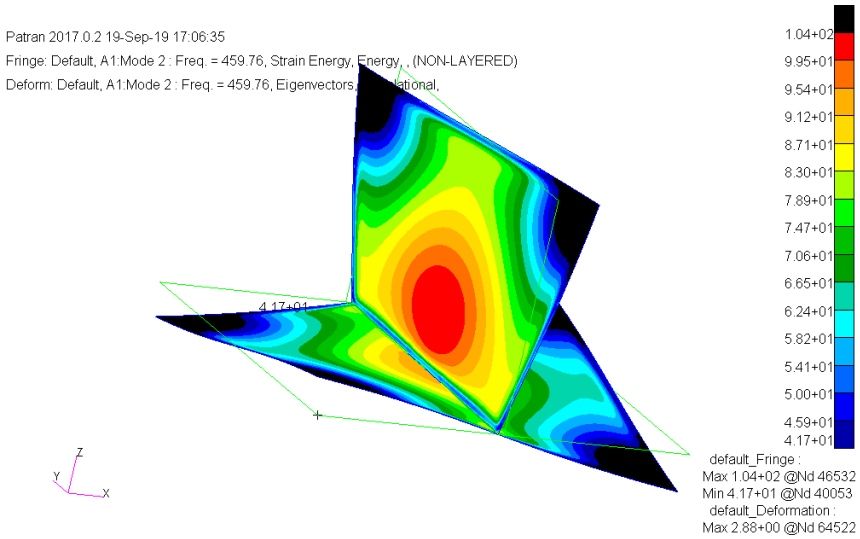

(b)

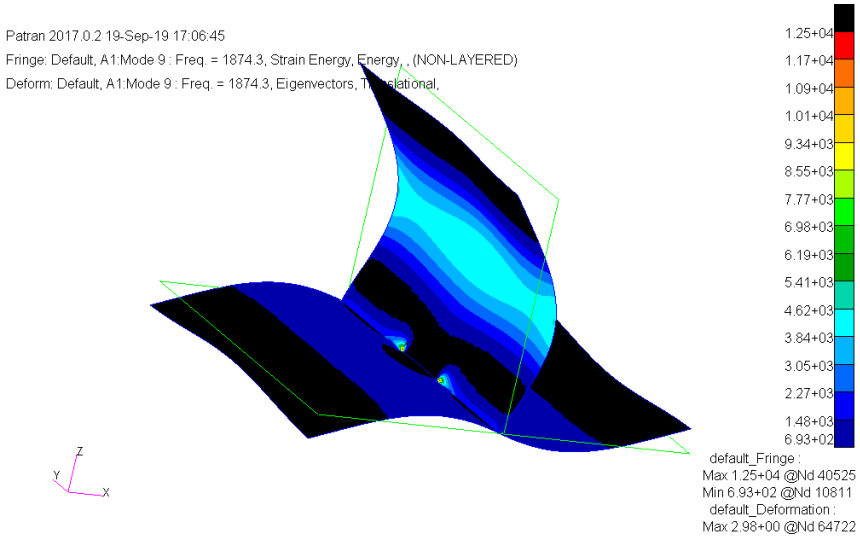

(c)

Figure 7-9 MSE distribution of the structure: (a) Mode 1; (b) Mode 2; (c) Mode 9.

Choosing the right MSE data is also a critical step. It must be made clear that not the MSEs of all modes can be used to identify damage. For example, in Figure 7-9 (b), the distribution of MSEs at the weld is primarily affected by the mode shape rather than damage. The reasonable choice should be to select the mode that the whole vertical plate bends in the same direction near the weld (Modes 1 and 9 are the available choices shown in Figure 7-9). Assuming that the damage in weld does not affect the order of the modes, in updating modes of the damaged structure must follow the mode of the initial theoretical model.

In this simulation, the MSE of the 1st mode is used for damage identification. The experimental MSE data are calculated by equation (7.9) using mode shape data extracted from the 1st model's Nastran output files — the MSE of a coarse-mesh element is obtained by integrating the MSEs of those fine-mesh elements inside it (see Figure 7-10). Note that in these figures the unit of the *x*-axis and *y*-axis is mm. As shown in Figure 7-9 (a), Figure 7-10 (b) and Figure 7-10 (c), in this mode the MSE values of the elements near the edges of the gap are extremely high, which indicates that the model updating procedure can get correct results.

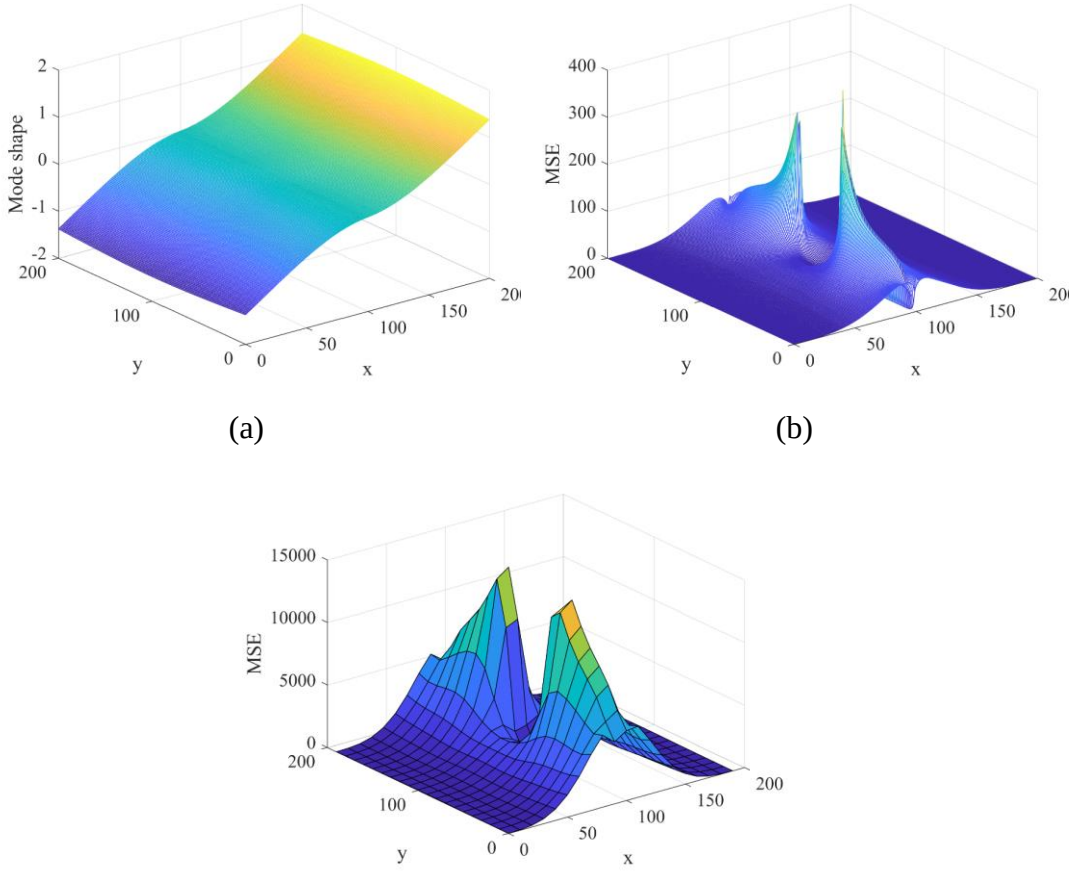

(a) (b)

(c)

Figure 7-10 Experimental data of the 1st Mode of the 1st model: (a) Extracted mode shape; (b) MSE of calculated by equation (7.9); (c) MSE of the coarse mesh corresponding to the 2nd model.

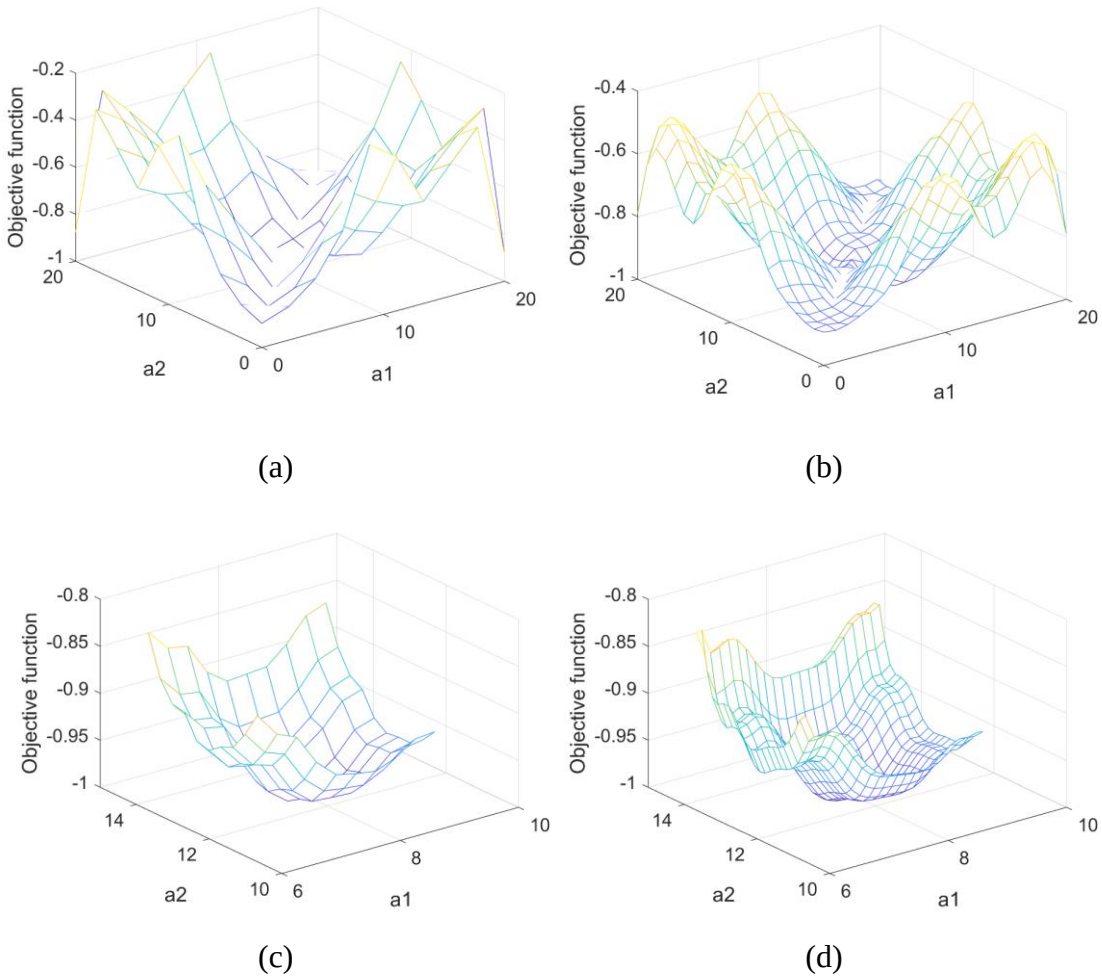

Figure 7-11 Response surface of the objective function: (a) Real response surface of the 1st step; (b) Kriging model of the 1st step; (c) Real response surface of the 2nd step; (c) Kriging model of the 2nd step.

During the updating, the response surfaces of the objective function is shown in Figure 7-11. Note that the axis a1 and a2 represent the location of the 2 edges (in no particular order) of the gap. Compared with directly using *a* and *b* to form a response surface of a triangular region, this setting is to ensure that the response surface of the 1st step is calculated in a rectangle region and is smooth near the axis of symmetry; otherwise the Kriging model can hardly describe that response surface. Actually, the real response surface of the 1st step (Figure 7-11 (a)) is still not smooth enough, and that is why the 2nd updating procedure is applied as an insurance based on the localization of the 1st step. If the wrinkles of that response surface are more severe, Equation (7.8) must be improved to allow proper solutions.

Table 7-3 Actual location and updating results of the gap.

Parameters	Actual value	Updating results	Error
a	7.9	7.76	1.8%
b	4.5	4.68	4%

After the optimization, the updated *a* and *b* are compared with their actual values in Table 7-3. It is clear that the damage gap can be identified correctly with tiny errors by this method. These errors are caused by inevitable modelling error which influences the updating result of the gap. The updated MSEs are compared with the experimental data shown in Figure 7-12 where the experimental data are normalized to have the same mean value with the updated data.

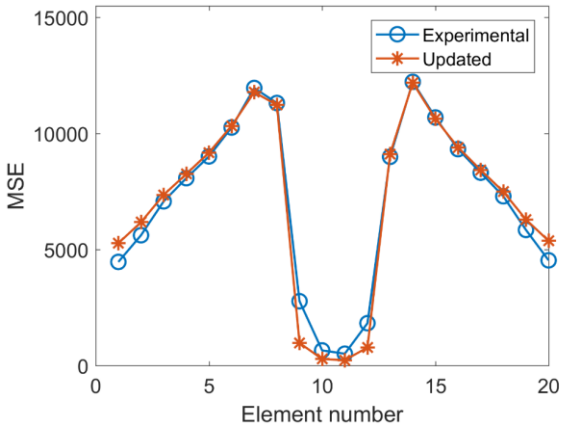

Figure 7-12 Comparison of element MSEs across the weld seam.

In this simulation, the proposed MSE-based model updating method can successfully identify the damage in the weld. It is illustrated that the MSE shape of one line of elements of the horizontal plate across the seam weld can provide enough information of the location of the gap. The experimental MSEs are calculated by the mode shape 'measurements'. Again, when the data are contaminated by noise, Gaussian smoothing technique must be used to obtain correct updating result, which is demonstrated in the next section.

7.6 Experimental results

In this section, 3 specially designed T-shaped steel structures with fillet weld connections are used to verify the proposed method. Their detailed design parameters and actual appearance are shown in the Figure 7-13. The 3 structures are referred to as T1, T2, T3 and their components are referred to as h1, h2, h3 for the horizontal plates (the left part is used for clamping) and v1, v2, v3 for the vertical plates, respectively. Initially, those 6 plates are cut from a single (larger) plate. Then, each pair of them are welded together by inert gas welding. Among them, T1 represents the intact model whose weld is designed Figure 7-13 (c) while T2 and T3 are 2 damaged structures whose damage scenarios are designed in Figure 7-14. The 2 gaps in both sides of the connection parts without any welding are considered as the damage to be identified, which is the main goal of this chapter.

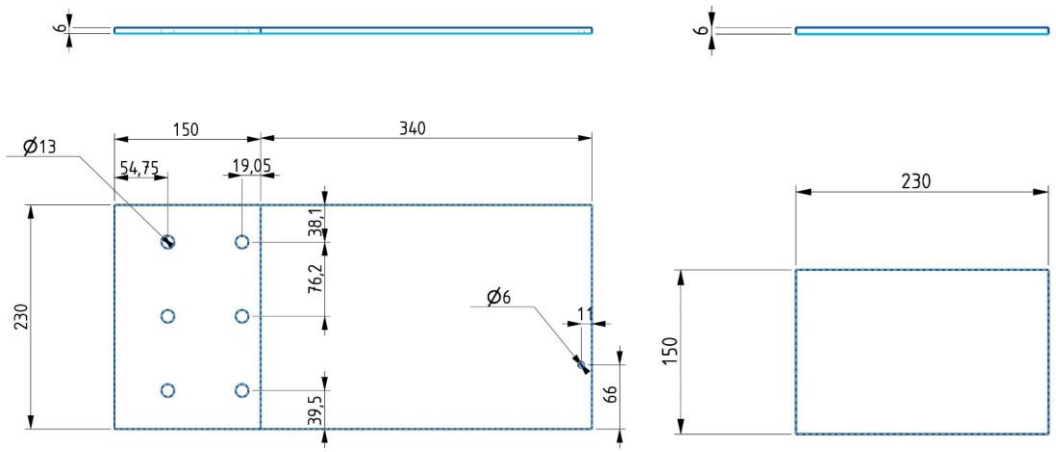

(a) (b)

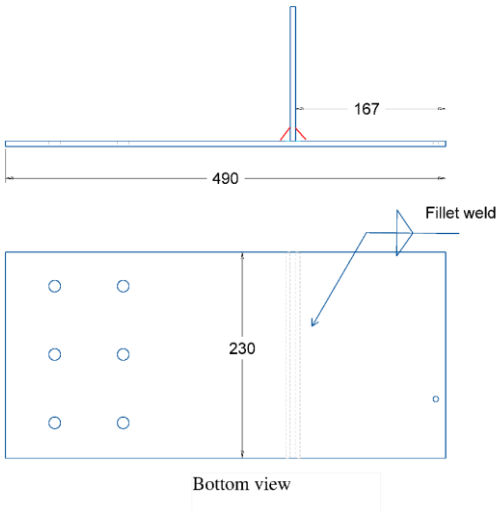

(c) (d)

Figure 7-13 Designed parameters of the T-shape structures (unit: mm): (a) Horizontal plate; (b) Vertical plate; (c) Weld connection for T1; (d) Actual appearance.

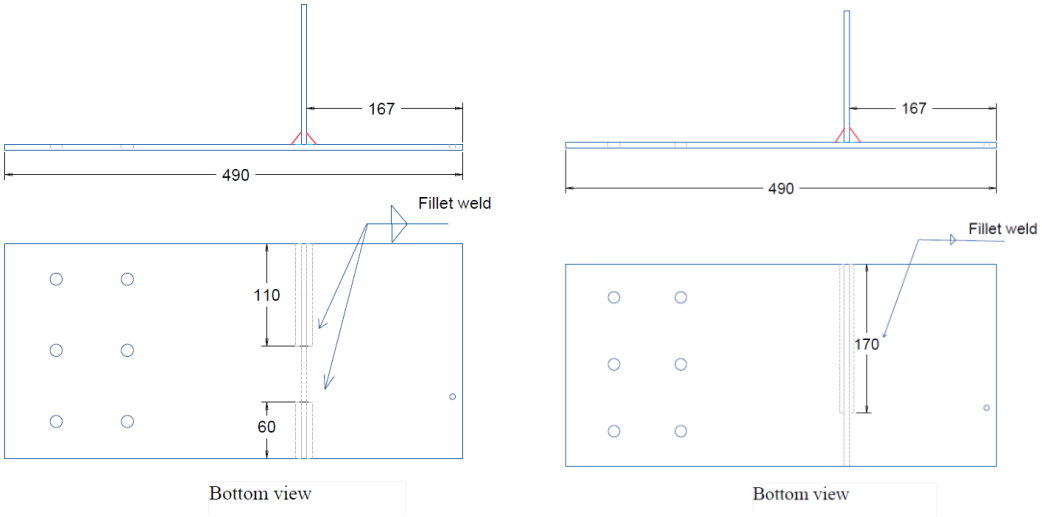

(a) (b)

Figure 7-14 Two damage scenarios: (a) Weld connection for T2; (b) Weld connection for T3.

The sizes of these real plates are very close to the design parameters. The mass densities of each plates are calculated by the measured weights shown in Table 7-4. Based on these, the Young's moduli and Passion's ratios are determined by model updating of plates h1, h2 and h3 and shown in Table 7-5. Finally, the averaged values of these material properties, which are regarded as the true material properties of the

original plate from which all the 6 component plates are cut, are used in the theoretical model.

Table 7-4 The measured weights (unit: kg) and calculated mass densities (unit: kg/m^3) of the plates.

	h1	h2	h3	v1	v2	v3	Average
Weight	5.28	5.28	5.26	1.62	1.62	1.63	
Density	7870.3	7873.3	7839.0	7826.1	7845.4	7874.4	7854.7

Table 7-5 Measured frequencies (unit: Hz) and updated *E* (unit: GPa) and ν of the horizontal plates.

Modes	h1	h2	h3	Average
1	42.81	42.6	42.66	
2	142.34	140	141.72	
3	265.47	262.9	264.53	
4	481.88	473.13	479.38	
5	667.19	666.88	665.78	
Updated *E*	196.4	191.6	194.8	194.3
Updated ν	0.3	0.295	0.3	0.30

In the theoretical model, the two plates are divided into 10-mm meshes and are connected by 46 CSEAM elements as shown in Figure 7-15 (a). This model is utilized to identify the damage in T2 and T3. Similar to section 7.5, at the beginning, the intact model T1 is used to obtain the initial Young's modulus (*E*) of CSEAM elements in the theoretical model based on the measured first six natural frequencies as shown in Table 7-6. Unlike the previous simulation, this updated *E* far exceeds that material property of the two plates. This means that this updating parameter only represents the strength of the weld itself, regardless of the actual physical meaning.

Table 7-6 Model updating of the *E* (unit: GPa) of the welding part based on natural frequencies (unit: Hz).

Modes	T1 measurements	Initial model	Updated model

1	36.72	5.88	36.95
2	103.75	39.03	107.23
3	180.94	79.04	183.78
4	233.59	164.62	228.25
5	340.31	166.32	333.82
6	410.78	187.12	398.72
E		194.3	7.37×10^{6}

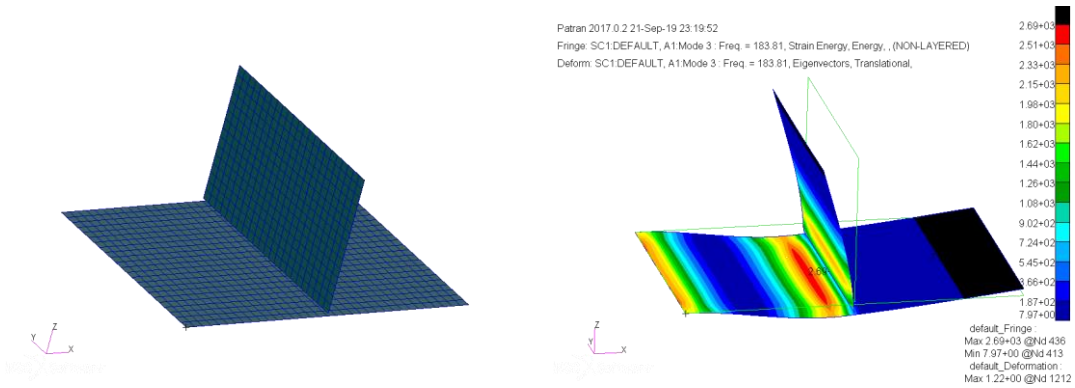

(a) (b)

Figure 7-15 (a) Theoretical model connected by CSEAM elements; (b) MSE distribution of the 3rd mode.

Next, FE analysis is applied to find effective modes for damage identification. It is required that the whole part of the vertical plate near the joint bends to one direction and thus the suitable ones are modes 3 and 4. Here, the 3rd order mode shape is adopted for both T2 and T3. The MSE distribution of the intact model of this mode is shown in Figure 7-15 (b). Note that the highest MSEs exist in the leftmost and middle left positions, as the structures are fixed at the left end.

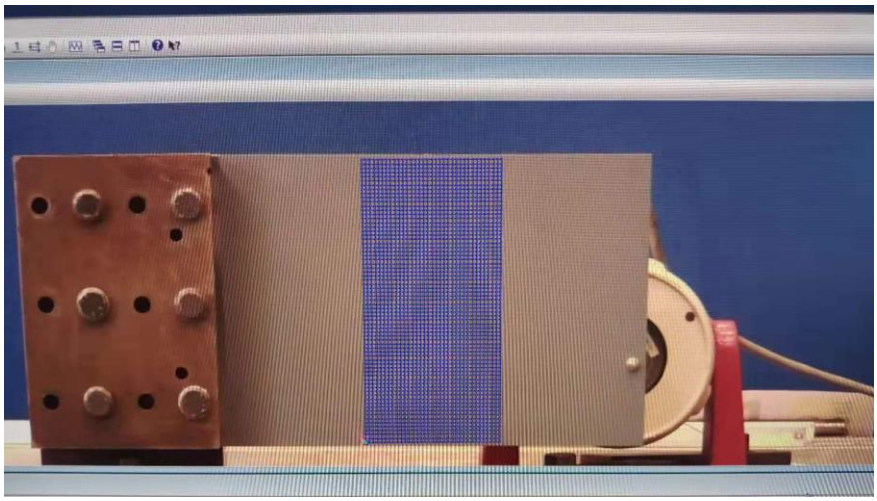

Figure 7-16 Grid of measurement points.

After that, the PSV-500 SLV is used to measure the 3rd mode shape of T2. The experimental set-up has been introduced in chapter 3. Only the area near the weld seam line is measured and a very fine measurement grid (71×35 points) is designed to improve the accuracy of the MSE calculation. For de-noising, the Gaussian smoothing technique is applied similarly to the 1-D problem in chapter 5. For example, the measured data can be recorded in a 71×35 matrix. When calculating the curvature of each point in the *x* direction, the data on each line of the matrix are calculated separately. By performing the same operation on each line as the 1-D de-noising used in chapter 5, the data can be greatly improved as shown in the Figure 7-17.

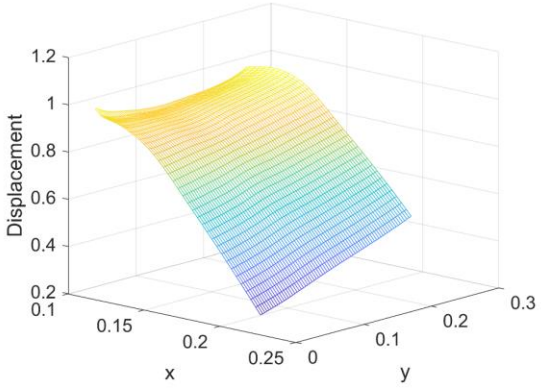

(a)

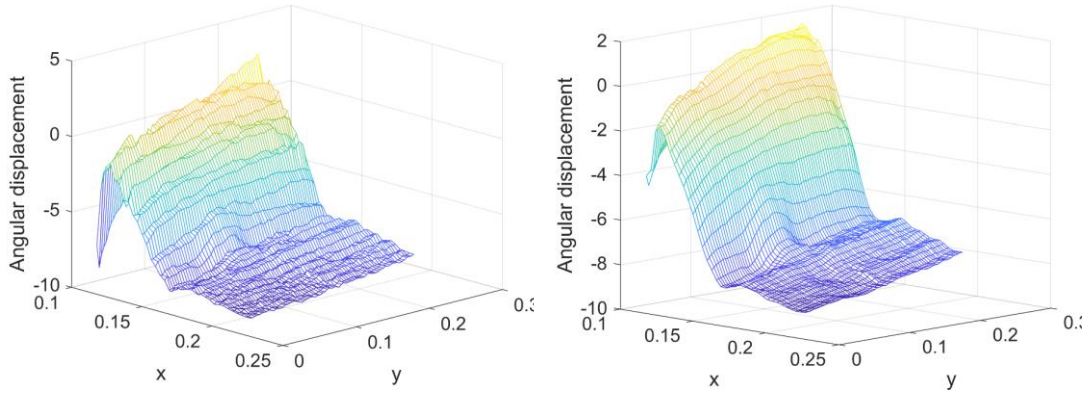

(b)

(c)

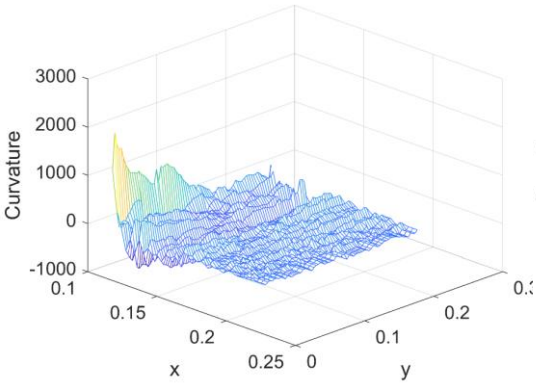

(d)

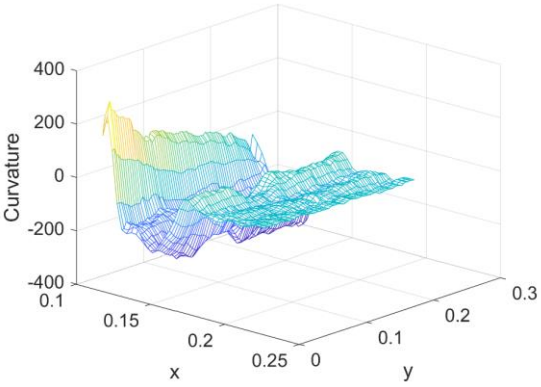

(e)

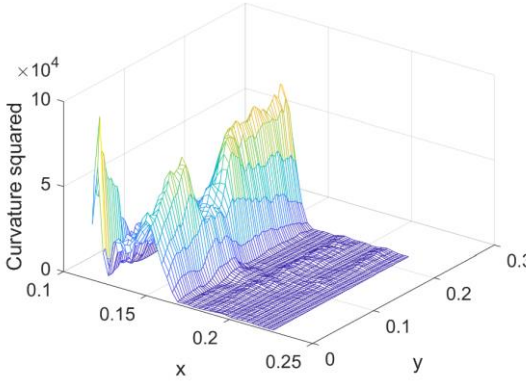

(f)

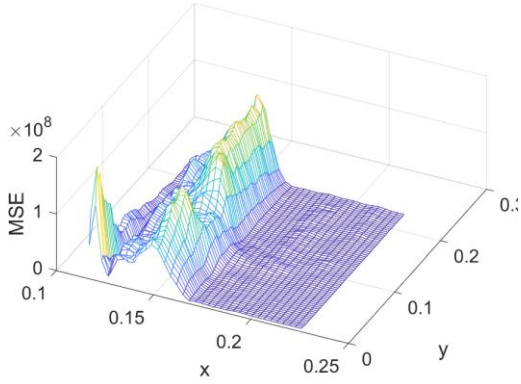

(g)

Figure 7-17 Performance of Gaussian smoothing technique applied on calculating x-direction curvature measurements: (a) Measured mode shape; (b) x-direction angular displacement calculated from (a); (c) x-direction angular displacement calculated from smoothed (c); x-direction curvature calculated from (b); (d) x-direction curvature calculated from smoothed (c); (e) Curvature squared from (d); (f) Final MSE density measurements.

Bringing the curvatures of a point into equation (7.9), the MSE density value of the point is obtained as shown in Figure 7-17 (g). Then, each element of the theoretical model is further subdivided, and the MSE density values on nodes of each sub-element are determined by the surface fitting of the MSE density values of the measuring points nearby. Finally, the actual measured MSE values corresponding to the theoretical model elements are obtained by integration of these sub-elements.

Similar to the FE analysis of the initial model, the region with the highest MSE value of T2 is on the left of the weld seam line. The MSE values of the elements in this area (between 0.14 m and 0.15 m from the left edge of the horizontal plate) should be selected as the reference responses because the high MSE value is less affected by noise and more sensitive to damage. Note that the leftmost high MSEs affected by the boundary conditions are not considered.

The proposed MSE based model updating method is applied for the damage identification of T2. The same process is performed again for T3. Their identification results are shown in Figure 7-18. Note that the experimental MSEs are normalized to have the same mean value with the updated MSEs for comparison. From these figures, it is clear that this method can localize the gaps quite well.

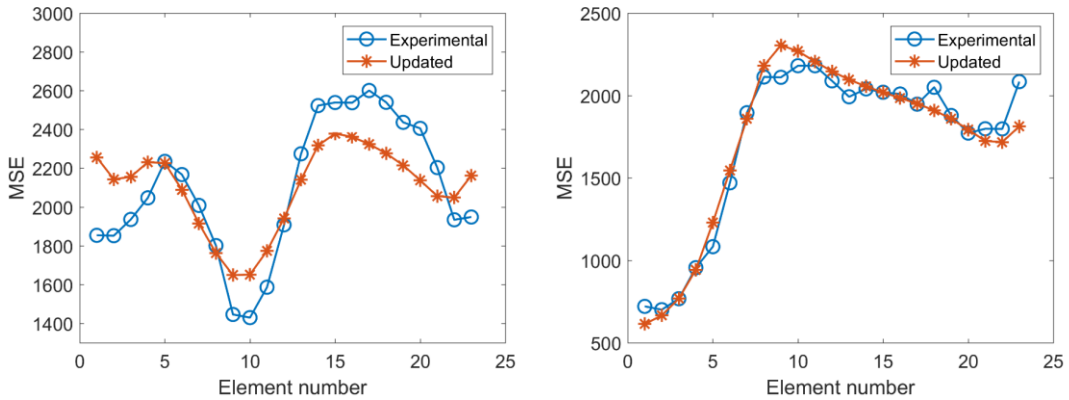

(a) (b)

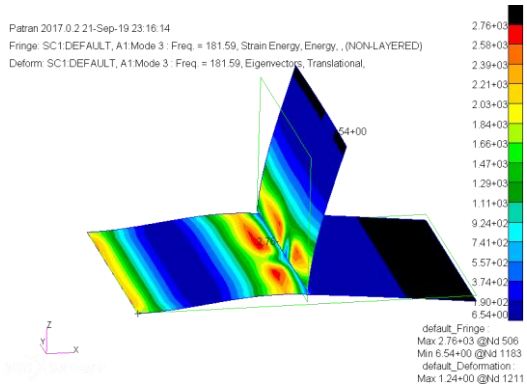

(c)

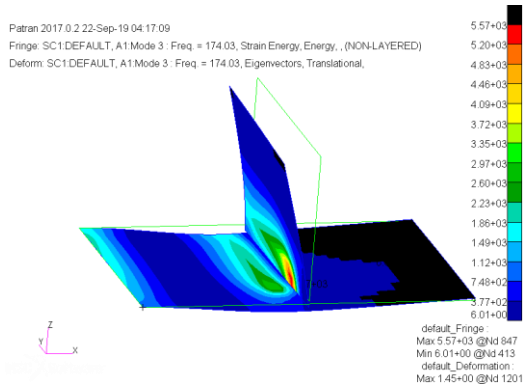

(d)

Figure 7-18 (a) Experimental and updated MSEs comparison of T2; (b) Experimental and updated MSEs comparison of T3; (c) The 3rd mode theoretical MSE distribution of T2; (d) The 3rd mode theoretical MSE distribution of T3;

Table 7-7 Updating results of T2 and T3 (unit: cm).

Parameters	T2	Updating results	Error	T3	Updating results	Error
a	6	6.3	5%	0	0	0%
b	6	5.4	10%	6	6.02	0.3%

Table 7-8 Computation time comparison of the 2 methods (unit: s).

	The proposed method	GA method
Time	581	11513

In addition, the contribution to saving computation time by introducing the Kriging model is demonstrated in Table 7-8. The computation time of the proposed method is directly recorded while the computation time of the GA method is estimated by multiplying the number of the objective function calculated (the number is obtained from applying GA on the Kriging model) by the time of the single response calculation. As can be seen the proposed method saves plenty of time when based on the Kriging model.

It is natural to consider whether the proposed method can be used for multi-gap identification. The first difficulty to face is the problem of parameter design. Assuming

that the structure has two both at both ends of the weld seam, then the two parameters corresponding to the length of the two gaps need to be identified. The proposed method can be applied and get good result, which has been proved by a simulation. However, if it is only known that there are two cracks, the problem becomes extremely complicated. Imagining the starting point and the length of two gaps as parameters (4 parameters), the cross and merge between two gaps will inevitably occur when constructing the response surface. This will cause the response surface to fail to meet the solution requirements. In addition, the number of updating parameters cannot be too large, as mentioned in Chapter 6. The problem of multi-notch recognition is a very challenging problem and will be explored in the future.

7.8 Conclusions

The purpose of this chapter is to study how to correctly construct a theoretical model to reflect the dynamic properties of a seam welded structure. First, the principle and process of connecting two plates using CSEAM element are described in detail. The CSEAM element is a Nastran-designed element that is provided for modelling a seam weld connecting two surfaces, which has many advantages in modelling. In practical applications, it is also necessary to update the theoretical model using the measured data such as natural frequencies. Note that although the CSEAM element has several parameters that can be adjusted, most of them only serve the modelling itself and have very little impact on the overall dynamic characteristics of a welded structure. For example, reducing the size of the seam element by 10 times will only result in less than 1% change in a frequency. Therefore, only the Young's modulus E of the CSEAM element is corrected and it is taken as reflecting the elastic property of a seam weld.

Next, based on the updated theoretical model, damage identification for two welded structures is also studied based on the CSEAM element. Here the damage is introduced as a gap in the weld and this research aim to establish a reliable method to locate the edges of the gap. Two common T-shaped structures are the object of study. Since the welding position is not suitable for measurement, identifying the damage through the dynamic characteristics of part of a structure (the horizontal plate in this case) is preferred and it is found that the modal strain energy (MSE) has an excellent potential

as the response in identification. At the same time, since the response of the theoretical model needs to be calculated by Nastran, the updating strategy based on the Kriging model proposed in Chapter 6 is adopted and a new MSE-based model updating method is established to realize the damage identification of the gap. This method is validated by a numerical simulation and two experimental cases, and demonstrates reliable identification results and high computational efficiency (compared with a direct GA method for solving the resulting optimization problems).

Chapter 8 - Conclusions and future work

8.1 Conclusions

This thesis focuses on the research of model updating-based damage identification methods. Model updating is a widely used optimization-based approach that makes the finite element model of a structure more accurate for subsequent structural analysis and design. When applied to the field of damage identification, this methodology can effectively determine the location and relative degree of the damage. At present, there are still some serious shortcomings in the application of model updating methods to large and complex structures. In this thesis, several original contributions have been made in computational efficiency, utilization of modal strain energy and application in the modelling and damage identification of welded joints by means of model updating methods, which are summarized as follows:

A unique contribution of this thesis is to propose a new model updating strategy based on Kriging model, which can easily use various types of dynamic responses to perform response surface-based model updating. The traditional approaches requires building a separate response surface for each response used, and that the response surface changes smoothly so that it can be described by mathematical tools. This results in only a few response types (usually the natural frequency and the modal assurance criterion value) that can be used, and the numbers of responses and updating parameters are limited. The newly proposed strategy only constructs the response surface of the objective function, so that the number of available responses is no longer restricted, and the number of updating parameters allowed is relatively increased. The efficient global optimization algorithm based solution scheme makes it possible to obtain reliable updating results only by ensuring that the response surface is smooth enough in the region near the optimal solution. Therefore, based on the proposed strategy, the model updating problem which requires finite element software to calculate specific responses can be efficiently solved by the evolutionary algorithm (genetic algorithm (GA) is used in this thesis) with only the requirement of designing the appropriate objective function.

The proposed model updating strategy is first applied to the utilization of frequency response function (FRF) data. The FRF is a typical response with highly nonlinear response surface, especially when the frequency point is chosen near resonance or anti-resonance. It is found that the objective function constructed by the summation of residuals of the Frequency Domain Assurance Criterion (FDAC) has a smooth response surface and can make full use of the vibration information contained in the FRF data. The robustness of this method is verified by a simulated cantilever beam and an experiment of a three-story building model structure. In the numerical simulation, the FRF based method can solve the model updating problem with 9 updating parameters, which is almost the maximum number allowed in the Kriging model in this problem; otherwise, the required sampling points will make the solution time of the problem unacceptable. In the experimental verification, when calculating the objective function of the FRFs close to the natural frequencies, it is necessary to use only the imaginary parts of the FRF to reduce the wrinkles of the response surface to improve the convergence of the problem. This emphasizes that the response surface is more important than the information of the response itself (the information in the real parts of the FRF is ignored). Finally, all 9 damage states can be identified by the proposed method.

In order to further validate the proposed strategy, the challenging problem of modelling and damage identification of the structures connected by the seam welded joint are investigated. The way of modelling the joint by Nastran-designed CSEAM elements is explored and many advantages of this modelling method are summarized. After the theoretical model is built, the Young's modulus of the CSEAM elements can be updated based on the measured natural frequencies, which is verified by an experiment of a T-shaped structure with 2 steel plates connected by fillet welds. The result shows that the updated theoretical model can reflect the natural frequencies of the actual structure quite well and the stiffness of the CSEAM elements is almost rigid.

For such T-shaped structures, the damage is introduced in the form of a weld gap. In the numerical simulation, it is found that the element modal strain energies (MSEs) of the horizontal plate rise and fall sharply along the direction of the weld due to the stress concentration at the edge of the gap. This indicates that this dynamic response can be

used to identify such gap damage. Of course, the premise of the use of the MSE is that it can be accurately measured. In this research, it is demonstrated that the available MSE test data can be obtained for two-dimensional plates and one-dimensional beams by the integration of curvature while the curvature is calculated by applying an finite difference method combined with Gaussian smoothing technique on the high-density mode shape data measured by a PSV-500 scanning laser vibrometer.

Then, a new MSE-related objective function is constructed and solved by the Kriging model based updating method. This method is applied in damage identification of the weld gap in which the left edge position and length of the gap are selected as updating parameters. There is a default constraint on the second updating parameter that the length of the gap is not less than 0, which results in constructing a response surface of a triangle region. However, the edge of this response surface is too steep and the updating cannot converge. Therefore, in practical application, the response surface is constructed with the left and right edges of the gap as variables, without restricting the orders of their numerical values. In this way, a smooth response surface of a rectangular region can be built and the optimization problem can be solved. The proposed method successfully identifies the location of the gaps of the two damaged T-shaped structures. In the experiment, it is also found that when the T-shaped structure is constrained as a cantilever, the most obvious position of MSE that reflects the damage (element MSE line with the maximum average value) appears outside the weld. This phenomenon is different from the situation under free boundary condition in simulation and requires special attention in practical application.

As a derivative of the mode shape, MSE is more sensitive to damage than the mode shape. The traditional damage identification methods utilizing MSE were mainly the damage index methods which determined the damage location based on the change of element MSE. Such methods are prone to misjudgement because they lack effective measurement methods and the damage index method itself does not make full use of the information contained in the MSE data. Therefore, this research also explores the general MSE based model updating method. Although the objective function constructed by MSE residuals can be solved directly by GA, the proposed sensitivity-based model updating method is more suitable for the problems with a large number

of updating parameters, such as model updating of truss structures. In addition, by normalizing the measured mode shape data with the theoretical mass matrix, the method can be used as a baseline-free damage identification method, which is verified by an experiment of a cantilever beam with cracks.

8.2 Future work

Although the proposed model updating methods in chapter 5 and 7 have successfully identified the damage in beams and seam welded joint and have been verified by experiments, there is still enough room for improvement.

(1) The MSE-based model updating method proposed in chapter 5 mainly uses the MSE test data extracted from the first four modes. For higher modes, the change in the element MSE caused by the damage is not outstanding. This means that when the number of updating parameters increases, the information provided by the MSE data may not be sufficient to identify the damage. Therefore, it is reasonable to consider using FRF data. Model updating methods based on strain energy of the shape of FRF are a direction that can be explored.

(2) In chapter 7, the damage of the weld is in the simplest form. Weld damage can take other forms, e.g., air bubbles inside welds, uneven thickness, etc. The challenge is that they usually cause small changes in stiffness (and even smaller changes in mass). It is also possible to study the performance of the proposed method under other damage forms, such as only one side of the weld has a gap or the positions of the weld gaps on both sides are different. The author is confident in that the proposed method can accomplish model updating with more than four updating parameters, and it is interesting to explore the maximum capability of this method.

(3) The ultimate goal of the seam welded joint damage identification problem is to effectively identify the minor damage. This requires that all Young's moduli of CSEAM elements are taken as updating parameters while the problem is solved efficiently using a reliable mathematical model. For this problem, the number of updating parameters is so large that the Kriging model cannot describe the complex

response surface through a limited number of sampling points. Thus, new mathematical tools need to be studied, and artificial neural network method is a potential choice.

Appendix A:

Nastran input file (.bdf) for Normal Modes analysis (SOL 103) of welded structures using CSEAM elements with PARTPAT format.

```
$ Direct Text Input for Nastran System Cell Section
$ Direct Text Input for File Management Section
$ Direct Text Input for Executive Control
$ Normal Modes Analysis, Database
SOL 103
CEND
$ Direct Text Input for Global Case Control Data
TITLE = MSC.Nastran job created on 06-Apr-18 at 16:03:06
ECHO = NONE
$ Using Nastran default values for RESVEC
SUBCASE 1
    SUBTITLE=Default
    METHOD = 1
    VECTOR(SORT1,REAL)=ALL
    SPCFORCES(SORT1,REAL)=ALL
$ Direct Text Input for this Subcase
BEGIN BULK
$ Direct Text Input for Bulk Data
PARAM       POST       0
PARAM     PRTMAXIM YES
EIGRL           1                1.              3000.           20              0
MASS
$ Elements and Element Properties for region : shell1
PSHELL     1          1          3.          1                   1
$ Pset: "shell1" will be imported as: "pshell.1"
CQUAD4     1          1          1          2          3          4
CQUAD4     2          1          2          6          7          3
```

```
$ Elements and Element Properties for region : shell2
PSHELL      2           1          3.          1                      1
$ Pset: "shell2" will be imported as: "pshell.2"
CQUAD4      3           2          8           9          11          10
$ Elements and Element Properties for region : shell3
PSHELL      3           1          3.          1                      1
$ Pset: "shell3" will be imported as: "pshell.3"
CQUAD4      4           3          12          13         15          14

swldprm,prtsw,101,chkrun,2

$
$ Pset: "PSEAM" will be imported as: "pseam.1000"
pseam,1000,2,,40.,10.
pseam,1001,2,,10.,5.

cseam,10001,1000,,pshell,1,3
,25.,0.,7.,25.,50.,14.
cseam,10002,1001,,pshell,1,2
,75.,0.,15.5,75.,50.,15.5

$ Referenced Material Records
$ Material Record : mat
$ Description of Material : Date: 06-Apr-18                Time: 16:00:40
MAT1        1       7.+7                .33       2.769-6
MAT1        2       7.+7                .33       2.769-6
$ Nodes of the Entire Model
GRID        1                    0.        0.        0.
GRID        2                   50.        0.        0.
GRID        3                   50.       50.        0.
GRID        4                    0.       50.        0.
GRID        6                  100.        0.        0.
GRID        7                  100.       50.        0.
```

GRID	8	50.	0.	3.
GRID	9	50.	0.	28.
GRID	10	50.	50.	3.
GRID	11	50.	50.	28.
GRID	12	10.	0.	14.
GRID	13	40.	0.	14.
GRID	14	10.	50.	14.
GRID	15	40.	50.	14.

$ Loads for Load Case : Default

$ Referenced Coordinate Frames

ENDDATA 7cde952a

References

[1] J.E. Mottershead, M.I. Friswell, Model updating in structural dynamics - a survey, J. Sound Vib., 167 (1993) 347-375.

[2] L. Deng, C.S. Cai, Bridge model updating using response surface method and genetic algorithm, J. Bridge Eng., 15 (2010) 553-564.

[3] B.R.M. Rabi, P. Nagaraj, Finite element model updating of a space vehicle first stage motor based on experimental test results, Aerospace Science and Technology, 45 (2015) 422-430.

[4] J.T. Wang, C.J. Wang, J.P. Zhao, Frequency response function-based model updating using Kriging model, Mech. Syst. Signal Proc., 87 (2017) 218-228.

[5] W. Fan, P. Qiao, Vibration-based damage identification methods: a review and comparative study, Struct. Health Monit., 10 (2011) 83-111.

[6] J.E. Mottershead, M. Link, M.I. Friswell, The sensitivity method in finite element model updating: A tutorial, Mech. Syst. Signal Proc., 25 (2011) 2275-2296.

[7] N.F. Alkayem, M.S. Cao, Y.F. Zhang, M. Bayat, Z.Q. Su, Structural damage detection using finite element model updating with evolutionary algorithms: a survey, Neural Comput. Appl., 30 (2018) 389-411.

[8] S.E. Fang, R. Perera, Damage identification by response surface based model updating using D-optimal design, Mech. Syst. Signal Proc., 25 (2011) 717-733.

[9] S.W. Doebling, C.R. Farrar, M.B. Prime, A summary review of vibration-based damage identification methods, Shock Vib. Dig., 30 (1998) 91-105.

[10] M.S. Cao, G.G. Sha, Y.F. Gao, W. Ostachowicz, Structural damage identification using damping: a compendium of uses and features, Smart Materials and Structures, 26 (2017) 14.

[11] Y. Yan, L. Cheng, Z. Wu, L. Yam, Development in vibration-based structural damage detection technique, Mech. Syst. Signal Proc., 21 (2007) 2198-2211.

[12] R. Adams, P. Cawley, C. Pye, B. Stone, A vibration technique for non-destructively assessing the integrity of structures, Journal of Mechanical Engineering Science, 20 (1978) 93-100.

[13] P. Cawley, R.D. Adams, The location of defects in structures from measurements of natural frequencies, The Journal of Strain Analysis for Engineering Design, 14 (1979) 49-57.

[14] A. Messina, E.J. Williams, T. Contursi, Structural damage detection by a sensitivity and statistical-based method, J. Sound Vib., 216 (1998) 791-808.

[15] O.S. Salawu, Detection of structural damage through changes in frequency: A review, Eng. Struct., 19 (1997) 718-723.

[16] Z.Y. Shi, S.S. Law, L.M. Zhang, Damage localization by directly using incomplete mode shapes, J. Eng. Mech.-ASCE, 126 (2000) 656-660.

[17] H.P. Chen, N. Bicanic, Assessment of damage in continuum structures based on incomplete modal information, Comput. Struct., 74 (2000) 559-570.

[18] E. Parloo, P. Guillaume, M. Van Overmeire, Damage assessment using mode shape sensitivities, Mech. Syst. Signal Proc., 17 (2003) 499-518.

[19] W.X. Ren, G. De Roeck, Structural damage identification using modal data. I: Simulation verification, J. Struct. Eng.-ASCE, 128 (2002) 87-95.

[20] W.X. Ren, G. De Roeck, Structural damage identification using modal data. II: Test verification, J. Struct. Eng.-ASCE, 128 (2002) 96-104.

[21] R.J. Allemang, The modal assurance criterion - Twenty years of use and abuse, Sound Vib., 37 (2003) 14-23.

[22] O.S. Salawu, C. Williams, Bridge assessment using forced-vibration testing, J. Struct. Eng.-ASCE, 121 (1995) 161-173.

[23] L.J. Hadjileontiadis, E. Douka, A. Trochidis, Fractal dimension analysis for crack identification in beam structures, Mech. Syst. Signal Proc., 19 (2005) 659-674.

[24] L.J. Hadjileontiadis, E. Douka, Crack detection in plates using fractal dimension, Eng. Struct., 29 (2007) 1612-1625.

[25] J. Wang, P.Z. Qiao, Improved damage detection for beam-type structures using a uniform load surface, Struct. Health Monit., 6 (2007) 99-110.

[26] K.M. Liew, Q. Wang, Application of wavelet theory for crack identification in structures, J. Eng. Mech., 124 (1998) 152-157.

[27] Q. Wang, X.M. Deng, Damage detection with spatial wavelets, Int. J. Solids Struct., 36 (1999) 3443-3468.

[28] E. Douka, S. Loutridis, A. Trochidis, Crack identification in plates using wavelet analysis, J. Sound Vib., 270 (2004) 279-295.

[29] C.C. Chang, L.W. Chen, Detection of the location and size of cracks in the multiple cracked beam by spatial wavelet based approach, Mech. Syst. Signal Proc., 19 (2005) 139-155.

[30] A. Pandey, M. Biswas, Damage detection in structures using changes in flexibility, J. Sound Vib., 169 (1994) 3-17.

[31] A.K. Pandey, M. Biswas, Experimental-verification of flexibility difference method for locating damage in structures, J. Sound Vib., 184 (1995) 311-328.

[32] J. Zhao, J.T. DeWolf, Sensitivity study for vibrational parameters used in damage detection, J. Struct. Eng.-ASCE, 125 (1999) 410-416.

[33] Z.D. Duan, G.R. Yan, J.P. Ou, B.F. Spencer, Damage localization in ambient vibration by constructing proportional flexibility matrix, J. Sound Vib., 284 (2005) 455-466.

[34] D. Wu, S.S. Law, Damage localization in plate structures from uniform load surface curvature, J. Sound Vib., 276 (2004) 227-244.

[35] Y.Y. Li, L. Cheng, L.H. Yam, W.O. Wong, Identification of damage locations for plate-like structures using damage sensitive indices: strain modal approach, Comput. Struct., 80 (2002) 1881-1894.

[36] Y.Y. Li, Hypersensitivity of strain-based indicators for structural damage identification: A review, Mech. Syst. Signal Proc., 24 (2010) 653-664.

[37] A. Pandey, M. Biswas, M. Samman, Damage detection from changes in curvature mode shapes, J. Sound Vib., 145 (1991) 321-332.

[38] M.M. Abdel Wahab, G. De Roeck, Damage detection in bridges using modal curvatures: Application to a real damage scenario, J. Sound Vib., 226 (1999) 217-235.

[39] C.P. Ratcliffe, Damage detection using a modified laplacian operator on mode shape data, J. Sound Vib., 204 (1997) 505-517.

[40] C.P. Ratcliffe, W.J. Bagaria, Vibration technique for locating delamination in a composite beam, Aiaa J., 36 (1998) 1074-1077.

[41] V. Amaravadi, V. Rao, L.R. Koval, M.M. Derriso, Structural health monitoring using wavelet transforms, in: L.P. Davis (Ed.) Smart Structures and Materials 2001: Smart Structures and Integrated Systems, Spie-Int Soc Optical Engineering, Bellingham, 2001, pp. 258-269.

[42] B.H. Kim, T. Park, G.Z. Voyiadjis, Damage estimation on beam-like structures using the multi-resolution analysis, Int. J. Solids Struct., 43 (2006) 4238-4257.

[43] N. Stubbs, J.-T. Kim, Damage localization in structures without baseline modal parameters, Aiaa J., 34 (1996) 1644-1649.

[44] N. Stubbs, J.T. Kim, C.R. Farrar, M. Soc Exptl, Field verification of a nondestructive damage localization and severity estimation algorithm, in: 13th Int. Modal Analysis Conf., Soc Experimental Mechanics Inc, Bethel, 1995, pp. 210-218.

[45] P. Cornwell, S.W. Doebling, C.R. Farrar, Application of the strain energy damage detection method to platelike structures, J. Sound Vib., 224 (1999) 359-374.

[46] Y.C. Li, S.Q. Wang, M. Zhang, C.M. Zheng, An improved modal strain energy method for damage detection in offshore platform structures, J. Mar. Sci. Appl., 15 (2016) 182-192.

[47] Z.Y. Shi, S.S. Law, Structural damage localization from modal strain energy change, J. Sound Vib., 218 (1998) 825-844.

[48] Z.Y. Shi, S.S. Law, L.M. Zhang, Improved damage quantification from elemental modal strain energy change, J. Eng. Mech.-ASCE, 128 (2002) 521-529.

[49] Z.Y. Shi, S.S. Law, L.M. Zhang, Structural damage detection from modal strain energy change, J. Eng. Mech.-ASCE, 126 (2000) 1216-1223.

[50] S.S. Law, Z.Y. Shi, L.M. Zhang, Structural damage detection from incomplete and noisy modal test data, J. Eng. Mech.-ASCE, 124 (1998) 1280-1288.

[51] P. Moradipour, T.H.T. Chan, C. Gallage, An improved modal strain energy method for structural damage detection, 2D simulation, Struct. Eng. Mech., 54 (2015) 105-119.

[52] P. Moradipour, T.H.T. Chan, C. Gallage, Benchmark studies for bridge health monitoring using an improved modal strain energy method, Procedia Engineering, 188 (2017) 194-200.

[53] Z. Wang, R.M. Lin, M.K. Lim, Structural damage detection using measured FRF data, Comput. Meth. Appl. Mech. Eng., 147 (1997) 187-197.

[54] G.M. Owolabi, A.S.J. Swamidas, R. Seshadri, Crack detection in beams using changes in frequencies and amplitudes of frequency response functions, J. Sound Vib., 265 (2003) 1-22.

[55] R.P.C. Sampaio, N.M.M. Maia, Strategies for an efficient indicator of structural damage, Mech. Syst. Signal Proc., 23 (2009) 1855-1869.

[56] R.P.C. Sampaio, N.M.M. Maia, J.M.M. Silva, Damage detection using the frequency-response-function curvature method, J. Sound Vib., 226 (1999) 1029-1042.

[57] N.M.M. Maia, J.M.M. Silva, E.A.M. Almas, R.P.C. Sampaio, Damage detection in structures: from mode shape to frequency response function methods, Mech. Syst. Signal Proc., 17 (2003) 489-498.

[58] M. Baruch, Optimization procedure to correct stiffness and flexibility matrices using vibration tests, Aiaa J., 16 (1978) 1208-1210.

[59] M. Baruch, Methods of reference basis for identification of linear dynamic structures, Aiaa J., 22 (1984) 561-564.

[60] F.S. Wei, Analytical dynamic-model improvement using vibration test data, Aiaa J., 28 (1990) 175-177.

[61] M.I. Friswell, D.J. Inman, D.F. Pilkey, Direct updating of damping and stiffness matrices, Aiaa J., 36 (1998) 491-493.

[62] M. Friswell, J.E. Mottershead, Finite element model updating in structural dynamics, Kluwer Academic, Dordrecht, 1995.

[63] R.L. Fox, M.P. Kapoor, Rates of change eigenvalues and eigenvectors, Aiaa J., 6 (1968) 2426-&.

[64] C.S. Rudisill, Y.-Y. Chu, Numerical methods for evaluating the derivatives of eigenvalues and eigenvectors, Aiaa J., 13 (1975) 834-837.

[65] R.B. Nelson, Simplified calculation of eigenvector derivatives, Aiaa J., 14 (1976) 1201-1205.

[66] I.-W. Lee, G.-H. Jung, An efficient algebraic method for the computation of natural frequency and mode shape sensitivities—part I. Distinct natural frequencies, Comput. Struct., 62 (1997) 429-435.

[67] I.W. Lee, D.O. Kim, G.H. Jung, Natural frequency and mode shape sensitivities of damped systems: Part I, Distinct natural frequencies, J. Sound Vib., 223 (1999) 399-412.

[68] E. Gorl, M. Link, Damage identification using changes of eigenfrequencies and mode shapes, Mech. Syst. Signal Proc., 17 (2003) 103-110.

[69] F. Sarvi, S. Shojaee, P. Torkzadeh, Damage identification of trusses by finite element model updating using an enhanced Levenberg-Marquardt algorithm, Iran University of Science & Technology, 4 (2014) 207-231.

[70] B. Moaveni, A. Stavridis, G. Lombaert, J.P. Conte, P.B. Shing, Finite-element model updating for assessment of progressive damage in a 3-story infilled RC frame, J. Struct. Eng., 139 (2013) 1665-1674.

[71] H. Ahmadian, J.E. Mottershead, M.I. Friswell, Regularisation methods for finite element model updating, Mech. Syst. Signal Proc., 12 (1998) 47-64.

[72] M.I. Friswell, J.E. Mottershead, H. Ahmadian, Finite-element model updating using experimental test data: parametrization and regularization, Philos. Trans. R. Soc. Lond. Ser. A-Math. Phys. Eng. Sci., 359 (2001) 169-186.

[73] P.C. Hansen, Analysis of discrete ill-posed problems by means of the L-curve, SIAM Rev., 34 (1992) 561-580.

[74] X.Y. Li, S.S. Law, Adaptive Tikhonov regularization for damage detection based on nonlinear model updating, Mech. Syst. Signal Proc., 24 (2010) 1646-1664.

[75] B. Weber, P. Paultre, Damage identification in a truss tower by regularized model updating, J. Struct. Eng., 136 (2009) 307-316.

[76] M. Imregun, W.J. Visser, D.J. Ewins, Finite element model updating using frequency response function data: I. Theory and initial investigation, Mech. Syst. Signal Proc., 9 (1995) 187-202.

[77] X.Y. Gang, S. Chai, R.J. Allemang, L.J. Li, A new iterative model updating method using incomplete frequency response function data, J. Sound Vib., 333 (2014) 2443-2453.

[78] A. Esfandiari, F. Bakhtiari-Nejad, A. Rahai, M. Sanayei, Structural model updating using frequency response function and quasi-linear sensitivity equation, J. Sound Vib., 326 (2009) 557-573.

[79] A. Esfandiari, Structural model updating using incomplete transfer function of strain data, J. Sound Vib., 333 (2014) 3657-3670.

[80] R. Pascual, J.C. Golinval, M. Razeto, M. Soc Exptl, A frequency domain correlation technique for model correlation and updating, in: Proceedings of the 15th International Modal Analysis Conference, Spie - Int Soc Optical Engineering, Bellingham, 1997, pp. 587-592.

[81] R. Pascual, M. Razeto, J.C. Golinval, R. Schalchli, A robust FRF-based technique for model updating, in: P. Sas, B. VanHal (Eds.) International Conference on Noise and Vibration Engineering, Katholieke Univ Leuven, Dept Werktuigkunde, Heverlee, 2002, pp. 1037-1045.

[82] F. Asma, A. Bouazzouni, Finite element model updating using FRF measurements, Shock Vib., 12 (2005) 377-388.

[83] K.S. Kwon, R.M. Lin, Frequency selection method for FRF-based model updating, J. Sound Vib., 278 (2004) 285-306.

[84] W. D'Ambrogio, A. Fregolent, On the use of consistent and significant information to reduce ill-conditioning in dynamic model updating, Mech. Syst. Signal Proc., 12 (1998) 203-222.

[85] W. D'Ambrogio, A. Fregolent, The use of antiresonances for robust model updating, J. Sound Vib., 236 (2000) 227-243.

[86] R.M. Lin, J. Zhu, Finite element model updating using vibration test data under base excitation, J. Sound Vib., 303 (2007) 596-613.

[87] S. Pradhan, S.V. Modak, Normal response function method for mass and stiffness matrix updating using complex FRFs, Mech. Syst. Signal Proc., 32 (2012) 232-250.

[88] A.J. Garcia-Palencia, E. Santini-Bell, A two-step model updating algorithm for parameter identification of linear elastic damped structures, Comput.-Aided Civil Infrastruct. Eng., 28 (2013) 509-521.

[89] M. Arras, G. Coppotelli, Finite-element structural updating using frequency response Functions, J. Aircr., 52 (2015) 1454-1468.

[90] T. Marwala, Finite element model updating using computational intelligence techniques: applications to structural dynamics, Springer Science & Business Media, 2010.

[91] M. Mitchell, An introduction to genetic algorithms, MIT press, 1998.

[92] V.R. Akula, R. Ganguli, Finite element model updating for helicopter rotor blade using genetic algorithm, Aiaa J., 41 (2003) 554-556.

[93] F.S. Almeida, A.M. Awruch, Design optimization of composite laminated structures using genetic algorithms and finite element analysis, Compos. Struct., 88 (2009) 443-454.

[94] O.E. Canyurt, H.R. Kim, K.Y. Lee, Estimation of laser hybrid welded joint strength by using genetic algorithm approach, Mech. Mater., 40 (2008) 825-831.

[95] T. Marwala, Finite element model updating using wavelet data and genetic algorithm, J. Aircr., 39 (2002) 709-711.

[96] R. Perera, A. Ruiz, A multistage FE updating procedure for damage identification in large-scale structures based on multiobjective evolutionary optimization, Mech. Syst. Signal Proc., 22 (2008) 970-991.

[97] J. Kennedy, R. Eberhart, Particle swarm optimization (PSO), in: Proc. IEEE International Conference on Neural Networks, Perth, Australia, 1995, pp. 1942-1948.

[98] Y.L. Lin, W.D. Chang, J.G. Hsieh, A particle swarm optimization approach to nonlinear rational filter modeling, Expert Syst. Appl., 34 (2008) 1194-1199.

[99] R. Kathiravan, R. Ganguli, Strength design of composite beam using gradient and particle swarm optimization, Compos. Struct., 81 (2007) 471-479.

[100] S.M. Seyedpoor, A two stage method for structural damage detection using a modal strain energy based index and particle swarm optimization, Int. J. Non-Linear Mech., 47 (2012) 1-8.

[101] L. Liu, W.X. Liu, D.A. Cartes, Particle swarm optimization-based parameter identification applied to permanent magnet synchronous motors, Eng. Appl. Artif. Intell., 21 (2008) 1092-1100.

[102] R.E. Perez, K. Behdinan, Particle swarm approach for structural design optimization, Comput. Struct., 85 (2007) 1579-1588.

[103] R. Hassan, B. Cohanim, O. De Weck, G. Venter, A comparison of particle swarm optimization and the genetic algorithm, in: 46th AIAA/ASME/ASCE/AHS/ASC structures, structural dynamics and materials conference, 2005, pp. 1897.

[104] S. Kirkpatrick, C.D. Gelatt, M.P. Vecchi, Optimization by simulated annealing, Science, 220 (1983) 671-680.

[105] E.W. McGookin, D.J. Murray-Smith, Submarine manoeuvring controllers' optimisation using simulated annealing and genetic algorithms, Control Eng. Practice, 14 (2006) 1-15.

[106] C.S. Pedamallu, L. Ozdamar, Investigating a hybrid simulated annealing and local search algorithm for constrained optimization, Eur. J. Oper. Res., 185 (2008) 1230-1245.

[107] R.I. Levin, N.A.J. Lieven, Dynamic finite element model updating using simulated annealing and genetic algorithms, Mech. Syst. Signal Proc., 12 (1998) 91-120.

[108] A. Kaveh, A. Zolghadr, Guided modal strain energy-based approach for structural damage identification using tug-of-war optimization algorithm, J. Comput. Civil. Eng., 31 (2017) 12.

[109] A. Kaveh, A. Zolghadr, Cyclical Parthenogenesis Algorithm for guided modal strain energy based structural damage detection, Appl. Soft. Comput., 57 (2017) 250-264.

[110] S.S. Jin, H.J. Jung, Sequential surrogate modeling for efficient finite element model updating, Comput. Struct., 168 (2016) 30-45.

[111] R.H. Myers, Response surface methodology - Current status and future directions, J. Qual. Technol., 31 (1999) 30-44.

[112] B.M. Rutherford, L. Swiler, T. Paez, A. Urbina, Response surface (meat-model) methods and applications, in: Proc. 24th Int. Modal Analysis Conf.(St. Louis, MO), 2006, pp. 184-197.

[113] S.E. Fang, R. Perera, A response surface methodology based damage identification technique, Smart Mater. Struct., 18 (2009) 1-14.

[114] W.X. Ren, H.B. Chen, Finite element model updating in structural dynamics by using the response surface method, Eng. Struct., 32 (2010) 2455-2465.

[115] S. Chakraborty, A. Sen, Adaptive response surface based efficient Finite Element Model Updating, Finite Elem. Anal. Des., 80 (2014) 33-40.

[116] A. Forrester, A. Sobester, A. Keane, Engineering design via surrogate modelling: a practical guide, John Wiley & Sons, 2008.

[117] L.R. Zhou, G.R. Yan, J.P. Ou, Response surface method based on radial basis functions for modeling large-scale structures in model updating, Comput.-Aided Civil Infrastruct. Eng., 28 (2013) 210-226.

[118] H.P. Wan, W.X. Ren, A residual-based Gaussian process model framework for finite element model updating, Comput. Struct., 156 (2015) 149-159.

[119] H.Y. Gao, X.L. Guo, H.J. Ouyang, F. Han, Crack Identification of Cantilever Plates Based on a Kriging Surrogate Model, J. Vib. Acoust.-Trans. ASME, 135 (2013) 10.

[120] Y. Liu, Y. Li, D.J. Wang, S.Y. Zhang, Model updating of complex structures using the combination of component mode synthesis and kriging predictor, Sci. World J., (2014) 13.

[121] H. Yin, J.J. Ma, K.L. Dong, Z.R. Peng, P. Cui, C.H. Yang, Model updating method based on Kriging model for structural Dynamics, Shock Vib., 2019 (2019) 12.

[122] E.J. Joy, A.S. Menon, N. Biju, Implementation of Kriging surrogate models for delamination detection in composite structures, Adv. Compos. Lett., 27 (2018) 220-231.

[123] F.L. Xie, Z.S. Jiang, J.W. Xiang, S.L. He, An improved two-step method based on Kriging model for beam structures, J. Low Freq. Noise Vib. Act. Control, 38 (2019) 1378-1390.

[124] C. Lu, Y.W. Feng, R.P. Liem, C.W. Fei, Improved Kriging with extremum response surface method for structural dynamic reliability and sensitivity analyses, Aerospace Science and Technology, 76 (2018) 164-175.

[125] J.L. Zapico, A. Gonzalez-Buelga, M.P. Gonzalez, R. Alonso, Finite element model updating of a small steel frame using neural networks, Smart Mater. Struct., 17 (2008) 11.

[126] Y. Zhu, L.M. Zhang, Finite element model updating based on least squares support vector machines, in: W. Yu, H.B. He, N. Zhng (Eds.) Advances in Neural Networks - Isnn 2009, Pt 2, Proceedings, Springer-Verlag Berlin, Berlin, 2009, pp. 296-303.

[127] M. Marcy, A. Brasiliano, G. Barbosa Lima da Silva, G. Doz, Locating damages in beams with artificial neural network, Int. J. Lifecycle Perform. Eng. (Switzerland), 1 (2014) 398-413.

[128] K.M. Hanson, F.M. Hemez, A framework for assessing confidence in computational predictions - Computational validation series: Part 3, Exp. Tech., 25 (2001) 50-55.

[129] C. Mares, J.E. Mottershead, M.I. Friswell, Stochastic model updating: Part 1 - theory and simulated example, Mech. Syst. Signal Proc., 20 (2006) 1674-1695.

[130] J.E. Mottershead, C. Mares, S. James, M.I. Friswell, Stochastic model updating: Part 2 - application to a set of physical structures, Mech. Syst. Signal Proc., 20 (2006) 2171-2185.

[131] C. Mares, B. Dratz, J.E. Mottershead, M.I. Friswell, Model updating using Bayesian estimation, Katholieke Univ Leuven, Dept Werktuigkunde, Heverlee, 2006.

[132] J.R. Fonseca, M.I. Friswell, J.E. Mottershead, A.W. Lees, Uncertainty identification by the maximum likelihood method, J. Sound Vib., 288 (2005) 587-599.

[133] H.H. Khodaparast, J.E. Mottershead, M.I. Friswell, Perturbation methods for the estimation of parameter variability in stochastic model updating, Mech. Syst. Signal Proc., 22 (2008) 1751-1773.

[134] G. Andriosopoulou, A. Mastakouris, K. Vamvoudakis-Stefanou, S. Fassois, Random vibration based robust damage detection for a composite aerostructure under assembly-induced uncertainty, in, Springer Singapore, Singapore, 2020, pp. 775-787.

[135] E. Simoen, G. De Roeck, G. Lombaert, Dealing with uncertainty in model updating for damage assessment: A review, Mech. Syst. Signal Proc., 56-57 (2015) 123-149.

[136] R.W. Messler, Joining of materials and structures: from pragmatic process to enabling technology, Butterworth-Heinemann, 2004.

[137] S.E. Hughes, A quick guide to welding and weld inspection, Matthews Engineering Training, Cambridge, England, 2009.

[138] D.M. Neto, P. Neto, Numerical modeling of friction stir welding process: a literature review, Int. J. Adv. Manuf. Technol., 65 (2013) 115-126.

[139] J.C. Shen, Z. Chen, Welding simulation of fillet-welded joint using shell elements with section integration, J. Mater. Process. Technol., 214 (2014) 2529-2536.

[140] M. Peric, Z. Tonkovic, A. Rodic, M. Surjak, I. Garasic, I. Boras, S. Svaic, Numerical analysis and experimental investigation of welding residual stresses and distortions in a T-joint fillet weld, Mater. Des., 53 (2014) 1052-1063.

[141] S. Nadimi, R. Khoushehmehr, B. Rohani, A. Mostafapour, Investigation and analysis of weld induced residual stresses in two dissimilar pipes by finite element modeling, Journal of Applied sciences, 8 (2008) 1014-1020.

[142] M. Nuruzzaman, C.Q. Wu, O. Ojo, Asme, Modeling of welding joint using effective notch stress approach for misalignment analysis, Amer Soc Mechanical Engineers, New York, 2016.

[143] A. Al-Samhan, S.M.H. Darwish, Finite element modeling of weld-bonded joints, J. Mater. Process. Technol., 142 (2003) 587-598.

[144] J.G. Fang, Y.K. Gao, G.Y. Sun, C.M. Xu, Y.T. Zhang, Q. Li, Optimization of spot-welded joints combined artificial bee colony algorithm with sequential Kriging optimization, Adv. Mech. Eng., (2014) 10.

[145] C.G. Matos, R.H. Dodds, Probabilistic modeling of weld fracture in steel frame connections - part I: quasi-static loading, Eng. Struct., 23 (2001) 1011-1030.

[146] Z.X. Song, Y.P. Xiong, J.L. Xie, J.T. Xing, Weld Root Magnification Factors for Semi-Elliptical Cracks in T-Butt Joints, Acta Mech. Solida Sin., 26 (2013) 317-330.

[147] M.P. Hu, X.D. Sun, J. He, Y.Y. Zhan, Double crack damage identification of welded steel structure based on LAMB WAVES of S0 mode, Materials, 12 (2019) 18.

[148] S.N. Zahari, A.A.R. Zakaria, M.S.M. Sani, I. Zaman, A review on model updating of joint structure for dynamic analysis purpose, in: S.A.C. Ghani, A. Alias, R. Mamat, M.M. Rahman (Eds.) 3rd International Conference on Mechanical Engineering Research, E D P Sciences, Cedex A, 2016.

[149] S. Xu, X. Deng, An evaluation of simplified finite element models for spot-welded joints, Finite Elem. Anal. Des., 40 (2004) 1175-1194.

[150] MSC.Software, MSC Nastran 2016 reference manual, 2016.

[151] J. Fang, C. Hoff, B. Holman, F. Mueller, D. Wallerstein, Weld modeling with MSC. Nastran, Proceedings 2nd MSC Worldwide, (2000).

[152] N.A. Husain, H.H. Khodaparast, A. Snaylam, S. James, G. Dearden, H. Ouyang, Finite-element modelling and updating of laser spot weld joints in a top-hat structure for dynamic analysis, Proc. Inst. Mech. Eng. Part C-J. Eng. Mech. Eng. Sci., 224 (2010) 851-861.

[153] M.N.A. Rani, S. Kasolang, M.H.O. Mohd, A. Yunus, W.I.I. Wan Iskandar Mirza, H. Ouyang, Finite element modelling and modal based updating for the dynamic behaviour of a laser spot welded structure, in: 23rd International Congress on Sound and Vibration, ICSV 2016, July 10, 2016 - July 14, 2016, International Institute of Acoustics and Vibrations, Athens, Greece, 2016, pp. 1-8.

[154] N. Abu Husain, A. Snaylam, H.H. Khodaparast, S. James, G. Dearden, H. Ouyang, FE model updating for damage detection - Application to a welded structure, in: Damage Assessment of Structures Viii, Trans Tech Publications Ltd, Stafa-Zurich, 2009, pp. 393-400.

[155] N. Abu Husain, H.H. Khodaparast, H.J. Ouyang, Parameter selection and stochastic model updating using perturbation methods with parameter weighting matrix assignment, Mech. Syst. Signal Proc., 32 (2012) 135-152.

[156] P. Zeng, Y. Gao, L.P. Lei, Local equivalent welding element to predict the welding deformations of plate-type structures, Sci. China Ser. E-Technol. Sci., 51 (2008) 1502-1506.

[157] N.C. Chee, A.R.A. Bakar, Finite element modeling of arc welded joints, Jurnal Mekanikal, 23 (2007) 15-30.

[158] R.A. Rahman, M. Zubair, N. Amin, Finite element modeling, correlation and model updating of stiffened plate, Jurnal Mekanikal, 16 (2003) 91-106.

[159] M. Garifullin, M. Bronzova, T. Jokinen, M. Heinisuo, B. Kovacic, Effect of fillet welds on initial rotational stiffness of welded tubular joints, in: S. Alpatov, O. Prentkovskis, R.L. Sterling, D. Kaliampakos (Eds.) 15th International Scientific Conference Underground Urbanisation as a Prerequisite for Sustainable Development, Elsevier Science Bv, Amsterdam, 2016, pp. 1643-1650.

[160] B. Horton, H. Gurgenci, M. Veidt, M. Friswell, Finite element model updating of the welded joints in a hollow section H-frame, in: International Conference on Applications of Modal Analysis: Recent Advances in Modal Analysis Practice, 1999, pp. 309-335.

[161] B. Horton, H. Gurgenci, M. Veidt, M.I. Friswell, Finite Element model updating of a welded space frame, in: Proceedings of IMAC, 2000, pp. 529-535.

[162] H. Ahmadian, J.E. Mottershead, M.I. Friswell, M. Soc Exptl, Joint modelling for finite element model updating, Soc Experimental Mechanics Inc, Bethel, 1996.

[163] S.N. Zahari, M.S.M. Sani, N. Abu Husain, M. Ishak, I. Zaman, Dynamic analysis of friction stir welding joints in dissimilar material plate structure, J. Teknol., 78 (2016) 57-65.

[164] S.N. Zahari, M.S.M. Sani, M. Ishak, Finite element modelling and updating of friction stir welding (FSW) joint for vibration analysis, in: S.A.C. Ghani, W.A.W. Hamzah, A. Alias (Eds.) 2nd International Conference on Automotive Innovation and Green Vehicle, E D P Sciences, Cedex A, 2017.

[165] L. Van Belle, D. Brandolisio, E. Deckers, S. Jonckheere, C. Claeys, B. Pluymers, W. Desmet, Experimental validation of numerical structural dynamic models for metal plate joining techniques, Journal of Vibration and Control, (2017) 1077546317704794.

[166] D.J. Ewins, Basics and state-of-the-art of modal testing, Sadhana, 25 (2000) 207-220.

[167] Z.-F. Fu, J. He, Modal analysis, Elsevier, 2001.

[168] B. Peeters, H. Van der Auweraer, P. Guillaume, J. Leuridan, The PolyMAX frequency-domain method: a new standard for modal parameter estimation?, Shock Vib., 11 (2004) 395-409.

[169] P. Avitabile, Experimental modal analysis - A simple non-mathematical presentation, Sound Vib., 35 (2001) 20-31.

[170] M.H. Richardson, Is it a mode shape, or an operating deflection shape?, Sound Vib., 31 (1997) 54-61.

[171] P. Qiao, K. Lu, W. Lestari, J. Wang, Curvature mode shape-based damage detection in composite laminated plates, Compos. Struct., 80 (2007) 409-428.

[172] R.M. Lin, Modelling, detection and identification of flexural crack damages in beams using frequency response functions, Meccanica, 51 (2016) 2027-2044.

[173] X.M. Yang, X.L. Guo, H.J. Ouyang, D.S. Li, Iop, A new frequency matching technique for FRF-based model updating, in: 12th International Conference on Damage Assessment of Structures, Iop Publishing Ltd, Bristol, 2017.

[174] Z. Zhang, A. Aktan, The damage indices for the constructed facilities, in: 13th Int. Modal Analysis Conf., SPIE INTERNATIONAL SOCIETY FOR OPTICAL, 1995, pp. 1520-1529.

[175] A. Alvandi, C. Cremona, Assessment of vibration-based damage identification techniques, J. Sound Vib., 292 (2006) 179-202.

[176] B. Jaishi, W.-X. Ren, Finite element model updating based on eigenvalue and strain energy residuals using multiobjective optimisation technique, Mech. Syst. Signal Proc., 21 (2007) 2295-2317.

[177] Y.J. Cha, O. Buyukozturk, Structural damage detection using modal strain energy and hybrid multiobjective optimization, Comput.-Aided Civil Infrastruct. Eng., 30 (2015) 347-358.

[178] W.J. Yan, W.X. Ren, A direct algebraic method to calculate the sensitivity of element modal strain energy, Int. J. Numer. Meth. Biomed., 27 (2011) 694-710.

[179] W.-J. Yan, T.-L. Huang, W.-X. Ren, Damage detection method based on element modal strain energy sensitivity, Adv. Struct. Eng., 13 (2010) 1075-1088.

[180] S. Seyedpoor, A. Gholizad, S.L. Arefi, Damage detection of structures using modal strain energy with guyan reduction method, Iranian J. Struct. Eng., 3 (2018).

[181] S. Wu, J. Zhou, S. Rui, Q. Fei, Reformulation of elemental modal strain energy method based on strain modes for structural damage detection, Adv. Struct. Eng., 20 (2017) 896-905.

[182] N. Guo, Z.C. Yang, L. Wang, O.Y. Yan, X.P. Zhang, Dynamic model updating based on strain mode shape and natural frequency using hybrid pattern search technique, J. Sound Vib., 422 (2018) 112-130.

[183] S.P. Robert Fisher, Ashley Walker, Erik Wolfart, Gaussian smoothing, in, 2004.

[184] X. Yang, X. Guo, H. Ouyang, D. Li, A Kriging model based finite element model updating method for damage detection, Applied Sciences, 7 (2017) 1039.

[185] J. Muller, C.A. Shoemaker, R. Piche, SO-MI: A surrogate model algorithm for computationally expensive nonlinear mixed-integer black-box global optimization problems, Comput. Oper. Res., 40 (2013) 1383-1400.

[186] W.X. Ren, S.E. Fang, M.Y. Deng, Response surface-based finite-element-model updating using structural static responses, J. Eng. Mech.-ASCE, 137 (2011) 248-257.

[187] H.H. Khodaparast, J.E. Mottershead, K.J. Badcock, Interval model updating with irreducible uncertainty using the Kriging predictor, Mech. Syst. Signal Proc., 25 (2011) 1204-1226.

[188] J. Sacks, W.J. Welch, T.J. Mitchell, H.P. Wynn, Design and analysis of computer experiments, Statistical science, (1989) 409-423.

[189] D.R. Jones, M. Schonlau, W.J. Welch, Efficient global optimization of expensive black-box functions, J. Glob. Optim., 13 (1998) 455-492.

[190] E. Figueiredo, G. Park, J. Figueiras, C. Farrar, K. Worden, Structural health monitoring algorithm comparisons using standard data sets, Los Alamos National Laboratory: LA-14393, 6 (2009).

[191] C. Zhan, D.S. Li, H.N. Li, A local damage detection approach based on restoring force method, J. Sound Vib., 333 (2014) 4942-4959.

[192] X. Yang, H. Ouyang, X. Guo, D. Li, Finite element modelling and damage detection of seam weld, in: Proceedings of the 13th International Conference on Damage Assessment of Structures, Springer, 2020, pp. 51-62.

[193] L. Van Belle, D. Brandolisio, E. Deckers, S. Jonckheere, C. Claeys, B. Pluymers, W. Desmet, Experimental validation of numerical structural dynamic models for metal plate joining techniques, Journal of Vibration and Control, 24 (2018) 3348-3369.

[194] S.N. Zahari, A.A.R. Zakaria, M.S.M. Sani, I. Zaman, A review on model updating of joint structure for dynamic analysis purpose, in: MATEC Web of Conferences, EDP Sciences, 2016, pp. 1-6.

[195] MSC.Software, MSC Nastran 2017 quick reference guide, 2016.

[196] M. Aygül, Fatigue analysis of welded structures using the finite element method, in, Ph. D. Thesis, Chalmers University of Technology, Gothenburg, Sweden, 2012.

[197] J.-L. Fayard, A. Bignonnet, K.D. Van, Fatigue design of welded thin sheet structures, in: European Structural Integrity Society, Elsevier, 1997, pp. 145-152.

[198] MSC.Software, MSC Nastran 2018 linear static analysis user's guide, 2017.